Incorporation of Non-Stationary Landcover into WATFLOOD Climate Change Scenarios

by

Shane Gregory Wruth

A thesis submitted to the Faculty of Graduate Studies of

The University of Manitoba

in partial fulfillment of the requirements of the degree of

MASTER OF SCIENCE

Department of Civil Engineering

University of Manitoba

Winnipeg, Manitoba

Abstract

In this thesis, a landcover simulator module is developed to incorporate non-stationary landcover into the hydrological model WATFLOOD. Objectives are to quantify the uncertainty inherent in assuming landcover stationarity in the Winnipeg River basin (WRB), and to improve the projections of future streamflow. Forest fires commonplace in the WRB are modelled through logistic regression and a generalized extreme value distribution for occurrence and extent respectively, fit from historical data. Fire regeneration and natural changes in landcover are modelled though a first order Markov chain, with transition probabilities derived from satellite imagery. Using satellite imagery directly into historical simulations in a sub-basin with substantial forest fire activity improved WATFLOOD results. With climate change, incorporating non-stationary landcover results in lower flows than assuming stationarity, albeit still greater than baseline (1971 - 2000) flows. Projected streamflow uncertainty under climate change also increases as a result of introducing non-stationary landcover in the WRB.

Acknowledgements

I would like to thank my advisor, Dr. Trish Stadnyk, for her support and assistance throughout my degree and previous work terms. You provided me with great academic experiences and have set a solid foundation for my career as an engineer.

I thank Manitoba Hydro for funding this project and participating in the NSERC Industrial Postgraduate Scholarship program. This program greatly enriched my degree and allowed me to draw on much appreciated expertise for my project. I also thank NSERC for supporting this partnership, and the Canadian Water Resources Association for additional support.

In the Water Resources Engineering Department at Manitoba Hydro, I would like to thank Kristina Koenig, Efrem Teklemariam, and John Crawford for helping make this project possible. I also thank Mark Gervais, Mike Vieira, Steve Bohrn, and Phil Slota for additional assistance throughout my degree.

I acknowledge the international modelling groups, the Program for Climate Model Diagnostics and Intercomparison (PCMDI), the JSC/CLIVAR Working group on Coupled Modelling (WGCM), and their Coupled Model Intercomparison Project (CMIP) and Climate Simulation Panel for providing, collecting, archiving, and organizing data analysis activity. As well as Ouranos Consortium for providing the global climate model data used in this thesis.

I thank Dr. Peter Rasmussen and Dr. Shawn Clark for helping me develop both interesting and necessary skill sets to be successful in this field. I also thank all the graduate and undergraduate students in the lab that I've had the privilege to work with. I thank the undergraduate students Wade Ambach and Mark Vogt for assisting with my project.

I also thank my parents, Marjorie and Melvin Wruth, and my sisters, Yasemin Keeler and Nicole Wruth for their support throughout my degree. Lastly, and definitely not least I thank Andrea Evans. Thanks for your unwavering support and enthusiasm throughout our degrees, and of course for sharing your statistical talents.

To my parents, Marjorie and Melvin Wruth

Table of Contents

List of Tables

List of Figures

List of Copyright Material for Which Permission was Obtained

List of Appendices

Chapter 1 Introduction

Climate change, and its effects on the hydrologic regime has been the topic of interest and focus of a significant amount of research in the water resources engineering field in the past decade (Velazquez, et al., 2013; Kim, et al., 2013; Bohrn, 2012; Poulin, et al., 2011; Samaniego & Bardossy, 2006). Future changes in water supply are projected to have impacts on the operations and design (both new and retrofit) of hydroelectric utilities; therefore understanding such change is paramount for future development, operation, and long term planning. Climate directly influences hydrologic processes through temperature and precipitation, and is not stationary through time. Landcover also directly affects the amount and timing of streamflow response, and is itself affected by climate change. The over-arching goal of this research is to incorporate landcover non-stationarity, influenced by climate change scenarios, into hydrological projections of future streamflow.

1.1 Project Motivation

Impacts of landcover change on the hydrologic regime are well known (Brown, et al., 2013; Kim, et al., 2013; Pomeroy, et al., 2012; Samaniego & Bardossy, 2006; Eschner & Satterlund, 1966) however many hydrologic studies do not yet consider non-stationary landcover and instead assert that its further study is warranted (Bohrn, 2012; Cuo, et al., 2011; Quilbe, et al., 2008). And while changes in climate have major impacts on runoff timing (such as snowmelt), changes in landcover more typically impact runoff volume thereby making its inclusion all the more necessary (Cuo, et al., 2011). Hydroelectric utilities, such as Manitoba Hydro, may be impacted by these changes in runoff induced by climatic and landcover change. This thesis serves to outline methodologies in quantifying the impact landcover changes, in the context of climate change, have on future hydrologic regimes. In addition to the knowledge of climate and landcover changes gained in this thesis, it will serve as a launching point for studies in additional watersheds. Many climate change impact studies in the literature can incorporate similar methodologies as this thesis into their own research to contribute to the broader understanding of climatic and landcover changes on various hydrologic regimes.

1.2 Scope

This research has can be divided into three distinct components: (1) a historical landcover change analysis at the sub-basin scale, (2) development of a pre-processing module to simulate future (or historical) landcover, and (3) application of the module in the Winnipeg River Basin (WRB) under climate change. Landcover change analyses presented are focussed on changes induced by forest fires over the study period and into the future, but the methodology derived is expandable to other types of landcover. For example, natural change is also addressed in this thesis.

The first component involves collection of historical LandSAT satellite imagery in two sub-basins: one with significant amounts of burn and transitional cover from historical forest fires, and one without significant burn. The landcover changes in these two sub-basins are assumed to be representative of changes throughout the entire WRB. Images are collected at regular intervals into the past, from the early '80s until present day. Used in the hydrological model WATFLOOD, historical simulations are conducted from 1980 – 2010 to reflect the time-period the images are collected from.

The second component of this thesis involves the development of the landcover simulator module; a pre-processing tool to run specifically alongside WATFLOOD that generates landcover forcing for the model. The module is linked with climate model outputs (temperature and precipitation), for the forest fire component to be impacted by climate change. The natural change and fire regeneration components are not linked with climate outputs, and depend solely on observed historical changes from satellite imagery.

The third component is the application of the module with WATFLOOD to simulate future streamflow in the WRB under climate change. Simulations are completed for non-stationary and stationary landcover, using three emissions scenarios (A1, A1B and A2) (IPCC, 2000) from the CGCM3.1 climate model (Scinocca, et al., 2008). Hydrologic simulation of climate change is conducted using the delta change method (Diaz-Nieto & Wilby, 2005; Hay, et al., 2000). While only one climate model is used, multiple ensemble members are simulated representing various initial conditions. Two future time periods are simulated: the 2050s (2040 – 2069) and 2080s (2070 – 2099). Climate change simulations are compared the baseline period of 1971 – 2000, consistent with studies in literature (Velazquez, et al., 2013; Roberts, et al., 2012; Veijalainen, et al., 2010).

1.3 Objectives

This thesis has three objectives:

- Develop methodologies to incorporate landcover changes into WATFLOOD;

- Quantify uncertainty in historical and future streamflow simulations resulting from changes in landcover (ex, forest fires) in the Winnipeg River Basin (WRB);
- Improve the accuracy of future streamflow projections in the WRB by incorporating non-stationary landcover in tandem with the existing climate change module using WATFLOOD.

1.4 Document Organization

The following is a brief outline regarding the organizational structure of this thesis, and is included as guide for finding specific sections of interest to the reader:

- Chapter 2: Background Information is included to provide the reader with relevant literature and hydrological modelling background (specifically WATFLOOD), and in particular its suitability for utilizing non-stationary landcover. Relevant literature is summarized pertaining to the hydrologic effects of changing landcover, including forest fires and climate change;
- Chapter 3: Study Area Description provides information on the spatial domain modelled in this thesis, the Winnipeg River Basin (WRB);
- Chapter 4: Sub-basin Historical Landcover Change Analysis describes the classification of LandSAT satellite imagery in two sub-basins and their application into WATFLOOD to examine the effects on model output and quantify the uncertainty inherent from changes in landcover alone;
- Chapter 5: Landcover Simulator Module describes the methodologies behind the pre-processing module and outcome of testing of each individual component;
- Chapter 6: Model Application describes and discusses simulation results using the landcover simulator module with WATFLOOD;

- Chapter 7: Conclusions and Recommendations summarizes the main conclusions resultant of this thesis and recommendations for future work. The significance of this research is also discussed.

Chapter 2 Background Information

This section contains background material on the core aspects of this thesis, including the WATFLOOD™ hydrological model, the study of climate change and how climate change studies are conducted with WATFLOOD. Also discussed is the concept and previous applications of non-stationary landcover in hydrological modelling, as well as methods of modelling forest fires.

2.1 Background on Hydrologic Modelling of Climate Change

Climate change is defined as statistically detectable changes in the mean and/or variability in properties of the earth's climate, which continue over long-term periods of ten years or more (IPCC, 2007). The IPCC has found overall increasing global warming trends over the past 100 years (1906-2005) of 0.74°C, and an average rise in sea level of 1.8 mm/year from 1961 – 2003 (IPCC, 2007). Trend analyses from 1900 – 2005 have also found increasing precipitation in North and South America (IPCC, 2007), which have implications for hydrologic modelling of future scenarios. When these increases (or potential decreases) in precipitation occur, they can affect the overall projected hydrographs in different ways. For example, depending on temperature, increased winter precipitation can result in increased spring freshet runoff (i.e., early year hydrograph not influenced by evaporation) versus increased summer precipitation results in more rain events affecting mid-late year hydrographs subjected to evaporation.

In the IPCC AR4 WGII report, section 19.3.6, various types of extreme events are discussed to have the possibility of increasing in size or frequency with climate change (IPCC, 2007). Large amounts of uncertainties are present however in future projections for the Boreal forest region, with choice of GCM being a significant factor (Bohrn, 2012), with increased burned area under climate change contributing to this (Liu, et al., 2010).

2.1.1 Emissions Storylines and Scenarios

The Intergovernmental Panel on Climate Change (IPCC) has developed four alternative storylines that qualitatively describe the future under various technological, social, and economic conditions (IPCC, 2000). The storylines form the basis of the quantification of climate change, and are further sub-divided into emissions scenarios that are specific in the amount of Greenhouse Gas (GHG) emissions each contribute to the atmosphere. Each scenario quantifies the extent of change in GHGs depending on world and regional policies, within the constraints of each storyline. The GHGs that contribute to climate change include, but are not limited to, carbon dioxide (CO_2), methane (CH_4), carbon monoxide (CO), sulfur dioxide (SO_2), and nitrogen oxides (NO_x). From the IPCC fourth assessment report (AR4), the B1, A2, A1B scenarios are selected and applied for this thesis and are described below. They range from low to high GHG emissions providing a variety of possible outcomes for this thesis, and tend not to diverge significantly until after the 2050s.

The A1 storyline and emission scenarios represent a future where per-capita income between countries come together, reducing quality of life disparities between regions (IPCC, 2000). Characteristics of this storyline include a commitment to market based solutions, high investment in education and technology, and international cultural and social interactions. Low population growth and rapid economic growth are also characteristic of this scenario. This storyline is split into a number of scenarios with varying amounts of technological change in terms of energy. The A1B scenario, which is used in this thesis, assumes a balanced approach with no single source of energy being dominant. Therefore while renewable and clean energies are pursued, fossil fuels are still used in significant amounts (IPCC, 2000). In this regard, A1B is considered to a 'middle ground' in that it's neither overly optimistic nor pessimistic.

The A2 storyline and emission scenario on the other hand are the most pessimistic considered in this thesis, characterized by high population growth and widening income gaps between the rich and poor. Economic development is regionally fragmented with resource-rich, low-income countries relying on fossil fuels for energy requirements and only resource-poor, high-income countries developing more advanced, renewable and clean energy. Therefore fuel use by region depends on resource availability; significantly slowing technological innovation in regards to clean energy, resulting in high GHG emissions (IPCC, 2000).

The B1 storyline and emission scenario consists of similar population growth patterns of the A1 storyline, however combined with a more dedicated approach to sustainable development. More emphasis is placed by society on environmental and social impacts of development, with significant investment into technological innovations and shifts to more resource-efficient energy sources (IPCC, 2000). In this regards, the B1 storyline is considered to be the most optimistic of those considered for this thesis.

2.1.2 Climate Change in Hydrological Modelling Studies

Using the output of climate models, numerous studies making hydrologic projections into the future have been conducted. Owing to the nature of these studies and lack of data for validation, it is well established that there are significant uncertainties in projected future streamflow from various sources and at varying significance levels. Poulin, et al., (2011), for example, conducted a hydrological modelling climate change impact study in the 6954 km^2 Ceizur River basin in south-western Quebec. Using the HSAMI and HYDROTEL hydrological models, parameter and model uncertainities are quantified in the context of climate change. Model selection was found to contribute more uncertainty than parameter uncertainty. A study by Velazquez, et al., (2013) also determined uncertainty in hydrological model selection the most significant source of uncertainty with climate change for basins in both Quebec and Barvaria, Germany; dominated by decidous and coniferous forests respectively.

Another hydrologic impact study modelling 21 watersheds in Quebec, made streamflow projections under climate change (Huziy, et al., 2013). This study used streamflow output from the Canadian Regional Climate Model (CRCM) for its projections of streamflow in watersheds varying from 13,212 km^2 to 143,241 km^2 in size, assuming stationary lancover. Of particular emphasis were extreme flows, with a generalized extreme value (GEV) distribution fit to historical extreme flows. Statistical tests were conducted to detect changes in magnitude and return period of extreme flows under climate change. Increases in flow for 30 and 10 year return periods were projected to occur for this region, with the trend being attributed to increased precipitation in the region consisting largely of boreal forest (Huziy, et al., 2013).

In a study by Veijalainen, et al., (2010), climate change impacts on the flow regime for the Vuoksi River basin (61,000 km^2) were conducted. This basin, residing in the Boreal forest region of Finland and Russia is heavily regulated for hydroelectric power production. Future streamflows were generated using meterological inputs from an ensemble of 19 GCMs and the lumped Watershed Simulation and Forecasting System (WSFS) hydrological model. Under climate change the normally snowmelt dominated basin recieved more precipitation in the winter, albeit more as rainfall due to warmer temperatures. With fall precipitation also increased, the peak average annual hydrograph was projected to shift from spring to fall or winter. Current regulation permits regarding control of water levels were deemed inadequate for these future conditions and modifications were recommended to account for changes in the hydrologic regime (Veijalainen, et al., 2010).

In Labrador the Pinus River (770 km^2), a sub-basin of the Churchill River, was modelled under climate change using WATFLOOD (Roberts, et al., 2012). Similar to the previous study, the Churchill River basin is relied upon for hydroelectric energy, with uncertainties in power production with climate change a driver of the reasearch. The closest metorological station to the Pinus River sub-basin is 90 km away, making the authors choose WATFLOOD to simulate flows due to its effectiveness in data sparse basins (Roberts, et al., 2012). Using an ensemble of regional and global climate models, precipitation in this sub-basin was projected to increase up to 25% in winter, with significant variability between ensemble members. Temperature was projected to increase up to 3.5°C in the sub-basin, shifting snowmelt runoff two weeks earlier than present. Overall, mean flows were projected to increase by 8.9% (2050s) in this sub-basin with climate change (Roberts, et al., 2012).

In the northern Canadian Mackenzie River basin (1.8M km^2) Yip, et al., (2012) conducted a trend analysis on historical climate and runoff. Trends were investigated using two meterological data sets: Environment Canada (EC) gridded data and European Centre for Medium-range Weather Forecasting (ECMWF) reanalysis data. Both datasets were input into the model WATFLOOD, with the hydrologic variable's sensitivity to the inputs quantified. Using historical data from 1961 – 2002, precipitation increases of 2.28 mm and 1.22 mm were found for the EC and ECMWF datasets respectively. Precipitation changes were more variable throughout the basin for both datasets, containing increasing and decreasing trends. Runoff experienced decreases with the EC dataset, and increases with the ECMWF dataset (Yip, et al., 2012). This highlights the importance of climate input selection to hydrological models and uncertainties, in particular in historic or climate change studies.

A recent study by Bohrn, (2012) performed a hydrologic climate change impact study on the Churchill River basin (280,000 km^2) in Manitoba, Saskatchewan, and Alberta. This is also a regulated basin, with significant contributions to hydroelectric power production. Using the HBV-EC, HMETS, and WATFLOOD hydrological models, climate change simulations were conducted and the uncertainties inherent in model selection quantified. Choice of hydrological model was found to significantly affect results, with HBV-EC resulting in the lowest projected flows. Common amongst the models was a shift in freshet timing with climate change despite differing projected volumes. All three models were calibrated and performed adequately to observed data, then produced diverging results under climate change, highlighting the importance of understanding the impacts (and uncertainties) from model selection and parameterization (Bohrn, 2012). This study showed model physical realism affects the quality of projections, where calibration to future flows is never possible. This study is consistent with several other studies in finding that GCM selection is also a large source of uncertainty in projected streamflows (Bohrn, 2012; Chen, et al., 2011; Prudhomme & Davies, 2009a; Prudhomme & Davies, 2009b; Minville, et al., 2008).

In all the hydrologic climate change and historical trend analysis studies examined in this section, landcover was held constant. A major reason for this assumption's prevalence in the literature is that no climate change enabled hydrological model is equipped to handle evolving landcover with climate change on the mesoscale (to the knowledge of the author), and data handling and processing requirements often make such studies infeasible. The WRNSHYD™ model has been used to model landcover effects on hydrology, but is most useful on small scales (Minister of Supply and Services, 1989). The effects of changing landcover on the hydrologic regime have however been tested in hydrological models under historical or current climates and its importance is well understood.

2.2 Landcover Non-Stationarity in Hydrological Modelling Studies

It is well established that changes in landcover and land use can have significant impacts on hydrologic regimes, including forest harvesting, forest fires, reforestation, and insect infestation (Eschner & Satterlund, 1966). In Eschner & Satterlund, (1966), landcover change in a coniferous forest dominated basin is documented from 1912 to 1962 as well as shifts in hydrologic response. The study area was the 1272 km^2 Sacandaga River basin in New York, and experienced extensive amounts of logging, forest fires, and insect outbreaks leading up to 1912, after the installation of a flow gauge, resulting in the lowest amount of forest cover density in recorded history. In the following years, after most of the basin became a national park and logging was reduced, the forest underwent a period of regeneration until 1950. At this time, a destructive storm occurred, regressing the landscape towards that of 1912. Streamflow implications for this period were quite significant, with large decreases in flow occuring between 1912 and 1950, and increasing to previous levels after the storm in 1950, and decreasing at a similar rate therafter to 1962. Various reasons for lower flows are discussed, including increased sublimation and evaporation losses from denser forest canopies, as well as an explosion of the beaver population by the mid 1910's being a factor. What's interesting about this study is that for a long streamflow record, hydrologic impacts directly arising from two massive forest disturbances in the same basin can be realized, with consistent results.

More recently, a study by Pomeroy, et al., (2012), investigated the effects of various forest disturbances in a small (9.4 km^2) mountainous basin, using the Cold Regions Hydrological Model (CRHM), as opposed to direct observation in the previous study. With CRHM, a large number of simulations were conducted with different landcovers to investigate the hydrologic effects of forest disurbances such as mounain pine beetle (MPB) infestation, forest fire, and clear-cut harvesting. The focus of this study was the immediate effects of such disturbances, with the effects of forest regeneration not included, and found that increases in flows occurred with the removal of forest cover. It was found that forest fires resulted in the greatest amount of increase in flows of up to 25%. Reduced sublimation from removed canopies was concluded to be the primary culprit for increasing flows for all disturbances. However because trunks are typically retained after forest fires, blowing snow sublimation losses are smaller than that of clear-cutting, causing forest fires to have the greatest increase in flows. This is due to the trunks inhibiting wind flow. On a small scale, this study highlights the importance of including forest-disturbance effects in hydrological models, as they can significantly affect the hydrologic response, and consequently the conclusions of hydrologic impact studies.

Long term effects of forest cover changes are also significant, and are investigated in Brown, et al., (2013). In this study, several catchments (27 – 350 ha) in South Africa and Austrailia that have undergone deforestation or afforestation were analyzed for there hydrologic responses (>50% total catchment area affected by landcover change in most cases). It was found that afforestation decreased total volumes of flow, and deforestation increased it. The main reasons for this were increased evapotranspiration from increased forest cover with afforestation, and the opposite for deforestation. Another finding of this study was the discovery of delays in total streamflow response over time with permanent forest cover change. Response times varied widely between dominate tree species, ranging from 8 – 25 years, showing that after forest cover change, either immediate or gradual, the time required to reach a new, stable hydrologic regime is not immediate and long-term analyis should be conducted.

With climate change becoming a global concern, it is becoming necessary for studies analyzing the hydrologic effects of landcover and land use change to include the meteorological effects of climate change (Kim, et al., 2013; Quilbe, et al., 2008; Samaniego & Bardossy, 2006). In Kim, et al., (2013), climate change simulations are conducted on a small (125.15 km^2) basin in the Republic of Korea, under various future landcover conditions. Using general meterological and landcover projections from the IPCC, and the Soil and Water Assessment Tool (SWAT) model, streamflow impacts under climate and landcover change were deduced. The focus of this study was more anthropogenic land use change, with the expansion of urban areas into countryside and forest. It was found that while climate change itself had a more significant impact on streamflow than changes in land use, land use did in fact have a significant effect. As a result, the climate and land use change simulations were similar to results with only climate change, albeit with greater seasonal variability with the former. Similarily in a study by Samaniego & Bardossy, (2006), the hydrologic effects of climate and landcover change were determined for a 126.3 km^2 basin. Again, the focus of land use change was mostly anthropogenic expansions of urban areas, however was simulated by coupling a statistical land use change model with a statistical hydrologic model, both developed by the authors. This study also found significant impacts on future streamflow with landcover changes, with 15 – 43% increases in annual peak flows as a result of greater impervious area, raising risks of floods. In Quilbe, et al., (2008) climate change simulations were conducted on the primarily agricultural Chaudière River basin (6682 km^2) in Quebec. Two future land use changes were simulated: progression towards lower intensity agriculture or continued intensive agriculture. The sustainable development case included a large portion of the basin reforested. Previous land use changes were determined through the use of LandSAT satellitte imagery, and projected 30 years into the future. The HYDROTEL hydrological model was used for hydrologic climate change simulation. The study found that historic agricultural land use changes have had significant impacts on the hydrologic regime, as well as with climate change. Annual runoff from the higher intensity and lower intensity (with reforestation) cases changed from 13.6% and -7.2% respectively. Land use changes actually had an equivalent or greater impact on future hydrology than climate change alone (Quilbe, et al., 2008). This difference from the previous study indicates that different types of landcover change can lead to different conclusions.

These studies illustrate the need for coupling landcover/land use changes with climate change in hydrologic models, and demonstrate the importance of considering such uncertainties in future streamflow projections. While each has its own methodology for incorporating land use/cover into hydrologic simulation, for this thesis investigating climate change impacts on disturbances such as forest fires are necessary for applicablity in the

Boreal region where fewer studies have been conducted and future water availability is required for hydroelectric operations.

2.3 Historical Forest Fires and Climate Change

In the Boreal forest, throughout history fire has been the dominant source of disturbance and has significant ecological effects such as increased biodiversity, changing energy flows, and impacts on the carbon cycle (Parisien, et al., 2006; Stocks, et al., 2003), as well as significant hydrologic effects (Pomeroy, et al., 2012; Eschner & Satterlund, 1966). Large forest fires (>200 ha), as classified by the Canadian Forest Service, are not as common as small fires in Canada and only account for 3% of all fires, however result in 97% of total burned area (Stocks, et al., 2003). These large forest fires are generally the focus of most studies' efforts to analyze historic trends and driving forces of the fire regime, as well as projections with climate change. Long term analysis of forest fire data however poses challenges, as despite the documenting of forest fire activity starting in 1918; actual recording in remote areas was not comprehensive until the 1950s and 1960s, and complete coverage not available until the advent of remote sensing via satellites in the 1970s. There has also been a shift in public attitudes in forest fire management over this recording period. Starting in 1918 and throughout most of the record, the focus of provincial fire management agencies was on fire suppression and conservation of the forests and "natural landscape". More recently, however, the ecological importance and benefits of fire to the forest are becoming more understood. This has resulted in a more balanced approach in that forest fires are generally allowed to run their natural course, with selective suppression to protect human settlements and maintain adequate timber stock (Stocks, et al., 2003).

In the Yukon boreal forest, McCoy & Burn, (2005), conducted historical analyses and climate change projections on the forest fire regime. Their results are clear, as for the A2 scenario in the 2080s, forest fire occurrences are projected to increase by two thirds over current conditions, with annual burned area increasing up to three times. Inter-annual variability however should remain constant, with some years experiencing more fires, and sometimes none at all. A study in the Boreal forest in central Quebec is consistent showing an overall increase in projected forest fires with climate change, although focussed on the temporal distribution of fires within the year (Le Goff, et al., 2009). Again with the A2 scenario in the 2080s, average monthly forest fire risk is projected to increase by 30%, with the highest increases in July and August of 70% and 100% respectively, and the lowest month being May with a decreased risk of 20%. This indicates that the peak in forest fire activity in this area is likely to shift towards the latter end of the forest fire season in July and August, however not enough data is available to actually conclude whether or not the forest fire season itself will shift. Overall though, the forest fire regime in the Canadian Boreal forest is projected to show signigicant changes in occurrences, burned area, and timing under climate change, and such changes are highly correlated to temperature and precipitation which are easily deduced from climate models (Le Goff, et al., 2009; McCoy & Burn, 2005).

2.4 WATFLOOD Hydrological Model

To incorporate non-stationary landcover into hydrologic climate change studies, a suitable model must be selected. For this thesis, the WATFLOOD hydrological model is used, and its suitability is discussed in this section. WATFLOOD is a semi-physically based, distributed hydrological model utilizing gridded input data sources such as DEMs, LandSAT imagery, and radar (Kouwen, 2012). WATFLOOD has a modular framework, separating input pre-processing (i.e. meteorological data, soil moisture initialization, etc.) from actual model simulation to enhance computational efficiency and model development. Being a distributed model, the watershed domain is divided into grids with runoff simulated for each grid and subsequently routed downstream. Each grid is sub-divided into several hydrologically-distinct landcover classes, with runoff generated individually within each class, and summed for total gridded runoff (Kouwen, et al., 1993). This concept is referred to as a Grouped Response Unit (GRU), and a graphical representation is shown on Figure 1.

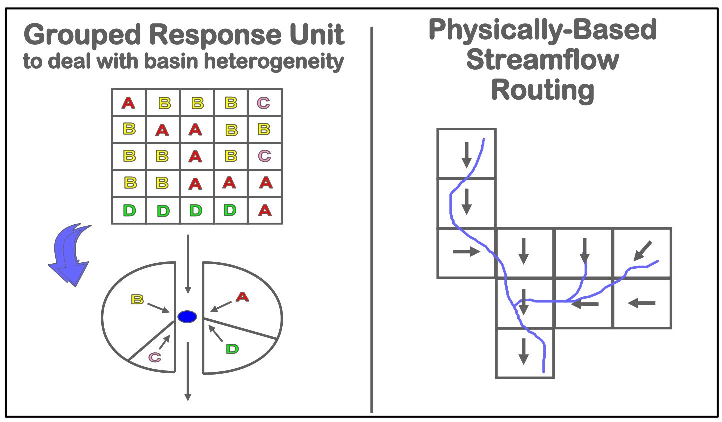

Figure 1 - WATFLOOD grouped response units (GRUs), from (Stadnyk-Falcone, 2008)

Derived from LandSAT imagery, each pixel within a grid cell is assigned a landcover class, and then grouped into a percent coverage as indicated on the left-hand side of Figure 1. This occurs for each grid cell (right-hand side of Figure 1); with gridded runoff then being routed downstream using simple storage routing. The benefit of this method in relation to this thesis is that percent landcover coverage for each grid can be changed dynamically throughout the simulation. This provides a means for studying the hydrologic impacts of landcover change, either historical or future. The hydrological processes that are simulated in WATFLOOD are included on Figure 2, with processes' parameters defined separately for each landcover.

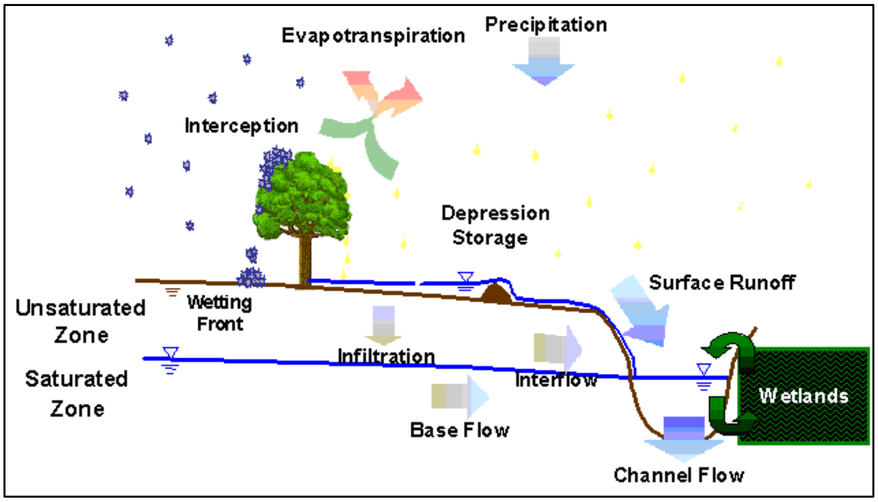

Figure 2 - Hydrological processes modelled in WATFLOOD, from (Stadnyk-Falcone, 2008)

As long as the internal hydrological processes are calibrated as an adequate representation of reality, changes in hydrologic responses and feedbacks within the system should be representative of actual changes in runoff responses associated with changing landcover. These internal processes have been validated by Bingeman, et al., (2006), as well as using stable-water isotope tracers (Stadnyk, et al., in press; Stadnyk, et al., 2005). Stable-water isotope tracers provide an additional means for validating internal model processes than streamflow response alone. These studies were conducted in areas of Boreal forest containing significant amounts of wetlands, both of which are characteristic of the Winnipeg River basin (the study domain for this thesis) and provides confidence in the model's hydrological response to changes in landcover.

This model is well suited to incorporating non-stationary landcover in simulations due to its separation of pre-processing (landcover and DEM data) from actual simulation, and because the majority of parameters are defined (and calibrated) separately on a per landcover basis. The parameters themselves are stationary through time. As landcover percentages are altered during simulation, hydrological responses will automatically adjust based on the different parameter definitions. The ability to change the landcover input files at any point during the simulation has been built into the development of the model (Kouwen, 2012), and a pre-processing module to generate future landcover files is all that is needed to incorporate non-stationary landcover into simulations.

2.4.1 Climate Change Module in WATFLOOD

A climate change module was incorporated into WATFLOOD by Slota (2009) and utilizes the delta change method (Diaz-Nieto & Wilby, 2005; Hay, et al., 2000). In the delta change method, temperature and precipitation forcing from a historical "baseline" timeframe are perturbed to values that would be expected under future climate change scenarios, in which the model output is considered to be future flow. This method captures changes in mean conditions projected under climate change, but does not reflect changes in frequency or variability (Diaz-Nieto & Wilby, 2005). Changes to diurnal temperature ranges are also held constant. To obtain delta values, GCMs are run under different GHG emissions scenarios, and the resulting temperature and precipitation outputs are compared to baseline values using Equations 2.1 and 2.2 from (Bohrn, 2012; Poulin, et al., 2011) respectively. Average monthly delta values are used, with the result being 12 deltas (one for each month) for each meteorological variable.

$$T_{future} = T_{observed} + \left[T_{GCM} - T_{GCM,present}\right] \tag{2.1}$$

$$P_{future} = P_{observed} * \left[\frac{P_{GCM,future}}{P_{GCM,present}}\right] \tag{2.2}$$

GCM results for the study area were provided by Ouranos from the CMIP3 dataset (Meehl, et al., 2007), in which the delta values were calculated and provided by Manitoba Hydro. Details of the delta values and GCM used for the study area are included in Section 3.4. The delta change method has commonly been used in various climate change hydrologic impact studies, such as Bohrn, (2012) and Poulin, et al., (2011), due to its ease of use and computational efficiency. A historical timeframe of 1971 – 2000 is used for the baseline flows to be consistent with literature (Velazquez, et al., 2013; Roberts, et al., 2012; Veijalainen, et al., 2010), is readily available from GCM output, and is consistent with the baseline period used by Manitoba Hydro's climate change studies.

Using stationary landcover is common amongst past and current climate change impact studies, despite a large body of literature that states the invalidity of this assumption. This not only includes forested basins as in the study area of this thesis, but also urban and agricultural basins. With forest fires a dominant feature of the study area (as described in Chapter 3), the literature reviewed demonstrated how forest fire behaviour is anticipated to be impacted by climate change. Various methods of simulating forest fire change under climate change in the Boreal region were presented. Implementing a methodology capable of evolving landcover in long-term hydrological simulation is the aim of this thesis. Due to its distributed nature, the use of GRUs, parameterization based on landcover, and suitability for long-term climate change studies, WATFLOOD was selected for this study. The built-in capability within WATFLOOD to dynamically swap landcover inputs throughout simulations assists in the development of a landcover simulation component of the model. The next chapter describes the study area in which the landcover simulator module is applied.

Chapter 3 Study Area Description

The Winnipeg River basin (WRB) is the domain of study for this project and is located in northwestern Ontario, with portions in Manitoba and Minnesota. This basin is large with an area of approximately 136,000 km^2 (WSC, 2013), and is a source of hydroelectric generation for Manitoba and Ontario. Understanding how climate change will impact future flow regimes is consequently of vital importance to utilities, and has been previously studied (Slota, 2009). Using the same study domain as previous studies, climate change impacts on the WRB are further assessed by incorporating the concept of non-stationary landcover and its inherent uncertainties. Similarly, since landcover alteration due to forest fire occurrence is the focus of this study, the WRB makes a suitable study domain based on extensive coverage by Boreal forest and known and well-documented impacts from forest fires, both historically and present-day. WATFLOOD setup of the WRB was provided by Manitoba Hydro, and is current as of January 2013 (Manitoba Hydro, 2013). A map of the basin is provided on Figure 3, with its Digital Elevation Model (DEM) on Figure 4. The St. Joseph Diversion on the figure is explained in more detail in Section 3.6.

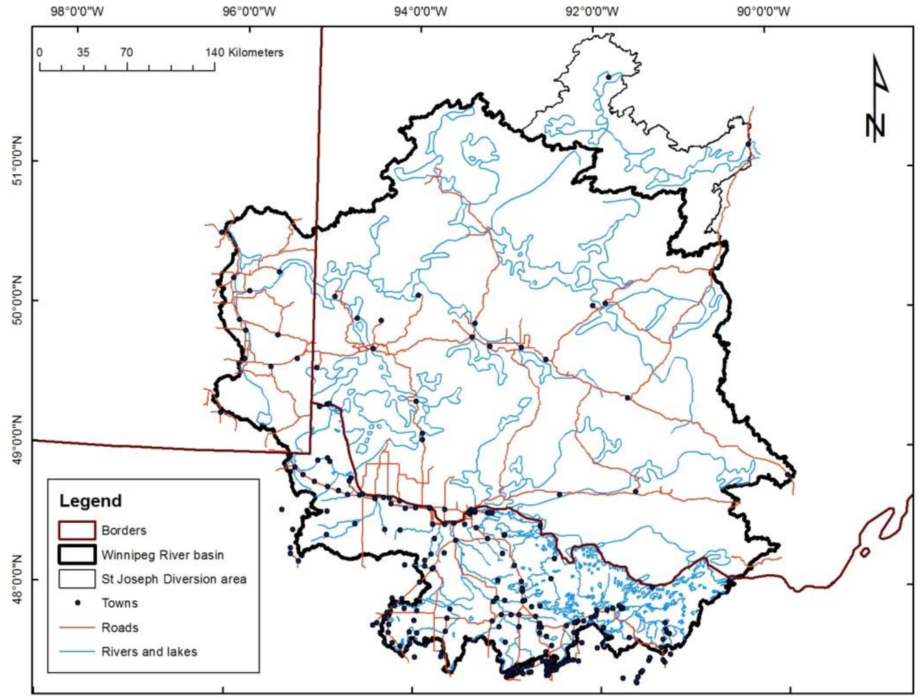

Figure 3 - Map of the Winnipeg River basin (study area)

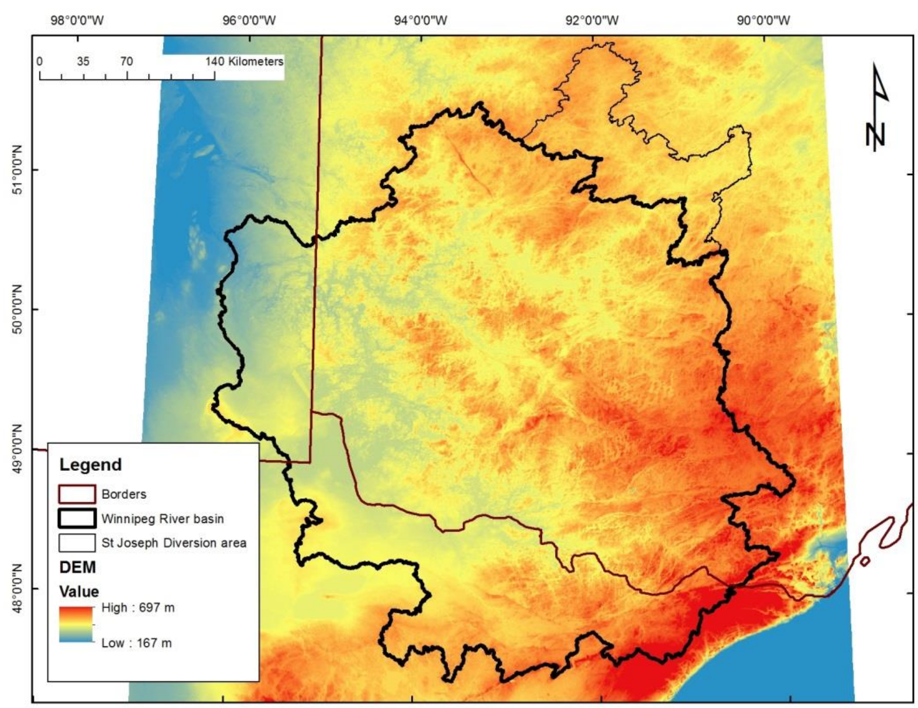

Figure 4 - Digital Elevation Model (DEM) of the WRB, 90 m resolution (Jarvis, et al., 2008)

Historically, the major rivers of this region have been of key importance to both Canada and the United States as an east-west transportation route before the railway, being home to Ojibway, Saulteaux, Cree, and Sioux Nations. The fur trade thrived and drove exploration in the area prior to the development of modern transportation routes (Lake of the Woods Control Board, 2002). After the railway was completed in 1881, major industries were established to include lumber, pulp and paper, mining, fisheries, and later energy through hydroelectric development. These industries continue to be important to this day, with the inclusion of a significant tourism industry, owing to the attractive Boreal forest landscape, large wilderness areas, and abundance of rivers and lakes (Lake of the Woods Control Board, 2002).

Various aspects of the WRB pertinent to this thesis are discussed below, including the hydrological model setup and context of the thesis in general.

3.1 Landcover

The Winnipeg River basin mostly resides in the Canadian Shield, and is described as occupying a transition zone of Boreal forest to the north, and mixed-deciduous forest in the south (St. George, 2007). Wetlands are prevalent throughout the basin, with significant concentrations in the southwest corner and the eastern Manitoba portion. This is evident on Figure 5, a map of the various dominant landcovers present in the basin.

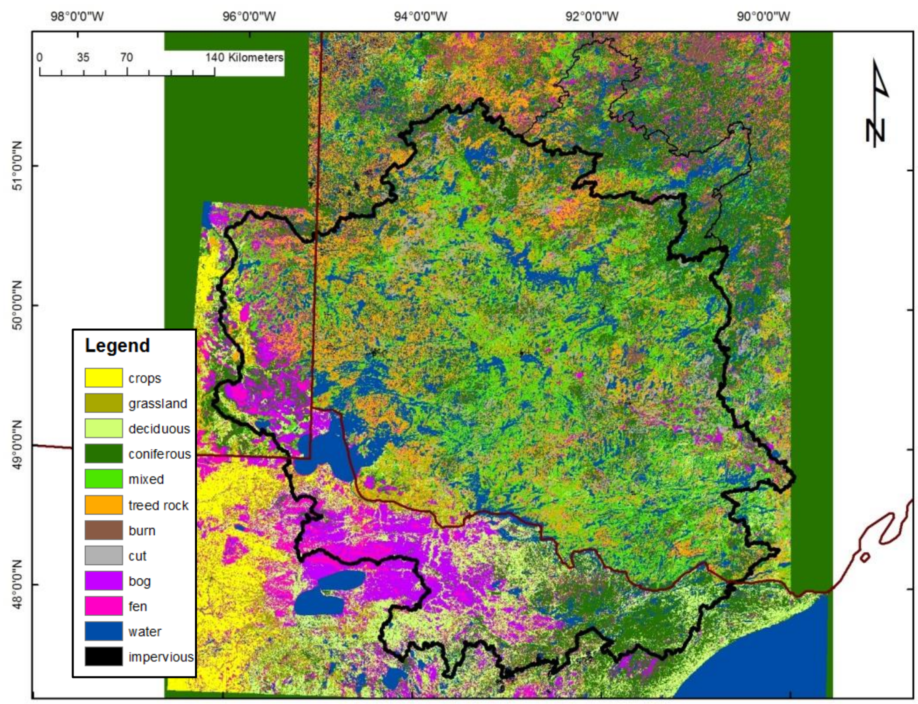

Figure 5 - Harmonized landcover map for the WRB, using ortho-imagery from 1999-2002 (MLI, 2013; MNR, 2013; Vogelmann, et al., 2001)

This map of classified landcover was provided for the project, and is an amalgamation of maps from the three sources: Manitoba Land Initiative (MLI, 2013), Ontario Ministry of Natural Resources (MNR, 2013), and the Multi-Resolution Land Characteristics Consortium (Vogelmann, et al., 2001). Each of these organizations used similar sources for their classifications, ortho-imagery from satellites mostly from the 1999 – 2002 time period, however, their methodologies and specific class descriptions are slightly different. The map on Figure 5 is therefore a simplification, as the most 'similar' land classes based on their descriptions and were grouped together into 12 hydrologically distinct classes as shown on the figure (Manitoba Hydro, 2013).

The *crops* class on Figure 5 is mostly seasonal farmland, with *grassland* consisting of pastures and natural grasslands. The *deciduous* class consists of dense areas of broadleaf trees that shed their leaves in winter, whereas *coniferous* forest is comprised of dense cone-bearing trees that retain their needles in winter. *Mixed* forest is a combination of the *coniferous* and *deciduous* classes, with both types of trees interspersed. The WRB resides mostly in the Canadian Shield, in which there are frequent exposed rock outcrops. Areas that contain significant amounts of exposed rock, intermingled with sparse *coniferous* and *deciduous* forest are referred to as *treed rock*. Areas affected by recent forest fires or logging are classified as *burn* and *cuts* respectively. *Bogs* refer to muskeg areas that can become saturated with water, while not connected to streams or rivers. *Fens* are classified as any type of wetland in which its water table is connected to nearby streams or rivers. Paved roads and towns that consist of surfaces impermeable to the soil are classified as *impervious*. The *water* class is any area that maintains open water on a yearly basis.

In WATFLOOD, each landcover class has unique parameters (i.e., for soil moisture, evaporation, etc.) that control the hydrological response of each class. Consequently model calibration is based on the primary assumption that the landcover represented on Figure 5 is reasonably correct for the year of simulation. This assumption is valid for simulations near the late 1990's and early 2000's, however poses a problem with longer term climate change simulations (50-100 years, for example) in which landcover cannot be expected to remain stationary through time as discussed in Section 2.2. When large scale disturbances, such as forest fires in the Boreal region are prevalent (Section 2.3), further consideration of landcover non-stationarity in the WRB is needed.

3.2 Forest Disturbances

Disturbances such as forest fires are a common phenomenon in the WRB, and are illustrated on Figure 6 for various time periods between jurisdictions spanning 1959 – 2012 (US Department of the Interior, 2013a; Canadian Forest Service, 2010). The figure shows the relative spatial distribution of forest fires in the basin, as well as the range in sizes. It is evident that small forest fires (<200 ha) are the most common, however still containing significant numbers of much larger fires. Fires are also relatively evenly spread throughout the basin, with the exception of the most wetland dominated regions in the southwest (comparing to Figure 5).

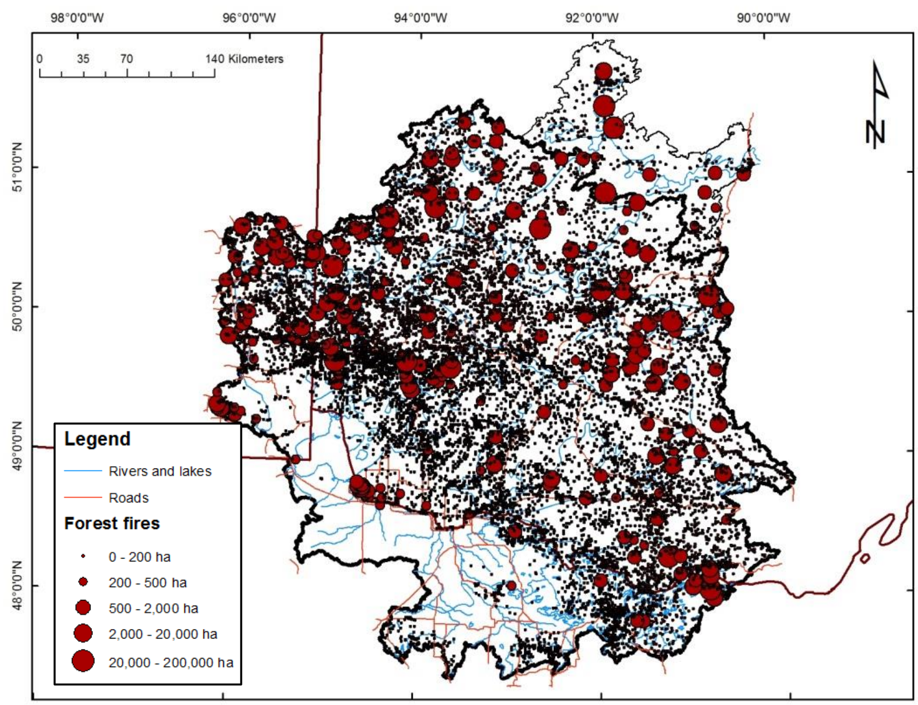

Figure 6 - Forest fires in the Winnipeg River basin, from 1959 – 2009 (Ontario); 1959 – 1999, 2005 – 2008 (Manitoba); 1980 – 2012 (Minnesota, USA). (US Department of the Interior, 2013a; Canadian Forest Service, 2010).

Other types of forest disturbance exist in the WRB, such as insect damage from Fall Cankerworm, Pinkstriped Oakworm, and White Pine Weevil (Scarr, et al., 2011). Diseases can also affect forest such as Spruce Needle Rust, Linospora Leaf Blight, and Anthracnose (Scarr, et al., 2011). These disturbances are considered negligible in this thesis, as the amount of impacted area is much less than that of forest fires. A logging industry also occurs in the basin, and is significant enough to be included in the landcover classification of

Figure 5. Logging is included in the developed landcover simulator module, although it is handled similarly to the natural, gradual changes of other land classes (details explained in section 5.1).

3.3 Geology

The geology of the WRB has been largely determined by glaciation and postglacial deposition, and is dominated by deposited glacial till (Baldwin, et al., 2000; Fulton, 1995). Veneer till (Tv) dominates most of the surficial material east of Lake of the Woods, which is a thin till with numerous rock outcrops (Fulton, 1995). These rock outcrops will form a significant portion of the treed rock land class. More common in the north of the basin is till blanket (Tb) material, which is thicker than Tv. Surrounding many of the lakes such as Lac Seul, as well the major inlet and outlet of Lake of the Woods is fine grained glaciolacustrine (fL) deposits, as a result of settlement from the (then larger) glacial lakes. Also, in most of southeastern Manitoba, and other wetland dominated areas, organic deposits (O) are widespread with layers of peat often in excess of 2 m thick (Fulton, 1995).

3.4 Climate and Climate Change

The WRB's climate can be defined as continental, characterized by large seasonal temperature differences between summer and winter (>36°C at Kenora), with significant amounts of precipitation occurring as snow (St. George, 2007). An east-west gradient in precipitation and overall moisture is evident in the basin, with much wetter conditions towards the east than in Manitoba. This is mostly due to increased summer and fall precipitation in the east (St. George, 2007), and this trend is evident upon examination of the climate normals at various locations in the basin on Figure 7 (Environment Canada, 2013).

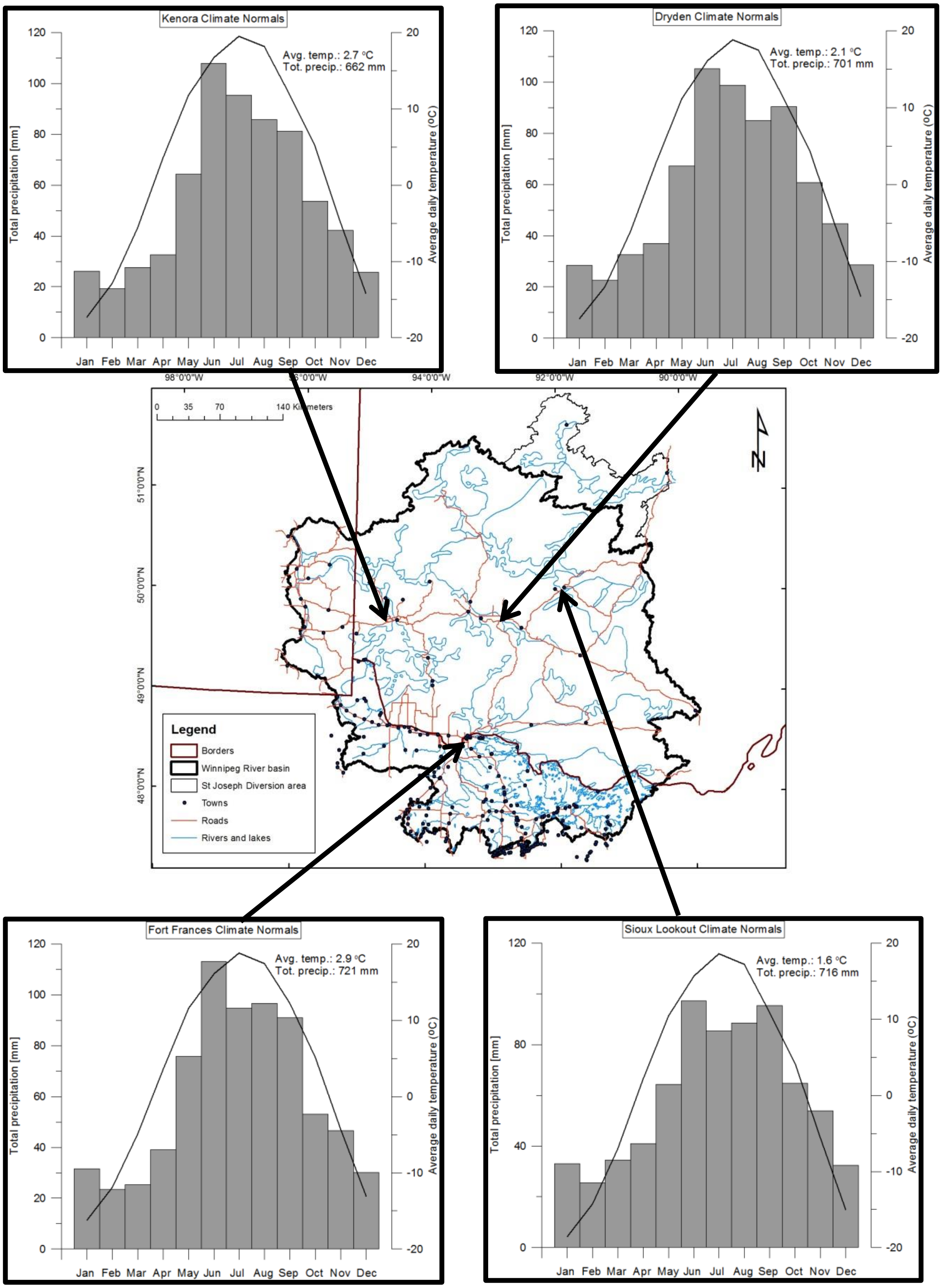

Figure 7 - Climate normals for Kenora, Dryden, Fort Frances, and Sioux Lookout in the WRB (Environment Canada, 2013)

These climate normals describe the overall climate at each location over 1971 – 2000, and are useful to examine in the context of climate change (Environment Canada, 2013).

Meteorological stations in the WRB are shown on Figure 8, with a DEM background. Due to a substantial area of the basin being unpopulated, distances between stations are often great, and stations are not evenly distributed. Considering that not all of these stations have long-term, continuous records, nor are they in operation over the same time intervals, adequately capturing all precipitation events for hydrological modelling is difficult.

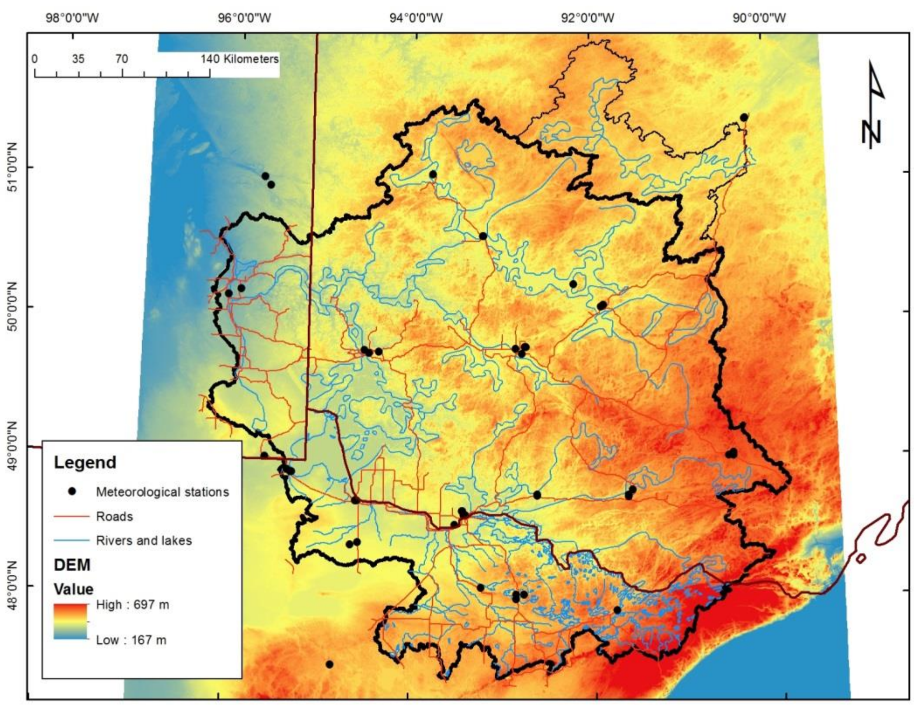

Figure 8 - Meteorological stations (current and discontinued) in the WRB

Improvements to WATFLOOD's inverse distance weighting spatial interpolation of the temperature and precipitation data to include lapse rates using grid elevation have improved temperature and precipitation fields, and are incorporated into this thesis (Manitoba Hydro, 2013). Further improvements to meteorological forcing are currently underway at the University of Manitoba's Water Resources Engineering group, to include the Canadian

Precipitation and Analysis (CaPA) as model forcing in data sparse regions (Evans, in press; Zhao, in press).

The effects of climate change have been documented to have significant impacts on the climate and hydrology of the WRB, including increased precipitation of 20% - 40% occurring at various locations from 1924 – 1998 (St. George, 2007). Alongside increasing temperature, this trend is projected to continue into the future according to CGCM3.1, as depicted on Figure 9. The CGCM3.1 model is used as it is a Canadian model, and has been used in other climate change impact studies with satisfactory results (Bohrn, 2012; Quilbe, et al., 2008). Also the goal of this thesis is to quantify changes in streamflow with landcover changes, to include multiple GCMs for testing of this module would be computationally prohibitive. Figure 9 shows the monthly climate deltas for all scenarios in the 2050s and 2080s over the entire WRB.

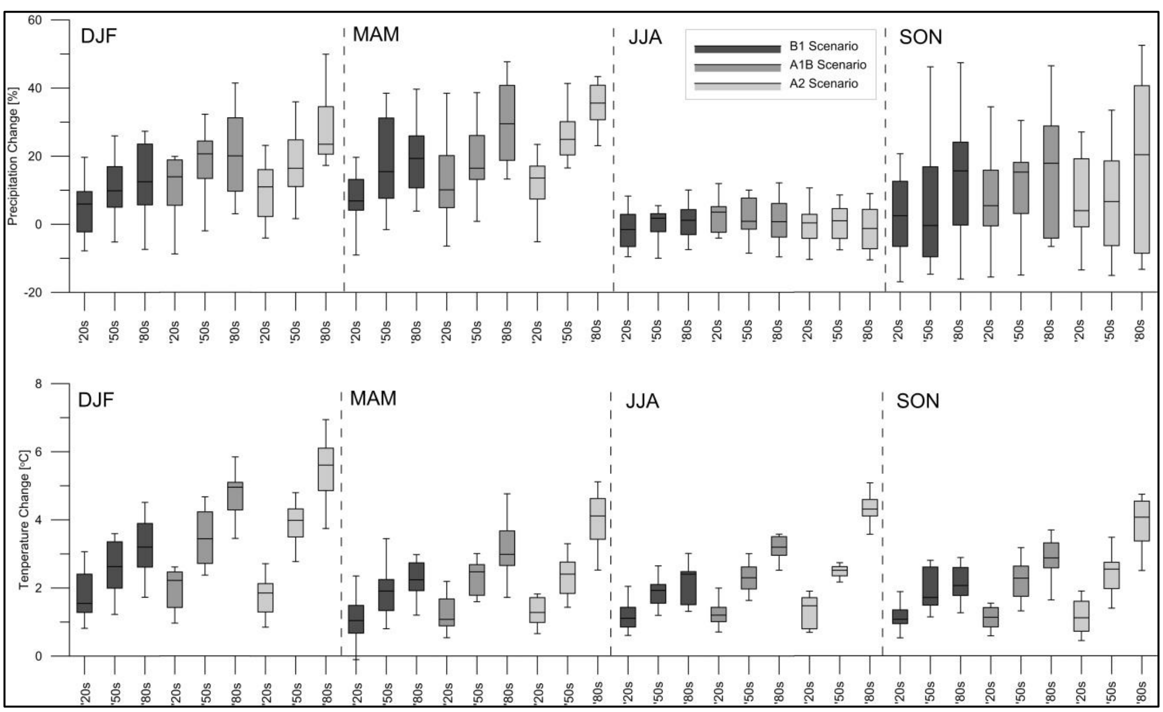

Figure 9 – CGCM3.1 monthly climate deltas for the B1, A1B, and A2 scenarios in the 2050s and 2080s, in the WRB

From the above figure, it is evident that the greatest precipitation increases are projected to occur in the winter (DJF) and spring (MAM) months (~50%), with increasing and decreasing shifts in the summer (JJA) and fall (SON) (lowest ~-15%), depending on the CGCM run. Uncertainty in fall precipitation is the highest and most variable. The least amount of change for both temperature and precipitation occurs in summer, with summer also having the least amount of uncertainty. Temperature is projected to increase in all scenarios and seasons except for two runs in the 2020s (B1), and in the most extreme case up to almost a 7°C increase (2080s A2). The CGCM used in this thesis was found to be within the 95% confidence bounds of similarity with other GCM output in terms of precipitation and temperature.

3.5 Drainage Network and Hydrology

Two major river-systems contribute to the Winnipeg River: The English River to the north and the Rainy River, which drains into Lake of the Woods, to the south. Consisting of over 100 lakes and a combined surface area of over 11,400 km^2, lakes play a major role in the basin's hydrologic regime (Lake of the Woods Control Board, 2002). Hydrometric stations within the basin are showed on Figure 10, with a DEM background. As with the meteorological stations on Figure 8, not all stations have an extensive record or are active today. However coverage of the WRB outlet and major sub-basin outlets is adequate for the study time-period of 1971 – 2000. Average annual flows at the Pine Falls hydrometric gauge (WSC #05PF069), outlet of the WRB, is 988 cms (WSC, 2013). Modelled drainage area is within 1% of measured, with the simulated area upstream of this gauge being 135,240 km^2, (Manitoba Hydro, 2013) and a WSC area of 136,000 km^2 (WSC, 2013).

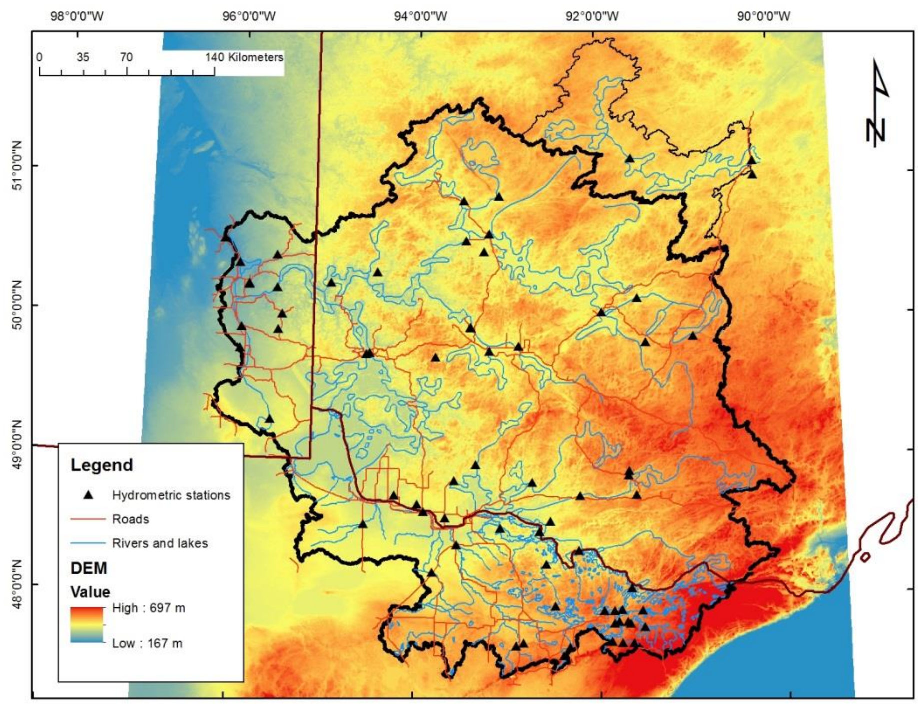

Figure 10 – Hydrometric (current and discontinued) stations in the WRB

The hydrologic regime is highly influenced by regulation of major lakes such as Lac Seul and Lake of the Woods, affecting the timing of peak flows at the outlet (St. George, 2007). At the outlet of the Winnipeg River, peak flows usually occur in June or July, with a rise in flows around the spring freshet in May. Upstream in non-regulated sub-basins, the hydrologic regime is more characteristic of a snowmelt dominated basin with peak flows earlier in mid-May to mid-April. Flows begin to decline in August and generally reach a minimum in October (St. George, 2007).

3.6 Basin Regulation and Hydroelectric Generation

In 1958, a diversion was constructed connecting the Albany and English River basins, on an old portage route for passage to Lake Winnipeg from James Bay (Lake of the Woods Control Board, 2002). The diversion channel (Figure 11) is controlled by the diversion dam (Figure 12) just downstream of the channel, and regulates the addition of flow into the

Winnipeg River basin for use in power generation by Ontario and Manitoba. The diversion increases the drainage area of the Winnipeg River basin by 9%, and on average contributes a flow of 80 cms (Lake of the Woods Control Board, 2002). Since flows through diversions are controlled, WATFLOOD forces them to observed flows. This is a model limitation, as future regulation of this diversion will potentially change with the climate.

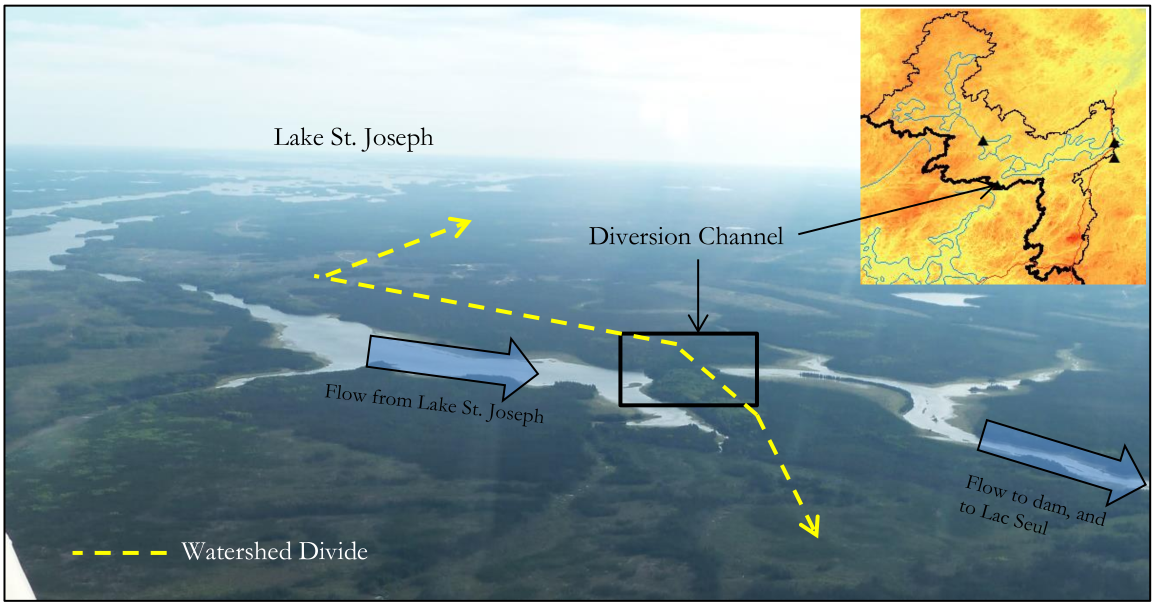

Figure 11 - Aerial photo of the Lake St. Joseph Diversion Channel (photo by author)

Figure 12 - Aerial photo of the Lake St. Joseph Diversion Dam (photo by author)

Other major sources of regulation occur at Ear Falls, outlet of Lac Seul, as well as Lake of the Woods. Outflows at these locations are managed by the Lake of the Woods Control Board (LWCB) to balance the needs of landowners, recreation, and hydroelectric generation (Lake of the Woods Control Board, 2002). While these regulatory actions have significant impacts on downstream hydrographs, for this thesis simulations are run in a "natural" state as if regulation was not occurring (other than the St. Joseph Diversion). This is preferable since with climate change, it's the trends in future streamflow that are of concern. Regulatory actions by the LWCB will change accordingly to climate induced hydrologic regime shifts to balance the needs of affected waterway users.

While only a small portion of the basin resides in Manitoba, Manitoba Hydro owns and operates six generating stations along the downstream section of the Winnipeg River. The Winnipeg River generating stations are shown on Figure 13.

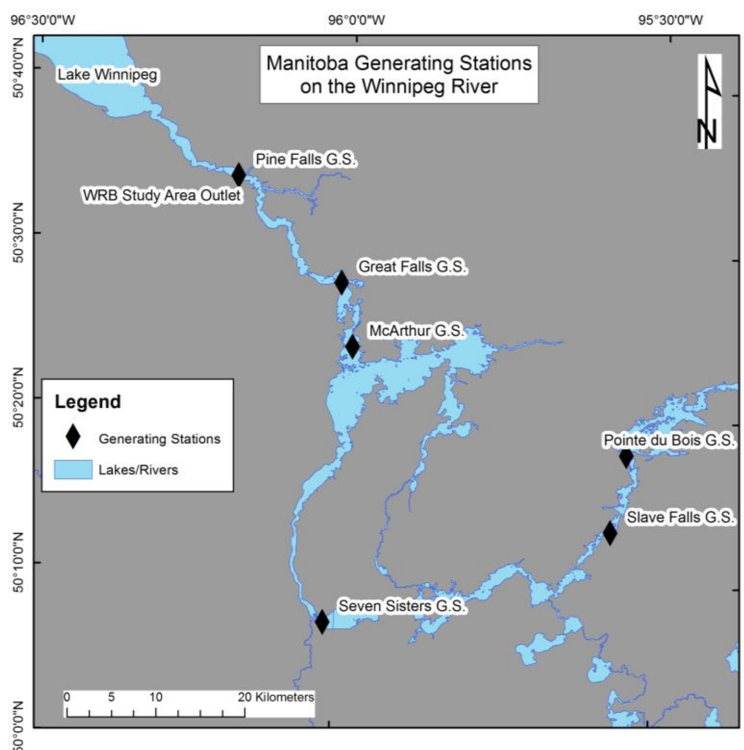

Figure 13 - Generating stations in Manitoba on the Winnipeg River

Generating stations and their capacities in the WRB are included in Table 1, from H2O Power Limited Partnership, Manitoba Hydro, and Ontario Power Generation.

Table 1 - Generating stations in the WRB (H2O Power Limited Partnership, 2013; Manitoba Hydro, 2012; Ontario Power Generation , 2011)

Generating Station	Net Capability (MW)
Great Falls	129
Seven Sisters	165
Pine Falls	88
McArthur	55
Pointe du Bois	75
Slave Falls	67
Whitedog Falls	68
Caribou Falls	91
Manitou Falls	73
Ear Falls	17
Lac Seul	12
Kenora	6
Norman	10
Fort Frances	10
Sturgeon Falls	7
Calm Lake	9

Most of Manitoba Hydro's generation capabilities lie in the Nelson River, north of Lake Winnipeg, and are shown in Table 2. These stations are the ultimate destination of flows from the Winnipeg River, which is part of the greater Nelson River basin. The Winnipeg River contributes ~39% of Manitoba Hydro's generation capacity (Manitoba Hydro, 2013). Climate change may have an impact on this streamflow.

Table 2 - Manitoba Hydro's generating stations on the lower Nelson River that receive contributions from the Winnipeg River (Manitoba Hydro, 2012)

Generating Station	Net Capability (MW)
Kelsey	250
Kettle	1220
Jenpeg	129
Long Spruce	1010
Limestone	1340

3.7 Historical WATFLOOD Simulation in the WRB

WATFLOOD setup of the WRB was provided by Manitoba Hydro, and is current as of January 2013 (Manitoba Hydro, 2013). Calibration on the Winnipeg River basin by Manitoba Hydro is currently ongoing, with developmental support from WATFLOOD's developer (Manitoba Hydro, 2013). Manitoba Hydro's collaboration with the University of Manitoba also contributes to the capability of WATFLOOD to model the WRB. This includes a recent investigation of lake evaporation methodologies to enhance WATFLOOD's ability in simulating the basin's abundant lake hydrology, with its incorporation into WATFLOOD ongoing (Slota, 2013).

For the 1971 – 2000 baseline period with the January 2013 WATFLOOD setup (natural flow conditions), Nash-Sutcliff (N_r) and Deviation of Runoff Volume (D_v) values of 0.50 and -5.52% at the Pine Falls outlet are obtained, with considerable variability amongst sub-basins. This time period is not used for calibration by Manitoba Hydro. Average annual hydrographs for observed and simulated streamflows are shown on Figure 14. An N_r of 1.0 is the best result, with 0.0 being that the model is no better than the mean in representing streamflow. Negative values indicate the model is worse than the mean. For D_v, a value of 0% indicates a perfect simulated match in volume, with positive or negative values indicating over or under-prediction respectively.

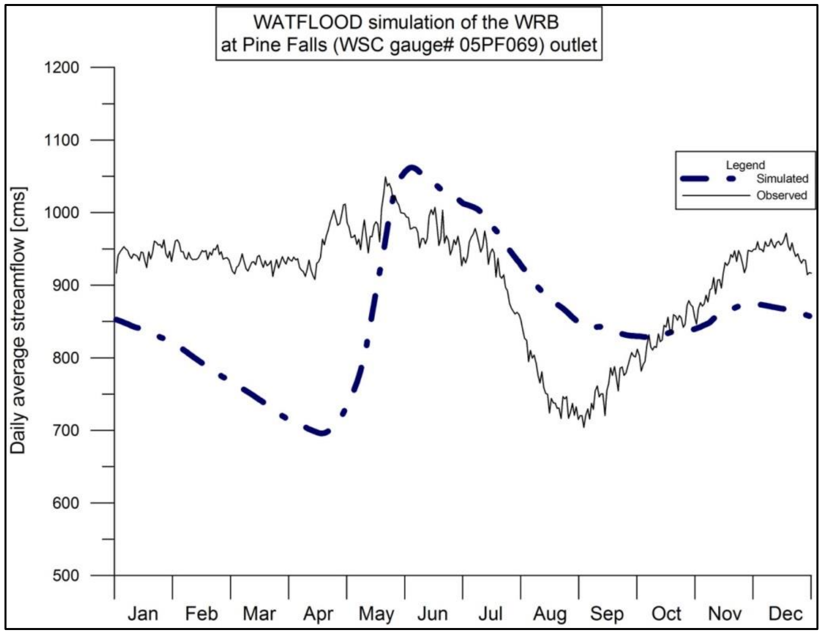

Figure 14 - WATFLOOD simulation of the WRB at the Pine Falls (WSC# 05PF069) outlet, for 1971 – 2000

Overall WATFLOOD tends to underestimate flows, particularly in the winter months. The spring peak is modelled consistently with observed flows, peaking in June or July with a rise beginning in May. As alluded to in the previous section, regulatory actions in the WRB prevent simulation of high skill scores involving timing (N_r) under natural flow conditions, particularly at regulated gauge locations such as Pine Falls (05PF069). Overall volume is well simulated, and the average D_v of -5.52% is considered reasonable. In the context of climate change, changes in runoff volume are very important for this thesis. With climate change simulations run with natural flows in this thesis, projected relative changes in volume and timing can still be deduced despite regulation.

In this chapter, the WRB was described in detail as the thesis study area, in which to derive, test and simulate non-stationary landcover and hydrologic climate change conditions. Most of this basin resides in the Boreal forest of the Canadian Shield, and is susceptible to regular disturbance by forest fires. With the hydrology of this basin contributing significantly to hydroelectric generation, it is important to understand the impacts of changing landcover on water supply. Evaluating the impacts of climate change on the hydrologic regime in tandem with evolving landcover is also important for future power planning. In the next chapter, two sub-basins of the WRB are selected for a historical landcover change analysis. Changes in landcover until present day are investigated, with its impact on sub-basin streamflow. This analysis then becomes the basis for methodologies in subsequent chapters in applying non-stationary landcover over the entire WRB.

Chapter 4 Sub-basin Historical Landcover Change Analysis

To document the change in landcover in the WRB from forest fires and natural, gradual changes, a historical landcover change analysis will be presented in this chapter on two sub-basins. Historical LandSAT satellite imagery is used for this analysis (US Department of the Interior, 2013c), and are classified into several distinct land classes. These classified images are directly incorporated into WATFLOOD to demonstrate the hydrologic effects of non-stationary landcover at the sub-basin scale, and are used as the basis for the forest fire regeneration and natural, gradual change components of the landcover simulator module in Chapter 5.

4.1 Sub-Basin Selection

Two sub-basins were chosen for a historical landcover change analysis (assumed to be representative of overall conditions in the WRB): one with a significant amount of forest fires, and one without. Basin 32 was selected to represent significant fire impact, and is located on the east end of the WRB as shown on Figure 15 on the Sturgeon River at McDougall Mills (WSC# 05QA004). The sub-basin selected as having very little forest fire activity was Basin 36, and is located on the north end of the WRB on Trout Lake River (WSC# 05QC003). Basins 32 and 36 have modelled drainage areas of 4453 km^2, and 2417 km^2 respectively. WSC listed drainage areas are 4450 km^2 and 2370 km^2 for Basins 32 and 36 respectively and are in relative agreement (WSC, 2013). Average annual flows for Basins 32 and 36 are 39.2 cms and 17.6 cms respectively (WSC, 2013).

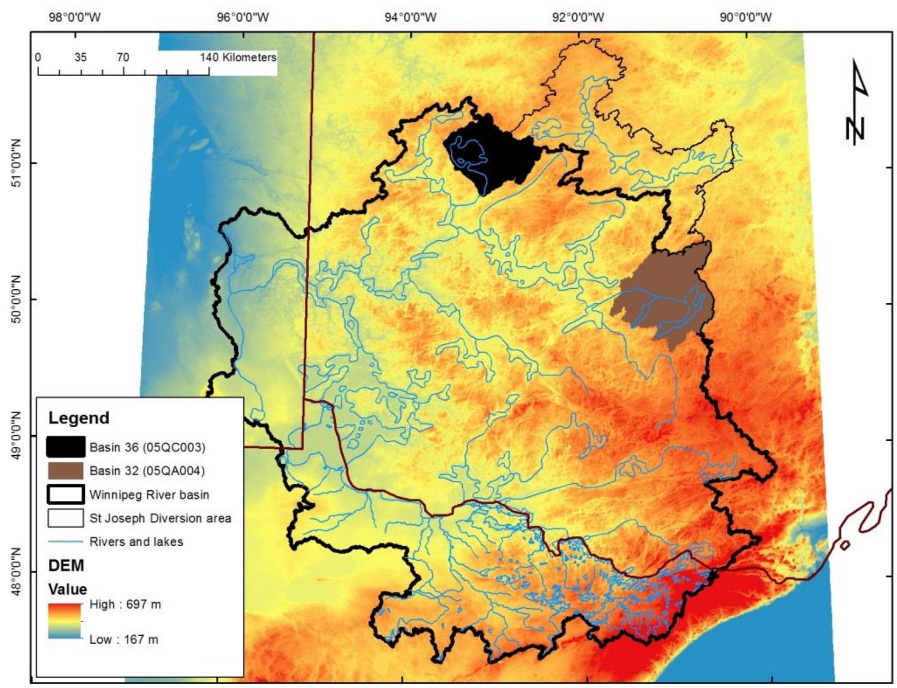

Figure 15 - Sub-basins chosen for historical landcover change analysis

4.2 Landcover Classification

4.2.1 Satellite Imagery

The main criteria for satellite image selection for the purposes of classification are: clarity of the image from clouds and weather, captured in the same month to reduce variations from changes in seasonality, and image is temporally far enough apart from other images to adequately detect change. Balancing these requirements, satellite images were gathered for Basin 32 in late-summer of 1984, 1991, 2003, and 2010. These sub-basins are spatially far enough apart that the satellites do not capture them in one rotation around the earth.

Therefore adverse weather conditions can develop in the intervening period that prevents high quality images at the same times between sub-basins being used. For Basin 36, images were gathered for 1985, 1994, 2003, and 2009. Images are provided as multi-band, geo-referenced TIFF format, one file for every band. Images from the LandSAT 5 and LandSAT 7 satellites are used, using the Thematic Mapper (TM), and Enhanced Thematic Mapper (ETM+) sensors respectively (US Department of the Interior, 2013b). The same bands are used from each satellite, cover approximately the same wavelengths, and have a resolution of 30 m (US Department of the Interior, 2013b). For landcover classification, bands 3, 4, 5, and 7 provide the best ranges of wavelengths for distinguishing between classes (Vogelmann, et al., 1998), and are used for this thesis (Table 3). An example of the spectral bands used in the landcover classification can be seen on Figure 16, for Basin 32.

Table 3 - LandSAT 5 (Thematic Mapper) and LandSAT 7 (Enhanced Thematic Mapper) spectral band information, from (Sanchez & Canton, 1999)

Band	Wavelength (μm)	Spectral Location
1	0.45-0.52	Blue
2	0.52-0.60	Green
3	0.63-0.69	Red
4	0.76-0.90	Near infrared
5	1.55-1.75	Mid infrared
7	2.08-2.35	Mid infrared
6	10.4-12.5	Thermal infrared

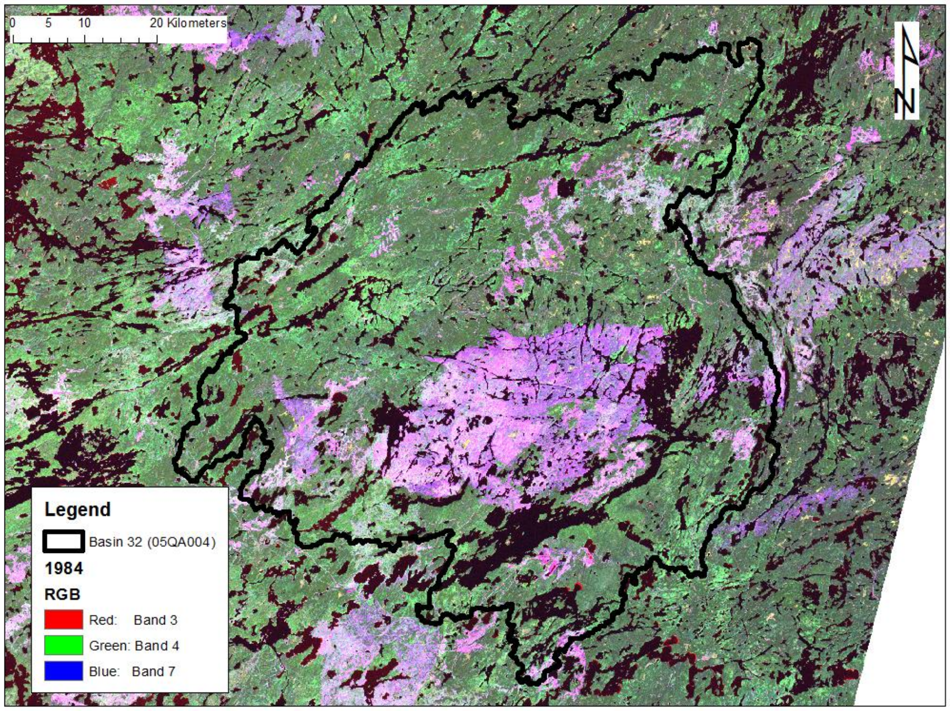

Figure 16 - Example of RGB composite image for bands 3, 4, and 7: Basin 32 in 1984 (band 5 not shown)

Note that while bands 3, 4, 5, and 7 are used in the classification, band 5 is not shown on Figure 16 as visualization is only possible in three dimensions. With these band combinations, it is possible to distinguish between land classes, particularly disturbances such as forest fires and recent logging, which show up in pink. Note the large pink area in the middle of the basin, which is the location of a large forest fire that occurred in 1980 with effects still quite visible in the 1984 image.

4.2.2 Classification Methodology

Using the composite images (bands 3, 4, 5 and 7), each of the two sub-basins were classified with ArcGIS 10.0, using a semi-automated approach utilizing the Classification Toolbar, the Spatial Analyst Toolbox, and Python. A flowchart of the methodology is shown on Figure 17, and is explained in the following sub-sections.

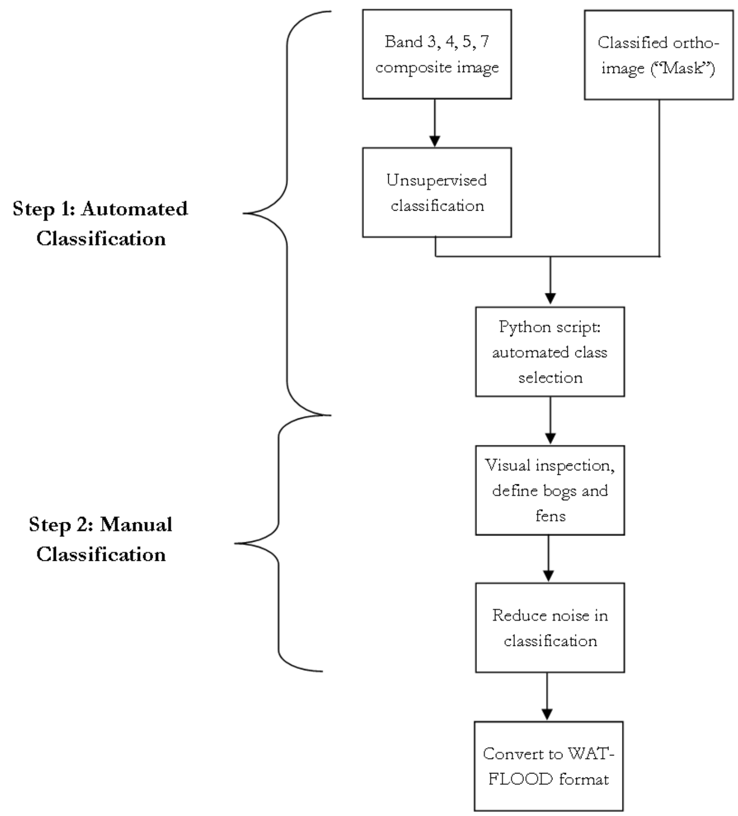

Figure 17 - Flowchart of landcover the classification methodology

Step 1: Automatic Classification

The automatic portion of the classification process is based on studies by Verhegghen et al., (2010), and Duveiller, et al., (2008). Firstly, each of the LandSAT images is classified into 25 clusters via maximum liklihood unsupervised classification. These clusters are not labelled as actual landcovers, but are divided into 25 distint clusters based on the brightness values of the spectral bands in each image. Therefore, similar combinatations of brightness values amongst the four bands spatially throughout the domain are grouped into the same cluster, and consequently the same land class. To assist in defining each of these clusters to an actual landcover, a Python script was programmed to automate this process and create a 'first guess' before more in-depth analysis is performed (Vogt, 2012). In this method, a pre-classified "mask" landcover image is used as a reference for classifying the images of interest, in this case, the ortho-classified image from the stationary landcover WATFLOOD simulations is used (i.e the image on Figure 5). The output of the script is a table that states the percentage of pixels in each cluster that lie in each landcover class of the mask. For example, one cluster from the unsupervised classification when overlayed by the mask image can be covered by 60% mixed forest, 10% coniferous forest, and 10% other classes. In this case, the cluster would be classified as mixed forest for the first step in the process. The assumption is that dense areas of landcover will remain similar over time despite natural changes, and that the method should capture this continuity with the mask classification, but will still show minor shifts over time while allowing for manual inspection (Verhegghen, et al., 2010; Duveiller, et al., 2008). This method contrasts with the manual approach using a supervised classification, which involves defining training samples of the image of known landcovers, typically from field surveys. The supervised approach works well for a single image in the present day, however would require the collection of training samples for every image, which is time conuming and not possible without aerial photographs at the times of analyses (Verhegghen, et al., 2010; Duveiller, et al., 2008). Despite the advantages of the unsupervised-automated approach used in this thesis, it is not completely accurate. Main sources of error are that disturbances such as forest fires and logging cannot be predicted from the mask image, as well as the further temporally the image is from the mask, deviations due to natural, gradual change will increase. This method does, however, provides a useful starting point for the manual classification, and in making decisions less subjective with the percentage output from the Python script.

Step 2: Manual Classification

The manual classification process is more subjective, and involves the use of the Python output from the automatic classification, as well as visual inspection of the composite images themselves, surficial soil maps, and aerial photography from a field excursion in early September 2012. Distinguishing forest fires from other classes is a straightforward process due to high reflectance values as illustrated on Figure 16, and an inconclusive result from the automatic classification (i.e., percentages in Python output equally spread amongst landcovers). Logging can also be distinguished from forest fires due to its regular spatial patterns and visual detection of logging roads, as evident on Figure 18.

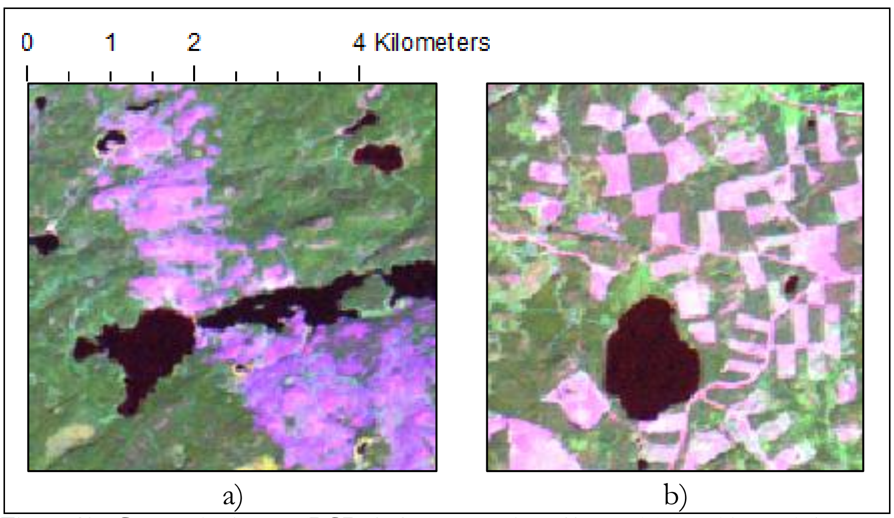

Figure 18 - Composite image (RGB: 3, 4, 7) examples of burned (a) and logged (b) areas

Wetlands also posed a challenge as detectability is significantly affected by amount of moisture (i.e., water level) in the wetland. An area might be readily detected as wetland in a wet year, however, may look more like a forest or shrubs in a dry year. Therefore emphasis for wetland classification was placed on the aerial photography specifically taken over areas of questionable wetland content from looking at the satellite and ortho-imagery. The aerial photography was captured in early September 2012, a slightly wetter than average year with annual precipitation greater than the 1971 – 2000 climate normal (716 mm and 662 mm respectively at Kenora Airport). The ortho-imagery is useful since it is captured over a larger time period, and has lower errors in wetland classification based on yearly variability. Also the difference between bogs (non-connected) and fens (connected) is mostly determined by relative location between wetlands and streams (i.e., water bodies), as well as the overall geography of the area and is not as easily classified from satellite images. So after the classification process in which only a single wetland class is identified, it is then split into bogs and fens based on distance to water features (i.e., lakes and streams). Through a process of trial and error, an 800 m buffer on either side of streams and lakes was determined to adequately separate bogs and fens based on visual inspection and the aerial photography. It is also important to note that the exact location of boundaries between landcovers is not the most important goal of this analysis, but rather determining the correct proportions of different landcover, on average, throughout the basins. WATFLOOD only uses the landcover after conversion to GRUs, so capturing the overall percentage of bogs and fens is the priority, not necessarily capturing the exact boundary and location of each bog and fen. The results of the classifications are shown on Figure 19 and Figure 20 for Basins 32 and 36 respectively.

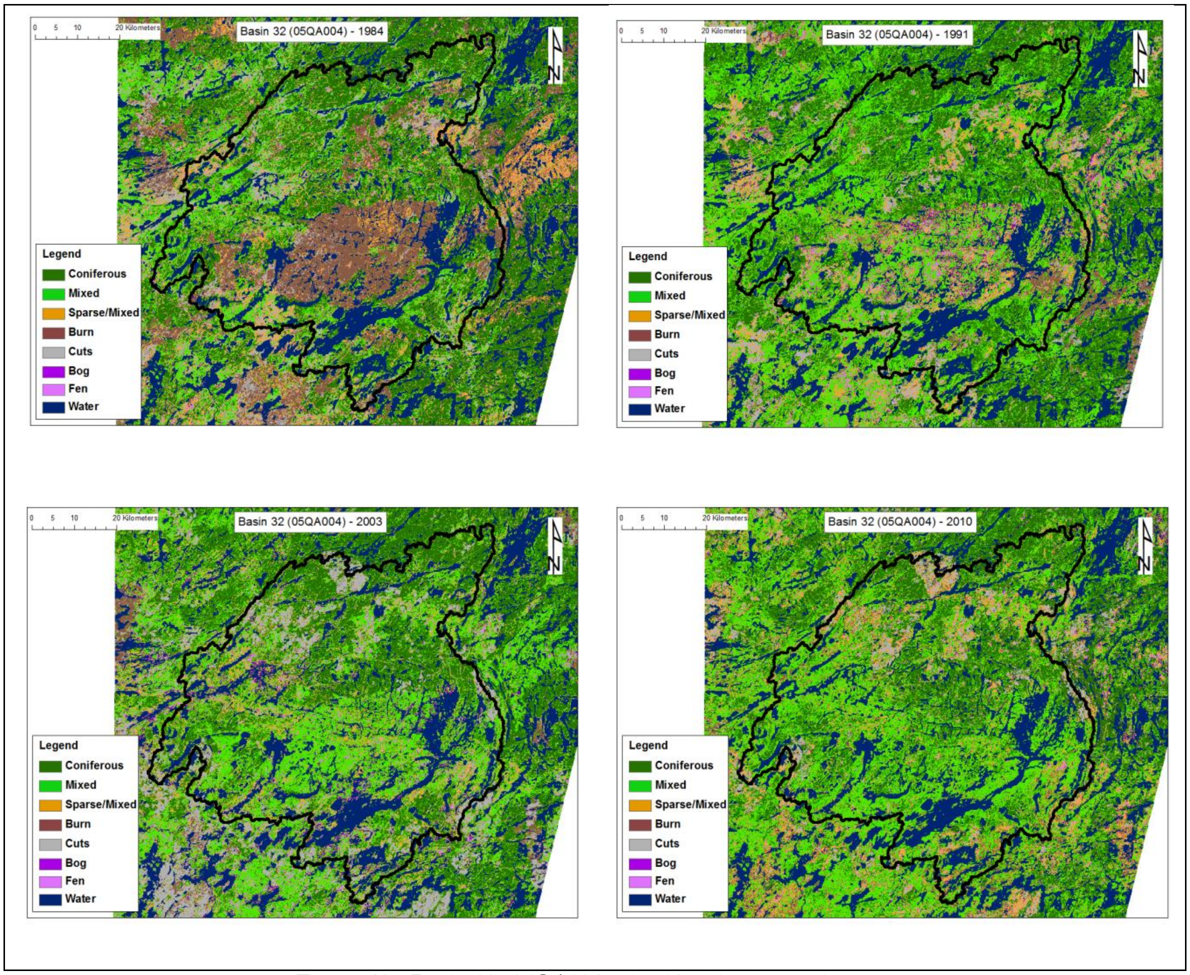

Figure 19 - Basin 32 (05QA004) classified landcover images

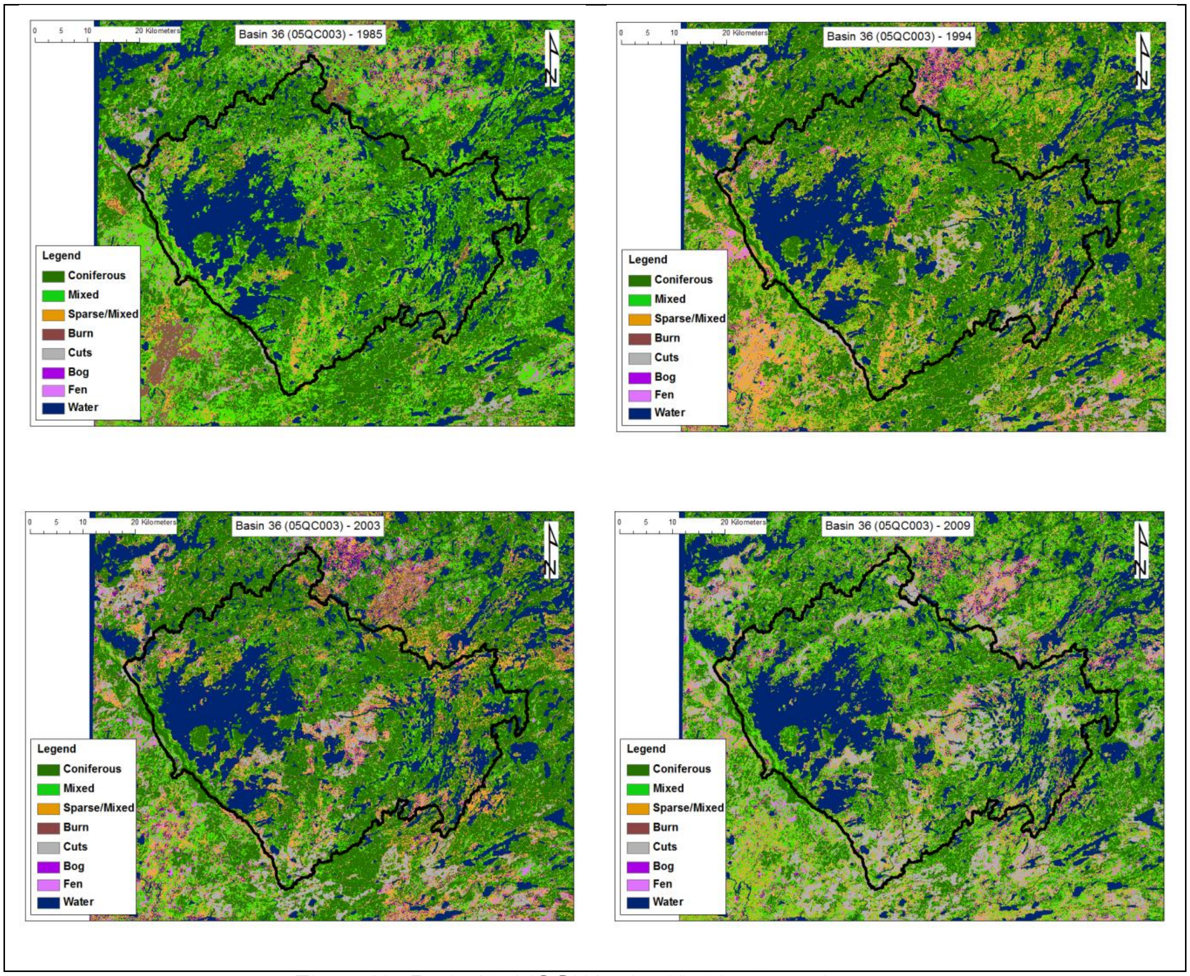

Figure 20 - Basin 36 (05QC003) classified landcover images

The classified images above have been smoothed to reduce noise, using the Majority Filter and Boundary Clean tools in ArcGIS. These tools are effective at removing small, isolated groups of pixels that either are errant classifications or are insignificant relative to the surrounding landcover, and are standard in landcover classification analyses (Lillesand & Kiefer, 1994).

As evident from Figure 19 and Figure 20, coniferous and mixed forest dominate the landscape in these sub-basins, with logging occurring in both basins, and forest fires more prevalent in Basin 32. The sparse/mixed class is described as mixed forest, however significantly less dense than the regular mixed forest, and can contain areas of exposed rock. Based on observations in this analysis, this class often acts as a transitional landcover after disturbances such as forest fires or logging and persists for several years until replaced by other types of forest. This is consistent with a study in the Experimental Lakes Area (ELA), residing in the WRB (Schindler, 1998). Forest fires in 1974 and 1980 in a small catchment caused >80 year old coniferous species to be mostly replaced by deciduous species. Throughout the regeneration period exposed bedrock was common in the affected area, previously covered by organic matter, with some persisting even 17 years later (Schindler, 1998).

4.3 Incorporation of Classified Landcover Images into WATFLOOD

The landcover images on Figure 19 and Figure 20 were converted to WATFLOOD format (.shd) using BSN.exe to enable simulation of non-stationary landcover on the hydrology of the sub-basins. The grid size was kept constant, and no recalibration was conducted. For each sub-basin, WATFLOOD simulations were run from 1980 – 2010 to cover the temporal domain of the images, and the non-stationary simulations were run such that the landcover file (.shd) was updated throughout the simulation. This time period differs from the climate change simulations baseline period (1971 – 2000) for the sole reason of satellite image availability. With LandSAT images available in a consistent format from the early 80's to present day, simulations from 1980 – 2010 are appropriate for analysis at the sub-basin scale in this chapter. The hydrographs are shown on Figure 21 and Figure 22 for Basin 32 and 36 respectively, with the vertical green bars indicating a historical change in landcover. The stationary run (in red), used the classified ortho-image, and derived from landcover mostly between 1999 and 2002. From 1980 to 1991 in Basin 32, there are overall increases in flow as compared to stationary landcover, including peak flow, as shown on Figure 21. This is a direct result of the significant amount of burned area in Basin 32, as evident on Figure 19 for the 1984 image. From 1991 onwards the difference between the runs is less significant, owing to the fact that the classified landcovers in the non-stationary runs are derived from a similar time period to the stationary runs. For Basin 36 on Figure 22, the differences between stationary and non-stationary runs are not as significant as in Basin 32, which is expected as this basin was specifically selected as being relatively unaffected by forest fires.

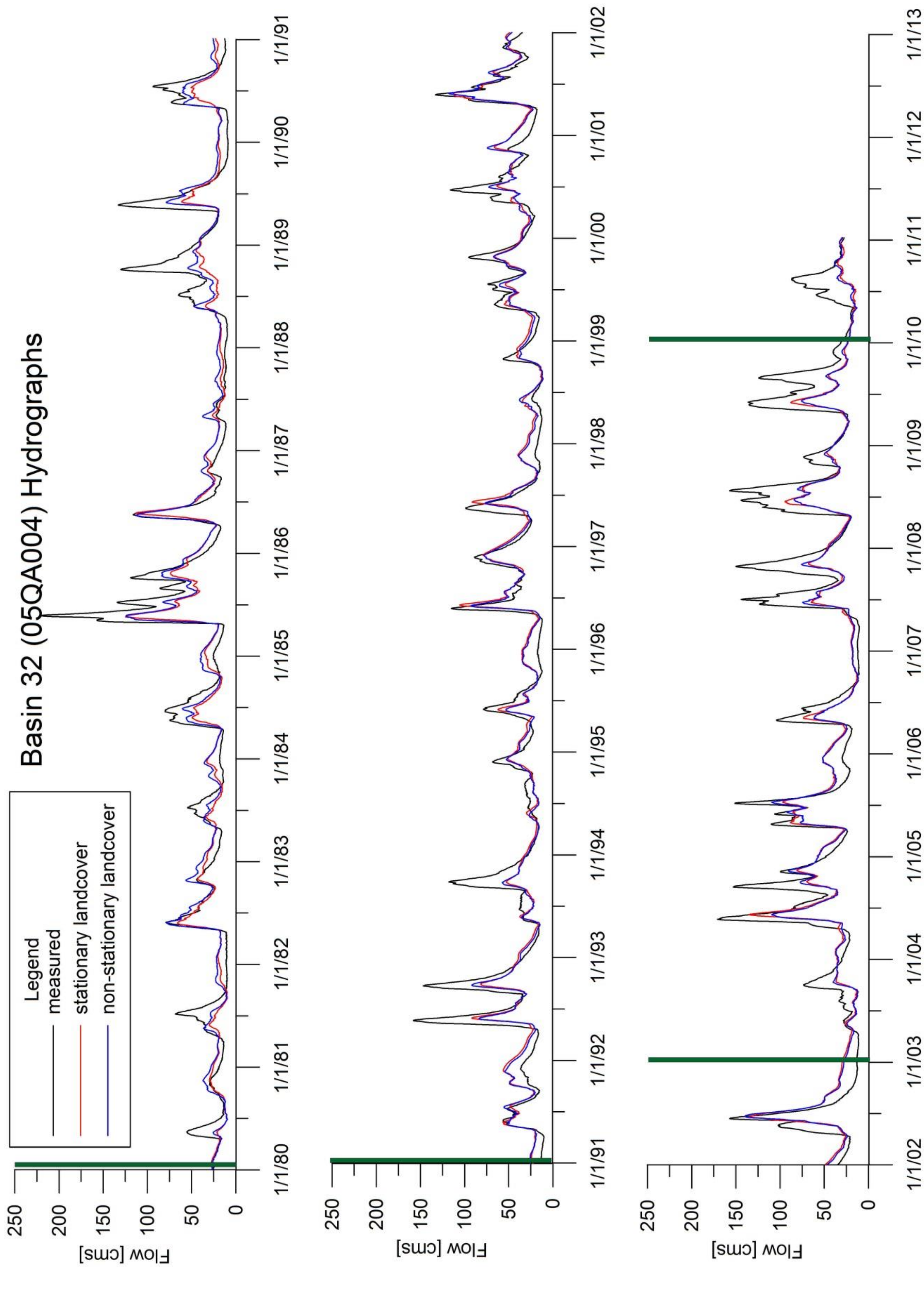

Figure 21 – Basin 32 (05QA004) hydrographs, green bars designate times a new landcover image is introduced to the simulation for the non-stationary (blue) run.

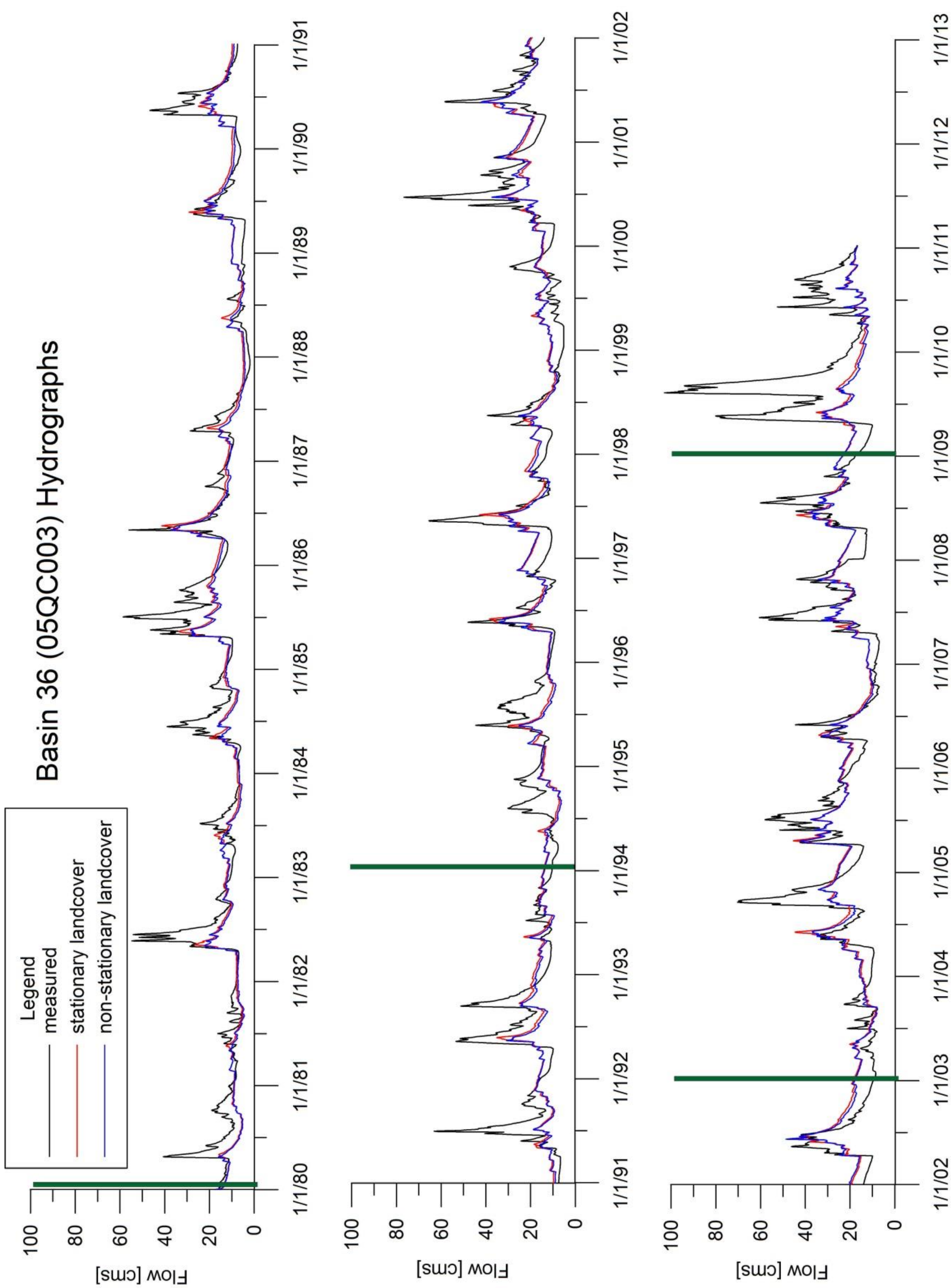

Figure 22 – Basin 36 (05QC003) hydrographs, green bars designate times a new landcover image is introduced to the simulation for the non-stationary (blue) run.

Examining the statistics for these runs in Table 4 and Table 5 for Basins 32 and 36 respectively, visual observations can be confirmed. Statistics are not calculated for 1980 to account for model-spin up. The tables are divided into 3 sections, 1981 – 1998, 1999 – 2002, and 2003 – 2010. The middle time frame was selected to coincide with the years that the ortho-imagery was classified (1999 – 2002 and used in the stationary simulation). Since imagery from 1991 (Basin 32), and 1994 (Basin 36) are used for the non-stationary simulations and are relatively close temporally to the ortho-image, the middle time frame's landcover can be considered the most similar for both non-stationary and stationary landcover simulations. Statistics over the entire time-period (1981 – 2010) are also included in the tables.

Table 4 - Statistical output for Basin 32 (05QA004) WATFLOOD simulations (1981 – 2010)

	Non-Stationary		**Stationary**	
	N_r	**D_v (%)**	**N_r**	**D_v (%)**
1981-1998	0.69	-1.24	0.58	-12.86
1999-2002	0.63	-1.48	0.59	0.56
2003-2010	0.47	-24.05	0.45	-22.73
All Years	0.61	-8.93	0.56	-11.08

Table 5 - Statistical output for Basin 36 (05QC003) WATFLOOD simulations (1981 – 2010)

	Non-Stationary		**Stationary**	
	N_r	**D_v (%)**	**N_r**	**D_v (%)**
1981-1998	0.48	-13.64	0.52	-8.1
1999-2002	0.43	-1.41	0.43	-0.35
2003-2010	0.27	-13.79	0.28	-12.63
All Years	0.43	-10.65	0.45	-8.04

Basin 32 shows improvement in the Nash-Sutcliff coefficient (N_r) and deviation in runoff volume (D_v), with the greatest improvements occurring during the 1981 – 1998 time period.

An increase in N_r from 0.58 to 0.69 is quite significant, and highlights the need to use accurate landcover inputs for the simulation time period especially if major disturbances (i.e., like forest fires) have occurred on the landscape. For the 1999 – 2002 time period, only a modest improvement in N_r occurs and a minor (net 1%) improvement in D_v, which is expected due to the similar landcover types in that period, and with the forest fire in the 1984 image mostly regenerated. The last time period from 2003 – 2010 yields the poorest results for both non-stationary and stationary landcover, with flows being underestimated and D_v values as low as -24.05%.

Basin 36 similarly shows poor results for the latter time period. The differences for this basin however, between stationary and non-stationary landcovers are less pronounced due to this basin's lack of drastic landcover change (in contrast to Basin 32), with near insignificant (net 1% change in D_v) change during the 1999 - 2002 period. One caveat to this however, is that the parameters for these simulations were calibrated using the stationary landcover, and results could improve if the model were calibrated using non-stationary landcover which is more representative of actual conditions. The fact that improvements in statistics are seen in Basin 32 inspires confidence in the calibration and that the parameters are adequately and physically representing the basin. However the implications of choosing to calibrate any model to one landcover input should not be discounted.

Proportionality plots of these simulations for Basin 32 are presented in the following figures, separated by time period (between landcover images on Figure 21) and with linear and log scales for Figure 23 and Figure 24, respectively. Similar plots for Basin 36 are on Figure 59 and Figure 60 in Appendix 1. Consistent with the D_v statistics in Table 4 and Table 5, flows are underestimated for both basins, particularly flows over 150 cms which are not simulated by the model for Basin 32 despite having observed flows of > 200 cms. These trends appear in both non-stationary and stationary simulations, and could be a result of missing precipitation events.

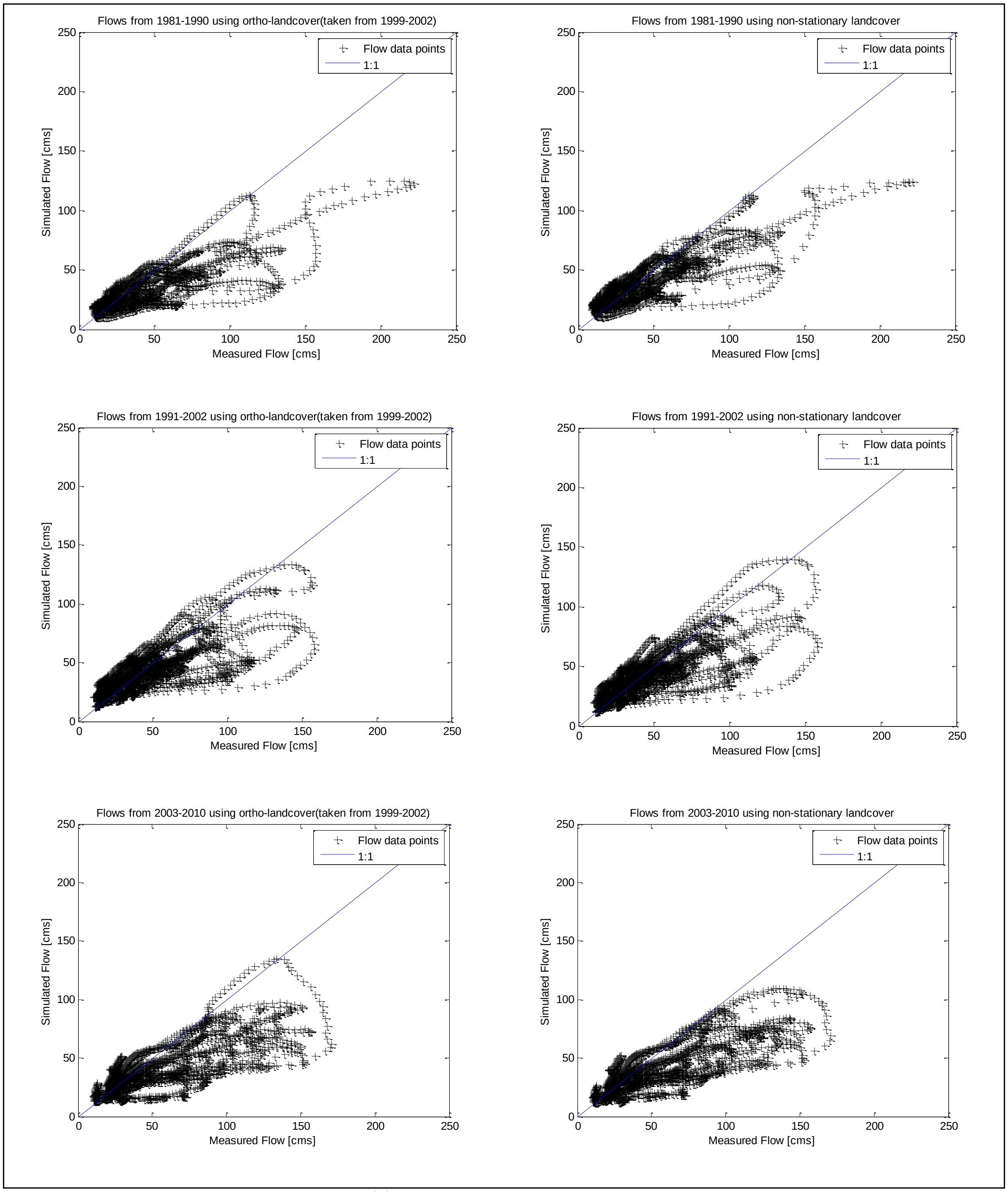

Figure 23 - Proportionality plots for WATFLOOD simulations on Basin 32 (05QA004) for stationary landcover (left column), and non-stationary landcover (right column)

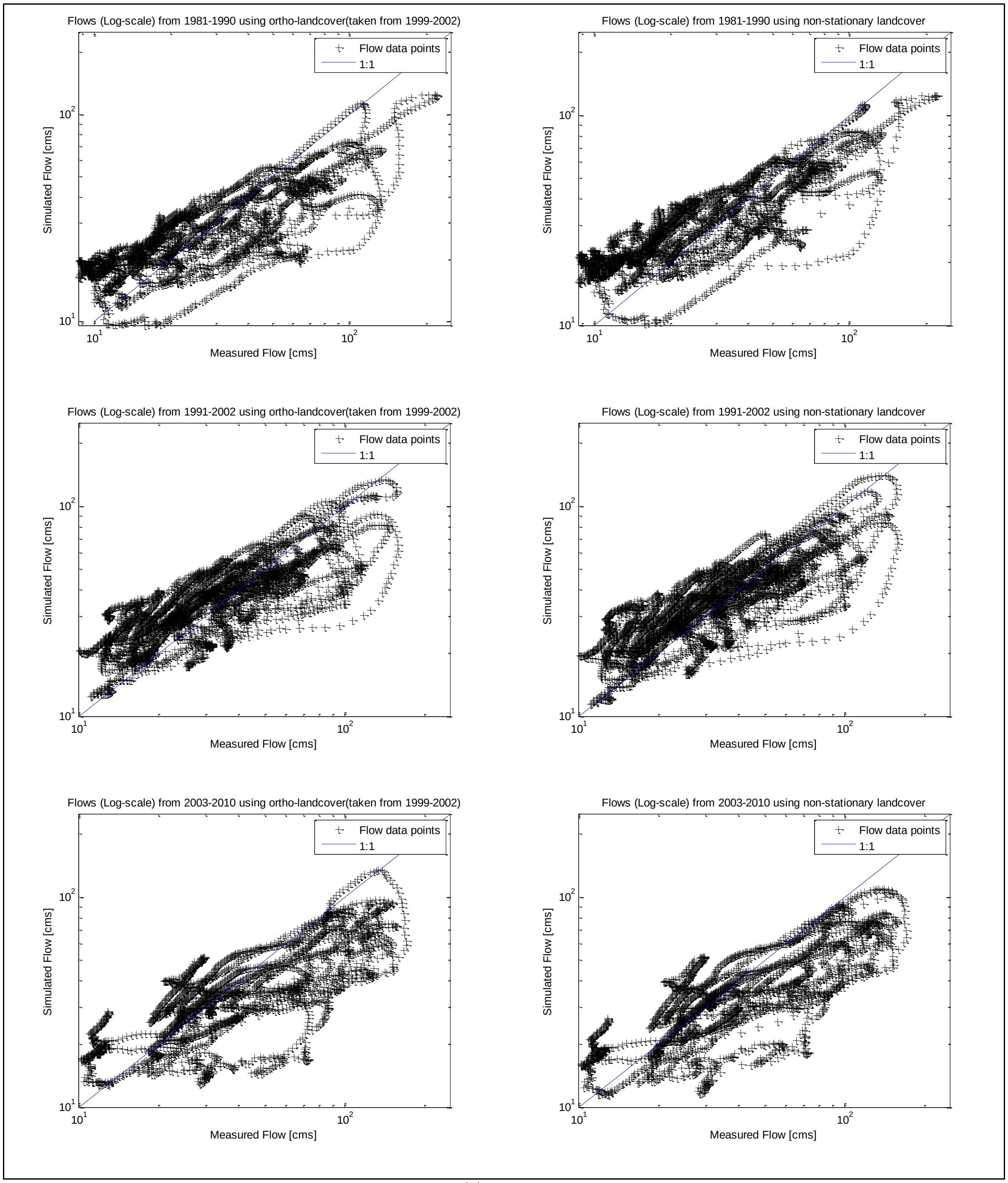

Figure 24 - Proportionality plots (log-scale) for WATFLOOD simulations on Basin 32 (05QA004) for stationary landcover (left column), and non-stationary landcover (right column)

Higher flows tend to be more drastically underestimated than lower flows since log scale proportionality plots show a better alignment between observed and measured flows for Figure 24 and Figure 60 for Basin 32 and 36 respectively. Errors in timing are also evident in both simulations for Basin 32, with significant tracking as opposed to more random scatter. Tracking tends to occur when timing of the hydrograph is in error, resulting in time-series discrepancies between observed and simulated flows particularly near the peaks. Even though volume of flow may be correct, errors in timing will result in a series of points partly above and below the 1:1 line in a non-random fashion. If tracking occurs when most points are above or below the 1:1 line, the simulation would have errors in over- and under-estimation respectively, as well as timing. In a few instances Basin 32 experiences tracking, in addition to underestimation. These observed high flows occur during the spring freshet. From the hydrographs on Figure 21, it is clear that the model often underestimates the spring freshet. Non-stationary landcover is an improvement over stationary landcover in this regard. Errors in timing are less of a factor for Basin 36, which displays more random scatter in all but the highest flows. These errors could be due to missing precipitation events, either summer or winter that results in errors from missed summer peak flows and snowmelt-driven runoff events.

Upon examining the log scale plots for Basin 32 during the time period of 1981 – 1990 on Figure 24, non-stationary simulated flows are more oriented towards the 1:1 line, indicating superior overall performance over the stationary simulation. These improvements in low flow, as emphasized by the log scale, are reflective of the improvements in N_r and D_v in Table 4. Higher flows for the same time period (Figure 23) do not show the same improvement and therefore low flows are a significant contribution to improvement of results.

With significant differences between stationary and non-stationary landcover being found on the sub-basin scale, it is clear that there will exist some uncertainty deriving from the selection of landcover images for the simulations. Selection of landcover images, as mentioned previously depends on image quality (mostly due to weather), as well as the ability to capture ~10 year intervals. When the images were captured and the frequency of the image replacement will influence the overall uncertainty. A visualization of the level of such uncertainty that can exist is shown on Figure 25 for Basin 32, with the annual average hydrograph for stationary (red), non-stationary (blue), and measured (black) flows. This figure shows that the averages of the entire simulation are very similar for non-stationary and stationary landcovers, however knowing the discrepancy in different time periods from Table 4, there is evidently some averaging of error. When each of the classified landcovers from Figure 19 are run through the simulation separately (i.e. stationary landcover, but for four different landcover images), the maximum and minimum daily average flows form the grey uncertainty envelope.

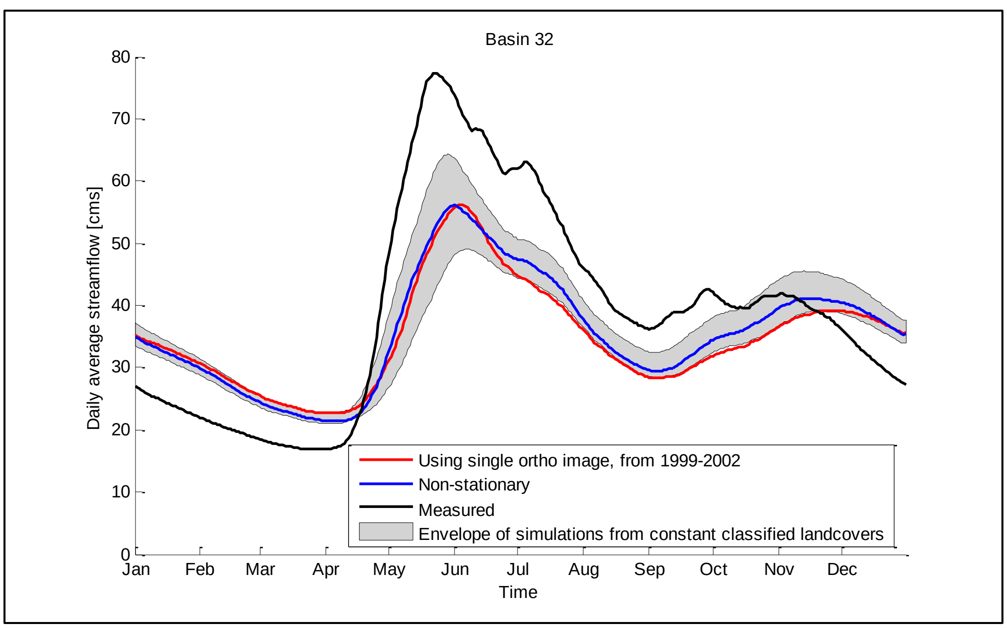

Figure 25 - Average annual hydrographs for Basin 32 (05QA004)

So while the red and blue lines are relatively consistent, there is a wider range (shown in the grey envelope) that represents the uncertainty associated with the selection of landcover image when stationarity of landcover is assumed. In particular, the peak of the hydrograph during spring freshet shows the highest amount of uncertainty. This contrasts with the same results from Basin 36 on Figure 26, in which there is less uncertainty than Basin 32 for the peak annual flow. This is not unexpected as Basin 36 has had significantly less forest fire alteration during the simulation period than Basin 32, and consequently exhibits less uncertainty in peak flow. There is still uncertainty, however, for both basins that highlights the need to consider the assumption of stationary landcover even in basins experiencing natural, gradual change alone.

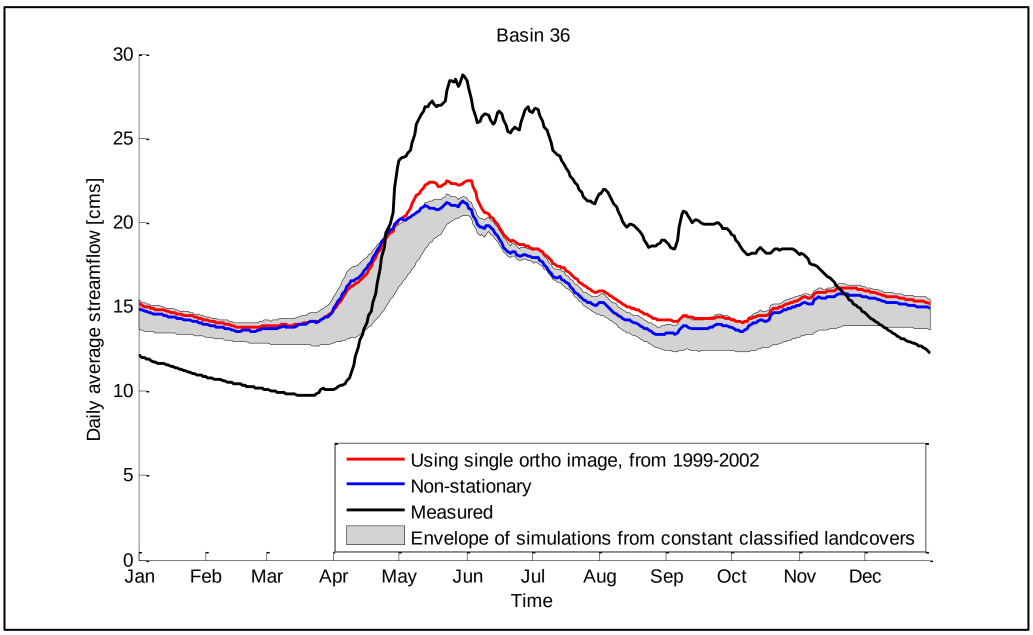

Figure 26 - Average annual hydrographs for Basin 36 (05QC003)

In this chapter, a straightforward approach was presented to incorporate non-stationary landcover, in the form of direct 'observations' from satellite imagery into a hydrological model. As discussed, the effects of running simulations with landcover temporally closest to the simulation period can improve results, and through calibration, can potentially provide more physically realistic parameters. This presumption is based on the principle of equifinality, in that if calibration was performed on landcover that is more representative of the physical system, the likelihood of producing the 'right results for the right reasons' is greater. Such an endeavor beyond the sub-basin scale is problematic given the size of most watersheds (and the WRB). Such a methodology can instead be applied in specific sub-basins of interest to gain an understanding of how sensitive parameters are to changing landcover, as part of a wider calibration effort. Of particular importance are the effects of climate change on changing landcover, and its hydrologic effects. A methodology to address such effects is discussed in the next chapter.

Chapter 5 Landcover Simulator Module

To adequately model climate change with non-stationary landcover, it is not possible to use the methodology of the previous chapter in incorporating 'observed' landcover derived from satellite images. While useful in historical streamflow analyses and operational purposes, assuming historical landcover is representative of future conditions neglects any perturbations of landcover in response to climate (changes in temperature and precipitation). This is especially troublesome for regions prone to forest fires and where, under hotter and drier conditions, the frequency of fires and average annual burned area will not remain stationary (Le Goff, et al., 2009; McCoy & Burn, 2005). This chapter describes the methodology developed to simulate hypothetical future landcover for the purposes of hydrological simulation in WATFLOOD under climate change. The module is developed in Fortran 95 and designed to run separately from WATFLOOD, directly producing landcover files that are to be used in climate change simulations. A schematic of the module's main components are on Figure 27, with each component and their methodologies outlined in the following sections.

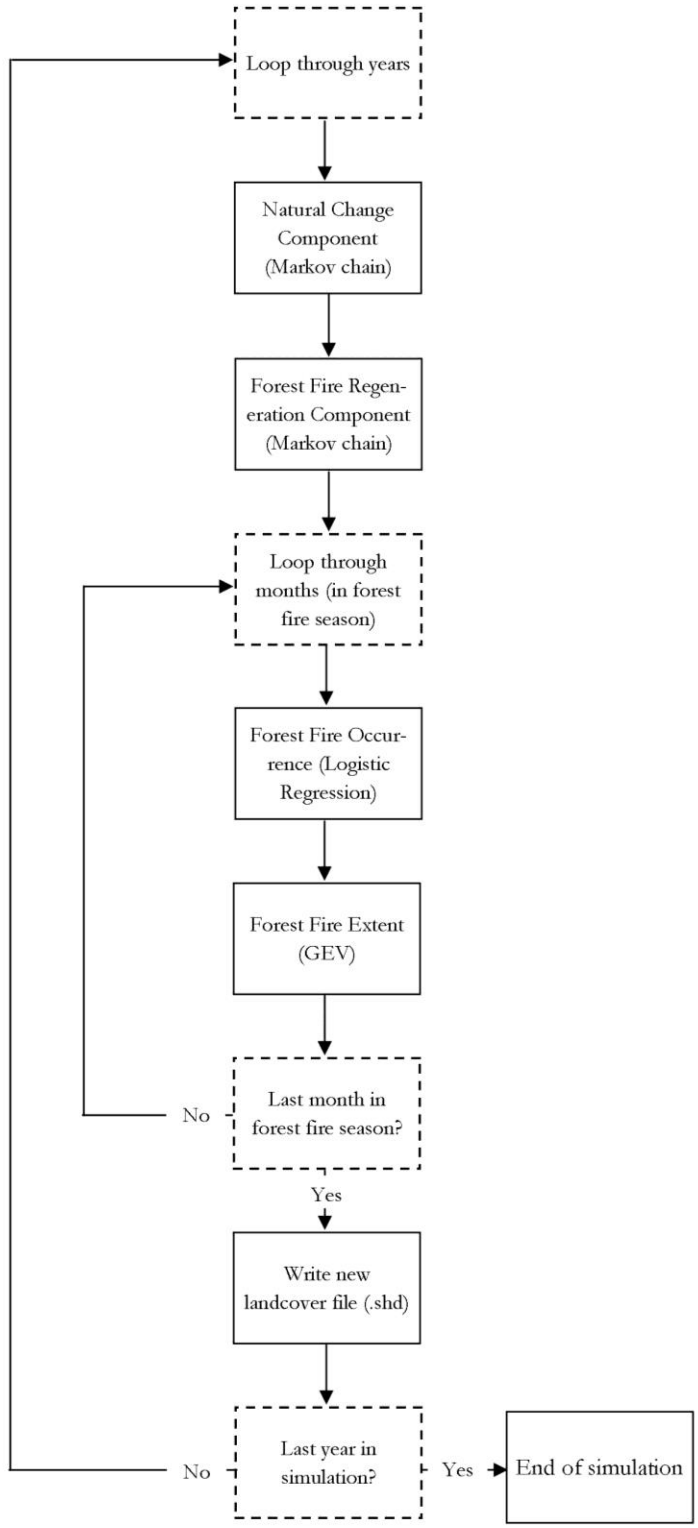

Figure 27 - Simplified schematic of the Landcover Simulator Module's main components

5.1 Natural Change Component

The natural, gradual change component in the landcover simulator module is modelled via a first order Markov chain, with transition probabilities derived from the satellite imagery classification (Section 5.1.1). A methodology is then constructed (Section 5.1.2) to select which images to use for transition probabilities in the landcover simulator module, and provides verification for its natural change component.

5.1.1 Natural Change Methodology

First order Markov chains are effective in predicting future landcover from historical data, particularly from satellite imagery (Kamusoko, et al., 2009; Pastor, et al., 1993; Hall, et al., 1991; Usher, 1981; Van Hulst, 1979). Well suited to remote sensing applications, Markov chains can describe how landcover has changed over time using a pixel by pixel analysis, and then provide future projections based on these historical changes. To do this, a transition probability matrix *P* is constructed between two landcover images, using Equation 5.1 (Pastor, et al., 1993).

$$P_{i,j,\tau} = \frac{n_{i,j}}{\sum_{j=1}^{m} n_{i,j}} \tag{5.1}$$

Where $P_{i,j,\tau}$ is the probability that any given pixel, over the time period in years τ, will transition from landcover class i to j, $n_{i,j}$ is the total number of pixels making such transitions, and m is the total number of land classes. Since the classified landcover images from Chapter 4 are not of regular τ (i.e. number of years between images is not constant), nor are the long time periods (~10 years) suitable for modelling landcover forcing for WATFLOOD on an annual basis, conversion to annual transition probabilities is necessary. A yearly landcover transition time step is preferred as the WRB WATFLOOD setup operates with yearly events, enabling a new landcover file to be read in every year (see Kouwen, (2012) for details on WATFLOOD setup). Equation 5.2 is used to normalize *P* to generate an annual transition probability matrix *N* (Pastor, et al., 1993).

$$N_{i,j} = 1 - \exp\left[\frac{\ln\left(1 - P_{i,j,\tau}\right)}{\tau}\right] \ when\ i \neq j$$

$$N_{i,j} = 1 - \sum_{j=1|j\neq i}^{m} N_{i,j} \ \ when\ i = j \tag{5.2}$$

Using the transition probabilities in *N* from Equation 5.2, landcover can be modelled on a yearly basis and to provide future projections based on historical trends (Kamusoko, et al., 2009). The main advantage to this method is that it provides a straightforward, easily implemented model to simulate processes that are seemingly very complex (Van Hulst, 1979). To physically model the processes governing changing landcover over decades is impractical due to the complexities (and computational requirements) including, but not limited to: the various plant species involved, the difficulty in measuring various vegetation and environmental variables governing the processes, lack of physical understanding of vegetative transitions, and the understanding of which variables are important and/or necessary to include. Using a Markov chain inherently assumes that all governing processes in landcover change can be described by a few parameters, that future change is governed by historical change, and that the large time scale (i.e., decades) makes modelling such small scale processes unnecessary (Van Hulst, 1979). This model tends to perform well in generating landcover changes temporally, while averaging out effects spatially (Kamusoko, et al., 2009; Usher, 1981). These properties are well suited for WATFLOOD, as landcover is averaged on a grid basis using the GRU concept for streamflow simulation. It should be noted that (in this research) it is the simulation and inclusion of trends in landcover change that is important, but not necessarily the exact placement of each pixel. So as long as the percent landcovers are well represented over a sub-basin, the placement of landcovers within the basin does not matter.

One limitation in using a Markov chain to model non-stationary landcover is that it assumes that transition probabilities are stationary through time. While this assumption may not be true, it is preferable to the uncertainties in adding additional variables involved in using transition probabilities as a function of time; and such modifications to the model would not necessarily mean better results due to higher uncertainties (Usher, 1981). Computational demand would also be increased with other, more complex Markovian models, which is a consideration given that WATFLOOD typically operates on large (mesoscale) domains.

Once computed, the transition probabilities from Equations 5.1 and 5.2 are entered into the landcover simulator's parameter file for every land class. Since forest fires are handled separately (Section 5.2), there is no need to include shifts in burned area in the transition probability matrix. Forest fire regeneration is however included, with the procedure to derive these probabilities described in Section 5.3. The parameter file used for simulations in this module is included in Appendix 2, along with definitions of all parameters.

To begin, the module requires a landcover input file to act as the initial condition for the model. The ortho-landcover image (derived from imagery mostly from 1999 – 2002) used in the stationary simulations was used for this research as it provides the most accurate baseline landcover, closest to the present time. Also this image covers the entire domain of the WRB, unlike the images in the previous chapter that only cover two sub-basins. Each year of the simulation, new landcover is generated using the transition probability matrix N, as provided to the module. Since landcover in each WATFLOOD grid is stored as a percent area coverage for every land class, each grid is divided into 0.1% pieces, with each piece being assigned a specific landcover. Every piece is then processed through the Markov chain individually to determine if they should be reclassified into a new class, reassembled, and a new percent landcover configuration for the grid formed. This process is repeated for every grid, on a yearly basis. The decision to use 0.1% sized pieces per grid is arbitrary, as physical size of the pieces varies by grid and grid size is typically not spatially constant (Kouwen, 2012). For example, grid size can be manually altered in WATFLOOD model setup, to take into account sub-basin boundaries residing in the middle of grids. For the WRB, the 'nominal' grid size (i.e. before any manual alterations) is 5595 ha, making the 0.1% pieces 5.595 ha for the average grid. These 0.1% pieces should be sufficiently small to reflect the fact that the transition probabilities were derived at the pixel-scale (30 m resolution, or 0.09 ha), but still computationally efficient and reflective of the pixel-scale. A balance between modelling at the pixel-scale and computational expense is desired given the size of the WRB (136,000 km^2 or 13.6M ha). Smaller pieces were tested (up to 0.01%, or 0.5595 ha average piece size) with negligible differences in generated landcover, so 0.1% was deemed sufficient.

5.1.2 Natural Change Analysis

Using the sub-basin classified landcover images from Chapter 4, transition probabilities were calculated with Equations 5.1 and 5.2 between each image using Matlab™ (version R2012b). Since burned areas and regeneration are handled separately and discussed in subsequent sections, burned pixels were removed from this analysis.

Basin 32

The transition probability matrix for Basin 32 between the 1984 and 1991 images from Figure 19 are presented in Table 6, and are converted to yearly probabilities in Table 7.

Table 6 - Basin 32 landcover transition probabilities [%], 1984 - 1991

	1991						
1984	**conif**	**mixed**	**sparse**	**cut**	**bog**	**fen**	**water**
conif	71.2	21.5	3.1	2.7	0.3	0.6	0.7
mixed	27.0	62.8	6.3	2.1	0.5	1.1	0.1
sparse	6.9	61.3	16.8	2.0	4.6	8.1	0.3
cut	1.1	69.5	21.4	2.6	2.1	3.3	0.1
bog	6.9	60.9	14.0	2.2	16.0	0.0	0.0
fen	9.6	61.6	16.2	1.0	0.0	10.9	0.6
water	1.7	0.7	0.2	0.0	0.0	0.1	97.3

Table 7 - Basin 32 landcover transition probabilities (annual) [%], 1984 - 1991

	1991						
1984	**conif**	**mixed**	**sparse**	**cut**	**bog**	**fen**	**water**
conif	95.6	3.4	0.4	0.4	0.0	0.1	0.1
mixed	4.4	94.1	0.9	0.3	0.1	0.2	0.0
sparse	1.0	12.7	84.1	0.3	0.7	1.2	0.0
cut	0.2	15.6	3.4	80.1	0.3	0.5	0.0
bog	1.0	12.6	2.1	0.3	84.0	0.0	0.0
fen	1.4	12.8	2.5	0.1	0.0	83.1	0.1
water	0.2	0.1	0.0	0.0	0.0	0.0	99.6

Coniferous (conif) and mixed forests (mixed) tend to be the most stable landcovers in this case, with any given pixel having a 71.2% and 62.8% probability of remaining in their land class over the entire seven year period (or 95.6% and 94.1% annually), respectively. Over this period (Table 6), coniferous forest has a 21.5% probability of converting to mixed forest and a 27% of mixed converting to coniferous (or 3.4% and 4.4% annual probability, respectively). This interchangeability and relative stability is expected due to their similarity, as mixed forest consists of coniferous and deciduous forest species types. The sparse class during the seven year time period converts mostly to the mixed class (61.3%). The classifications are essentially the same type of tree species, but with the sparse class being significantly less dense and often characterized by exposed rock. Usually serving as a transitional landcover, a significant amount of this sparse class is likely lost by recovery areas from previous forest fires or logging re-growing (into the mixed classification). Wetlands (bogs and fens) also show a shift towards the forest classes, including mixed (~61%) and sparse (~14-16%) over the simulation period. Fens have a 0.6% probability of transitioning to water, which is expected due to the proximity of fens to water (changing water levels could account for this in fens due to their connectivity to water). Water has a 97.3% probability of remaining in the same class, as the water area typically stays constant and should be as close to 100% as possible. A discrepancy of ~3% can be attributed to classification error, or changes with the fens.

In order to establish a level of confidence in the transition probabilities derived from these images, a series of simulations were conducted in Matlab™ to generate future landcover based on the computed transition probabilities. The Matlab™ script uses annual transition probabilities between two images (e.g. between 1984 and 1991) to generate landcover at the time of the third (future) image (e.g. from 1991 to 2003). The simulated future (i.e., 2003 for model verification) landcover can then be compared to observed, as shown on Figure 28. The y-axis of this plot has been converted to equivalent grid sizes (a representation of area) for ease of interpretation, being 5595 ha in size for the WATFLOOD setup of the WRB.

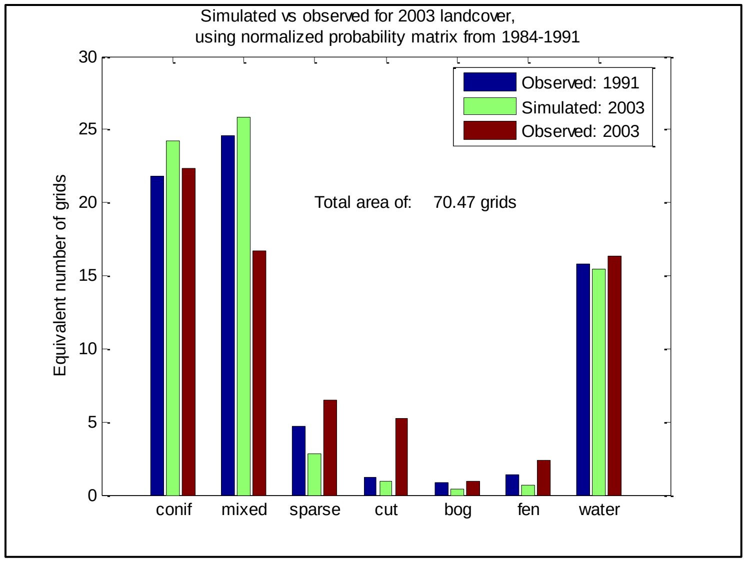

Figure 28 - Basin 32 Matlab™ simulation of natural change for 1991 – 2003 (using annual transition probabilities from 1984 – 1991)

It is important to note that for these simulations, the cut landcover refers to recently logged areas and is relatively unpredictable, in particular when considering climate change. Trends in logging can be captured using the transition probabilities between images, and is included in the scope of this thesis as any other landcover type would. This is not an ideal assumption as logging practices can change over time. How the forestry sector will adapt to climate change in regards to yearly cut area (i.e. size, placement, and frequency of logging), and type of harvest (i.e. clear-cut verses selective logging) is outside of the scope of this thesis. Cuts are, however, of hydrologic importance due to their impact on runoff generation (Pomeroy, et al., 2012) and are simulated through the Markov chain in WATFLOOD simulations. On Figure 28, the cut's lack of predictability has to be considered in the Matlab™ simulation results. The dominant change in observed (1991) and 'future' (2003) images are found within the mixed forest class, which the script fails to accurately reproduce by 2003. A significant portion of the modelling error in the mixed classification is likely attributable to increased logging activity that occurred during the 1991

– 2003 period that is not included in the annual transition probabilities from 1984 – 1991. Classification error could also be a factor. This highlights a limitation of the Markov chain using historical data to predict future events, as it doesn't take into account anthropogenic and other unforeseen effects.

Regular and annual transition probabilities for the 1991 to 2003 time period are shown in Table 8 and Table 9, respectively. Using the annual probabilities, simulation results from 2003 to a 'future' time period (2010) using the Matlab™ script are shown on Figure 29.

Table 8 - Basin 32 landcover transition probabilities [%], 1991 - 2003

	2003						
1991	**conif**	**mixed**	**sparse**	**cut**	**bog**	**fen**	**water**
conif	66.7	11.6	6.7	11.9	0.2	0.3	2.6
mixed	23.2	43.9	14.6	8.9	2.1	6.7	0.5
sparse	8.5	49.3	14.3	12.3	4.6	10.6	0.4
cut	1.1	48.1	9.5	26.3	5.4	9.5	0.2
bog	6.8	67.9	13.8	6.0	5.3	0.0	0.2
fen	5.2	66.2	13.5	6.4	0.0	8.0	0.7
water	0.9	0.3	0.2	0.1	0.0	0.0	98.6

Table 9 - Basin 32 landcover transition probabilities (annual) [%], 1991 - 2003

	2003						
1991	**conif**	**mixed**	**sparse**	**cut**	**bog**	**fen**	**water**
conif	97.1	1.0	0.6	1.0	0.0	0.0	0.2
mixed	2.2	94.9	1.3	0.8	0.2	0.6	0.0
sparse	0.7	5.5	91.3	1.1	0.4	0.9	0.0
cut	0.1	5.3	0.8	92.5	0.5	0.8	0.0
bog	0.6	9.0	1.2	0.5	88.6	0.0	0.0
fen	0.4	8.6	1.2	0.6	0.0	89.1	0.1
water	0.1	0.0	0.0	0.0	0.0	0.0	99.9

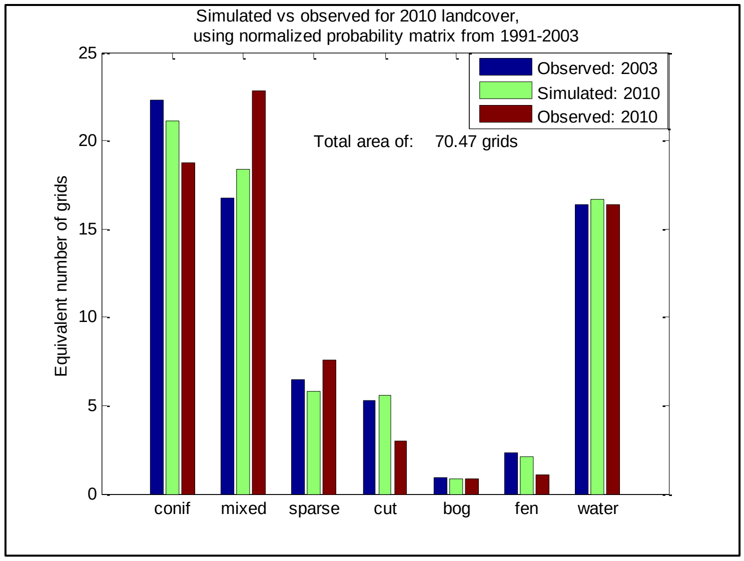

Figure 29 - Basin 32 Matlab™ simulation of natural change from 2003 – 2010 (using annual transition probabilities from 1991 – 2003)

This simulation is characterized by a shift from coniferous to mixed landcover, including significant amounts of cut and little change in the sparse class (Figure 29). These trends are not as clear when looking solely at the transition probabilities. The sparse class, for example, only has a 14.3% probability of remaining the same class as from 1991 – 2003 (Table 8), yet in the simulation, there is only a small decrease in landcover area, based on equivalent number of grids affected (Figure 29). This is because the sparse class acts as a transitional landcover in a basin where there was a significant amount of logging from 1991 – 2003, which is represented in Table 8 by a significant amount of landcover that is converted to cuts. Similarly, cuts are readily converted to mixed and sparse, with sparse in turn converted to mixed. Also, while the results from Figure 29 do not exactly match observed 'future' landcover in 2010, the overall transitional trend from coniferous to mixed landcover is honoured, and is only its somewhat delayed with the Markov chain.

Transition probabilities between the final two landcover images: from 2003 to 2010, are shown in Table 10 and Table 11. Since there is no observed landcover image available after

2010, the Matlab™ script was not run (for verification purposes) using these probabilities. This time period shows similar transitional probabilities as previous ones (1991 – 2003; Tables Table 8 and Table 9), except for showing significantly less cut. There is also double the transition from coniferous to mixed during the 2003 – 2010 time period (from 11.6% to 26.2%).

Table 10 - Basin 32 landcover transition probabilities [%], 2003 - 2010

	2010						
2003	**conif**	**mixed**	**sparse**	**cut**	**bog**	**fen**	**water**
conif	63.6	26.2	3.4	3.8	0.6	0.8	1.5
mixed	20.8	61.8	11.5	1.7	1.6	2.0	0.5
sparse	18.0	49.5	23.2	2.5	2.4	3.4	1.0
cut	10.6	16.2	40.9	24.4	3.5	4.0	0.4
bog	2.5	56.9	28.6	6.1	5.9	0.0	0.0
fen	2.8	72.2	19.1	2.1	0.0	3.3	0.5
water	2.8	0.3	0.1	0.1	0.0	0.1	96.6

Table 11 - Basin 32 landcover transition probabilities (annual) [%], 2003 - 2010

	2010						
2003	**conif**	**mixed**	**sparse**	**cut**	**bog**	**fen**	**water**
conif	94.3	4.3	0.5	0.6	0.1	0.1	0.2
mixed	3.3	94.1	1.7	0.2	0.2	0.3	0.1
sparse	2.8	9.3	86.6	0.4	0.3	0.5	0.1
cut	1.6	2.5	7.2	87.5	0.5	0.6	0.1
bog	0.4	11.3	4.7	0.9	82.7	0.0	0.0
fen	0.4	16.7	3.0	0.3	0.0	79.5	0.1
water	0.4	0.0	0.0	0.0	0.0	0.0	99.5

Basin 36

The same verification methodology used for Basin 32 was applied to Basin 36. Regular and annual transition probabilities between the first two images (1985 and 1994) were computed and are shown in Table 12 and Table 13 respectively, with output from the 'future' Matlab™ simulation from 1994 – 2003 shown on Figure 30.

Table 12 - Basin 36 landcover transition probabilities, 1985 - 1994

	1994						
1985	**conif**	**mixed**	**sparse**	**cut**	**bog**	**fen**	**water**
conif	79.3	5.9	9.0	3.8	0.0	0.1	1.9
mixed	34.2	33.9	24.4	2.3	1.7	2.5	0.9
sparse	15.2	23.2	50.3	2.5	2.7	5.0	1.1
cut	2.4	9.8	42.8	30.7	10.0	2.2	2.1
bog	14.5	26.7	47.4	1.3	9.9	0.0	0.1
fen	16.4	26.1	42.7	1.5	0.0	12.0	1.2
water	0.6	0.1	0.1	0.0	0.0	0.0	99.2

Table 13 - Basin 36 landcover transition probabilities (normalized), 1985 - 1994

	1994						
1985	**conif**	**mixed**	**sparse**	**cut**	**bog**	**fen**	**water**
conif	97.6	0.7	1.0	0.4	0.0	0.0	0.2
mixed	4.5	91.6	3.1	0.3	0.2	0.3	0.1
sparse	1.8	2.9	94.0	0.3	0.3	0.6	0.1
cut	0.3	1.1	6.0	90.9	1.2	0.2	0.2
bog	1.7	3.4	6.9	0.1	87.8	0.0	0.0
fen	2.0	3.3	6.0	0.2	0.0	88.4	0.1
water	0.1	0.0	0.0	0.0	0.0	0.0	99.9

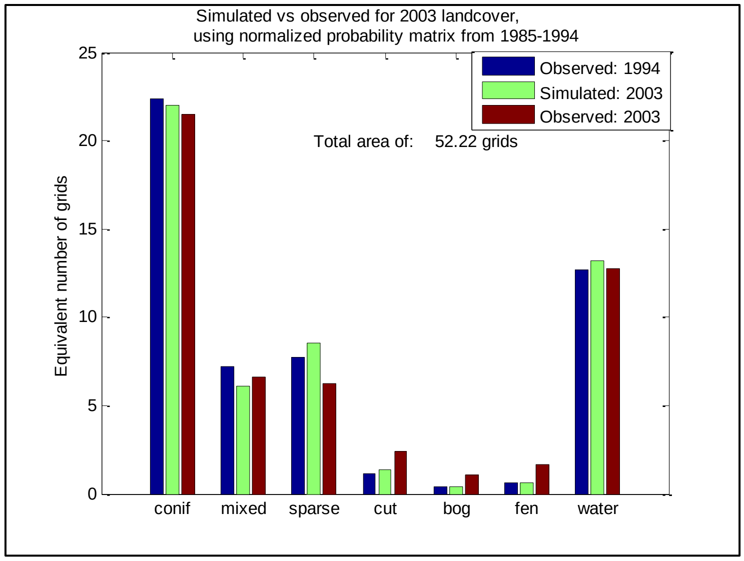

Figure 30 - Basin 36 Matlab™ simulation of natural change from 1994 – 2003 (using annual transition probabilities from 1985 – 1994)

From Figure 30 there is little change in landcover between the observed (1994) and 'future' (2003) images, and this is well reflected using the 1985 – 1994 annual transition probabilities from Table 13. The main reason for this consistency is that the sub-basin is predominantly coniferous forest (Figure 30), with coniferous landcover having a yearly retention probability of 97.6% (Table 13).

Transition probabilities for the second time period (1994 – 2003) are shown in Table 14 and Table 15, with the corresponding Matlab™ simulation from 2003 to the 'future' (2009) time period shown on Figure 31.

Table 14 - Basin 36 landcover transition probabilities [%], 1994 - 2003

	2003						
1994	**conif**	**mixed**	**sparse**	**cut**	**bog**	**fen**	**water**
conif	82.0	5.3	5.9	5.4	0.1	0.2	1.2
mixed	31.6	37.7	18.9	5.4	1.9	4.2	0.2
sparse	9.1	32.8	34.5	6.5	6.6	10.3	0.2
cut	0.6	1.6	53.4	19.8	10.8	13.5	0.3
bog	0.3	12.8	21.7	3.0	62.2	0.0	0.0
fen	0.8	10.8	31.5	2.6	0.0	54.0	0.3
water	1.0	0.1	0.2	0.2	0.0	0.0	98.6

Table 15 - Basin 36 landcover transition probabilities (annual) [%], 1994 - 2003

	2003						
1994	**conif**	**mixed**	**sparse**	**cut**	**bog**	**fen**	**water**
conif	98.0	0.6	0.7	0.6	0.0	0.0	0.1
mixed	4.1	92.2	2.3	0.6	0.2	0.5	0.0
sparse	1.1	4.3	91.9	0.7	0.8	1.2	0.0
cut	0.1	0.2	8.1	88.7	1.3	1.6	0.0
bog	0.0	1.5	2.7	0.3	95.4	0.0	0.0
fen	0.1	1.3	4.1	0.3	0.0	94.2	0.0
water	0.1	0.0	0.0	0.0	0.0	0.0	99.8

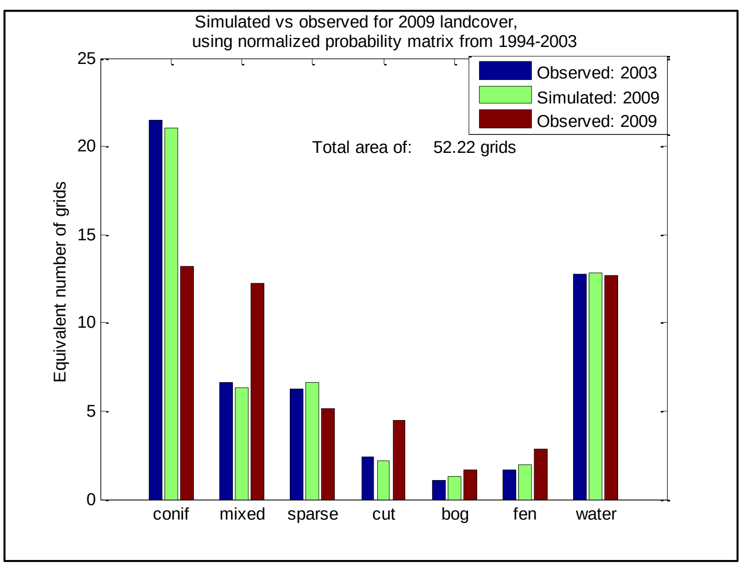

Figure 31 - Basin 36 Matlab™ simulation of natural change from 2003 – 2009 (using annual transition probabilities from 1994 – 2003)

The transition probabilities are again similar during this time period (1994 – 2003) relative to previous (1985 – 1994), particularly for the dominant coniferous and mixed classes. In this regard, the Matlab™ simulation performs quite similar between the two time periods (Figure 30 and Figure 31). The observed 'future' landcover image in 2009, however, shows significant discrepancies for both the coniferous and mixed classes between 2003 and 2009. While a transition from coniferous to mixed forest from 2003 – 2009 is consistent with Basin 32 and not unexpected in Basin 36, the magnitude of the transition for Basin 36 seems unlikely, and could be in part due to other factors. For example, transition probabilities between 2003 and 2009 (Table 16 and Table 17) show a significant reduction in the retention probability of coniferous forest over this period (58.8%), with the bulk of the probability transferred to mixed (28.5%) and to cut (7.8%).

Table 16 – Basin 36 landcover transition probabilities, 2003 - 2009

	2009						
2003	**conif**	**mixed**	**sparse**	**cut**	**bog**	**fen**	**water**
conif	58.8	28.5	2.3	7.8	0.8	1.4	0.4
mixed	3.8	48.3	20.0	7.3	8.6	12.1	0.0
sparse	1.6	29.3	29.8	11.2	8.1	19.5	0.5
cut	0.4	8.2	23.0	62.5	2.5	2.9	0.4
bog	0.2	30.9	29.4	5.4	34.2	0.0	0.0
fen	0.7	34.1	34.6	4.0	0.0	26.5	0.2
water	1.4	0.1	0.1	0.0	0.0	0.0	98.4

Table 17 - Basin 36 landcover transition probabilities (normalized), 2003 - 2009

	2009						
2003	**conif**	**mixed**	**sparse**	**cut**	**bog**	**fen**	**water**
conif	92.4	5.4	0.4	1.3	0.1	0.2	0.1
mixed	0.6	90.8	3.6	1.2	1.5	2.1	0.0
sparse	0.3	5.6	87.1	2.0	1.4	3.6	0.1
cut	0.1	1.4	4.3	93.3	0.4	0.5	0.1
bog	0.0	6.0	5.6	0.9	87.5	0.0	0.0
fen	0.1	6.7	6.8	0.7	0.0	85.6	0.0
water	0.2	0.0	0.0	0.0	0.0	0.0	99.7

Wetlands appear to be a factor in this transition, where bogs and fens had only 12.8% and 10.8% probability of transition to mixed from 1994 – 2003, respectively; this increases to 30.9% and 34.1% for 2003 – 2010, respectively. Another contributing factor would have been infestation of the Jack Pine Budworm, which caused damage to 262,245 ha of forest from 2007 – 2009 in the Red Lake area, which includes part of the surroundings of Trout Lake in Basin 36 (Scarr, et al., 2011). This infestation affected Jack Pine (*Pinus banksiana*), classified as coniferous in the landcover classification, and would contribute to the actual depletion of this land class from 2003 – 2009, but was not captured by the model.

5.1.3 Incorporation of Natural Change into WATFLOOD

One transition probability matrix for the natural change component must be selected for use in the landcover simulator module for the WRB in order to conduct climate change simulations with non-stationary landcover. It is assumed that the transition probabilities derived for one sub-basin from one time period are representative of the entire WRB and simulation period (1971 – 2000). This assumption is quite broad, and generally not true. From the analysis conducted in Section 5.1.2, however, the transition probabilities were shown to represent overall shifts in landcover over a 30 year period and are therefore assumed to be reliable enough to provide a 'best guess' of future landcover in the WRB. Being able to validate these probabilities using this analysis was a priority for incorporation into the module. From that analysis, the transition probabilities that best fit the overall trends in landcover change experienced by the sub-basins are from the 1991 – 2003 time period in Basin 32 (Table 9). As explained above, the probabilities in this time period describe a shift from coniferous to mixed forest (Figure 29), albeit gradually, which is preferable to prevent unrealistic rapid changes in landcover. This shift between classes is not unexpected, as previous studies have found that boundaries between coniferous dominated and deciduous dominated forest types will likely shift north with climate change (Ehman, et al., 2002; Thompson, et al., 1998). These probabilities also simulate and maintain a significant amount of cut area, which is useful given significant cutting was known to have begun in 1991 and is not otherwise addressed in this thesis or modelling methodology. Cuts also won't simply accumulate over time, as generated cuts with the Markov chain are subsequently converted to other classes over time.

5.2 Forest Fire Modelling Component

Landcover alteration from forest fire is modelled separately from the natural change component to account for landcover-based feedbacks due to climate change (i.e., changes in temperature and precipitation). Forest fire occurrences in the module are simulated consistent with literature-based approaches using a logistic regression model linked to temperature and precipitation forcing with extents determined from a generalized extreme value (GEV) distribution fit from historical forest fire data.

5.2.1 Forest Fire Occurrence Methodology

Logistic regression is commonly applied in the literature to describe forest fire occurrence (Woolford, et al., 2010; Le Goff, et al., 2009; Chou & Minnich, 1993). Operating at a monthly time step, forest fire occurrence acts as a binomial variable due to the large numbers of months where fires would not occur (i.e. over the entire fire record in the WRB), making logistic regression well suited to this application (Le Goff, et al., 2009). For this thesis, a forest fire is defined as a fire having a burned area of at least 2000 hectares. The nominal grid size in the WRB is 5330 ha and it is prudent to only model fires that would be hydrologically relevant (i.e., would affect runoff generation processes within the WATFLOOD model). The logistic regression model is described by Equation 5.3.

$$
\begin{gathered}
Prob = \frac{\exp(U)}{1 + \exp(U)} \\
U = b_0 + b_1 * Pcp + b_2 * Tmp
\end{gathered}
\tag{5.3}
$$

Prob is the probability of forest fire (>2000 ha) occurring in any given month, with a monthly average basin temperature *Tmp* [°C], monthly cumulative precipitation *Pcp* [mm] in the hydrologic year, and regression coefficients $b_{0..2}$. The hydrologic year for the WRB is October 1 to September 30, which is included in the logistic regression to account for the contribution of snowmelt to moisture conditions during the forest fire season. Using forest fire data regressed with monthly *Tmp* and *Pcp*, coefficients and p-values of the logistic regression can be found in Table 18.

Table 18 - Logistic regression of forest fire occurrence variables: coefficients and p-values

Case	b_0	b_0: p-value	b_1	b_1: p-value	b_2	b_2: p-value
Pcp	-0.2745	0.6834	-0.0037	0.0140	--	--
Tmp	-3.5267	<0.0001	--	--	0.1221	0.0217
Tmp & Pcp	-1.1080	0.2384	-0.0081	0.0021	0.2124	0.0017

Results of the regression are shown in Table 18 for three cases: each of *Pcp* and *Tmp* separately, and combined. Whether regressed together or separately, *Pcp* and *Tmp* are significant at the 5% level, with decreasing *Pcp* resulting in increased probability of fires, and increased *Tmp* with increased probability of fires, as was intuitively expected. *Pcp* and *Tmp* are most significant (p-values of 0.0021 and 0.0017 respectively) when regressed together, as opposed to separately, indicating that including both variables are preferable for projecting forest fire occurrence. Graphically, the results of the logistic regression for both *Pcp* and *Tmp* combined are presented on Figure 32. In this figure, probability of forest fire is shown as a function of *Pcp*, for two constant *Tmp*'s of 10°C and 20°C. Note that probability of forest fire decreases rapidly with increasing precipitation and decreasing temperature.

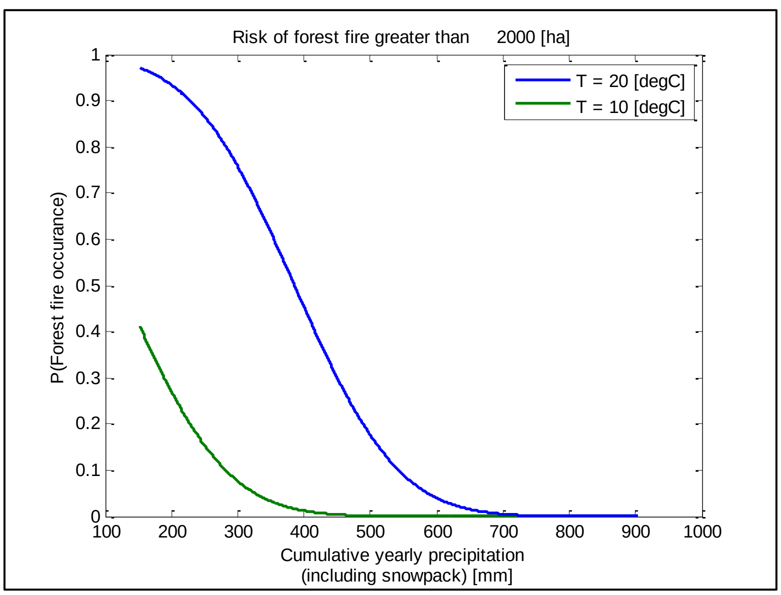

Figure 32 - Logistic regression of forest fire occurrence with monthly average temperature and cumulative yearly precipitation

While basin averages of *Pcp* and *Tmp* are used for fire occurrence prediction, actual location of the fire within the basin is determined at the grid scale. Equation 5.3 is applied to every grid to compute probabilities of occurrence for all grids in the WRB (using gridded temperature and precipitation), with a randomizing component to the model applied, and the fire is placed in the grid having the highest probability. Determination of forest fire location based on the logistic regression and random component is completely separate to determining occurrence. Fires larger than one grid size are "spilled" over into neighbouring grids, and are explained in detail in Section 5.2.4. The equation for the random component is shown below.

$$\begin{aligned} R &= Prob - [rand * wt] \qquad when\ Prob > 0.5 \\ R &= Prob + [rand * wt] \qquad when\ Prob < 0.5 \end{aligned} \tag{5.4}$$

Where *rand* is a random number between 0 and 1 drawn from a uniform distribution, *wt* is a weighting factor between 0 and 0.5, and *R* is the "adjusted" *Prob*, taking the random component into account. The weighting factor is included to provide control on the degree to which *Prob* is adjusted. A *wt* of 0 would have no effect on *Prob*, and 0.5 (the maximum allowable value) would have a significant effect. If a *wt* of 0.5 is not exceeded, *R* will not leave the constraints of [0,1]. From trial and error, a *wt* of 0.45 was used in the WRB to ensure an adequate spread in forest fire occurrence throughout the basin; lower values of *wt* tend to concentrate forest fires in the west of the WRB due to generally higher average temperatures (Section 3.4). A randomized component in the model is necessary as actual location of a fire depends on more factors than solely temperature and precipitation; factors that are not included in the WATFLOOD model. The goal of the landcover simulator module is not to reproduce past fires in terms of specific date, location or extent, but rather to simulate future *trends* in landcover change. Therefore, specific locations of fires are not as important as the fact they have simply occurred somewhere within the basin and altered the overall landcover distribution (and therefore runoff generation) through time. The logistic regression model doesn't work very well in placing fires because that was not a specific design criteria: it was calibrated (and works well) to simulate occurrence more accurately than location. The logistic regression model provides a physical basis, albeit a simple one, to place the fire within the basin of interest. The random component to the model is also coded in such a way that should more inputs be added to the WATFLOOD model, it can be replaced or refined in the future as desired.

5.2.2 Forest Fire Extent Methodology

Once a forest fire is known to occur in the landcover simulator module, its size is determined by a generalized extreme value (GEV) distribution, fit from historical forest fire data available in the WRB. A study by Jiang & Zhuang, (2011), found that burned area from forest fires in the Boreal region of Canada (which includes the the WRB) can be described with a GEV distribution. The cumulative distribtion function (CDF) of the GEV distribution is shown in below.

$$F(x|k,\mu,\sigma) = \begin{cases} \exp\left[-\left[1+k\left(\frac{x-\mu}{\sigma}\right)\right]^{-1/k}\right], 1+k\left(\frac{x-\mu}{\sigma}\right) > 0, k \neq 0 \\ \exp\left[-\exp\left(-\frac{x-\mu}{\sigma}\right)\right], \quad k = 0 \end{cases} \tag{5.5}$$

With x as the forest fire size in hectares, and $k, \mu,$ and σ as the shape, location, and scale parameters respectively. The special case of $k = 0$ is referred to as the Gumbel distribution and is often used when k is not necessary to adequately describe the data in order to simplify analyses. However the Gumbel distribution was not found to adequatly describe the data at a significant level in this thesis, requiring the shape parameter, k, to be used in the full GEV distribution (Equation 5.5). For this analysis, coefficients for the three parameters are determined using historical forest fire data, with forest fire extent modelled in the landcover module by the inverse CDF shown below using those parameters.

$$x(F|k,\mu,\sigma) = \left[\frac{(-\ln F)^{-k} - 1}{k}\right]\sigma + \mu \tag{5.6}$$

Every time a fire is determined to occur using the logistic regression subroutine (Section 5.2.1), a random number is generated between 0 and 1 and is directly entered into Equation 5.6 to calculate an extent of burn in hectares.

In order to determine if the GEV distribution is appropriate for modelling forest fire extent in the WRB specifically, Kolmogorov-Smirnov (KS) tests were conducted using the historical forest fire data from both a calibration (1960 – 1980) and validation (1981 – 2003) time period. Parameters for the GEV distribution were fit with data from the calibration period, then tested for both the calibration and validation periods and are shown in Table 19.

Table 19 - GEV distribution parameters for calibration (1960 - 1980) period

	k (shape)	σ (scale)	μ (location)
Parameter values	1.5842	3193.3	3830.1

For the KS tests, the null hypothesis is that the GEV CDF from the calibration period is an adequate representation of the empirical CDF for the calibration and validation periods that are shown on Figure 33.

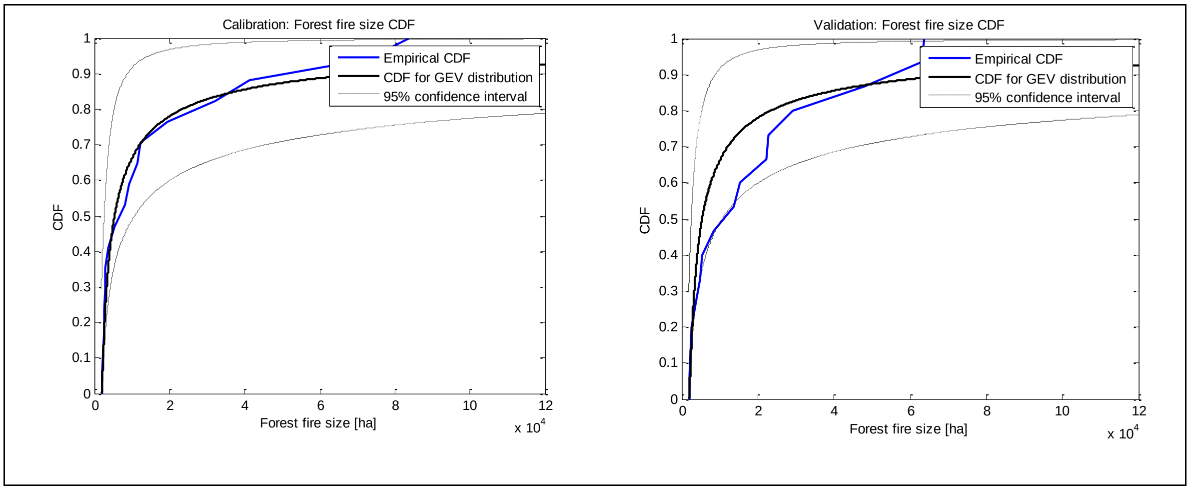

Figure 33 - GEV distribution CDFs for KS tests

The solid black lines indicate results of a large sample (10,000 random numbers [0,1] from a uniform distribution) using the GEV parameters, with the blue lines representing the empirical CDFs from historical fire data. The p-values of these KS tests are 0.567 and 0.360 respectively, indicating that the null hypothesis has failed to be rejected for both cases at the 5% level. This indicates that using the GEV distribution with these parameters is appropriate for use in the WRB. This is illustrated on Figure 33 with the blue lines both lying within the 95% confidence bounds of the solid black lines.

5.2.3 Coupled Forest Fire Occurrence and Extent

In the preceding two sub-sections, models for forest fire occurrence and extent were derived and justified based on literature and statistical testing in the WRB study domain. Coupling two such models, however, has not before been attempted for a hydrological modelling application. To do so, additional consideration is needed in order to gain confidence in such a model. As a result, 1000 simulations were conducted in Matlab™ using logistic regression (Section 5.2.1) and GEV distribution (Section 5.2.2) methodologies to visualize results and validate against observed forest fire data. Results are shown on Figure 34.

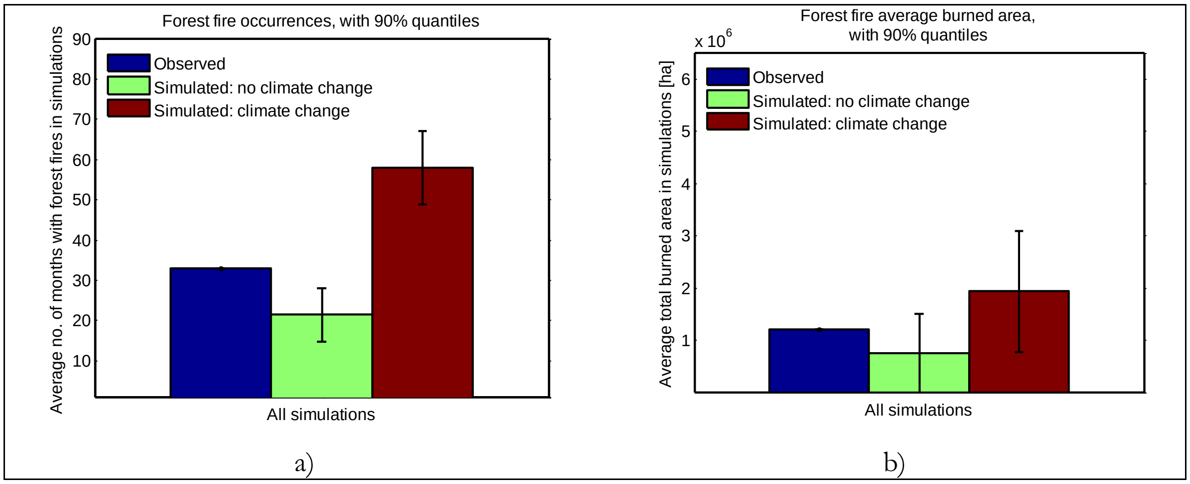

Figure 34 - Coupled forest fire (a) occurrence and (b) extent Matlab™ simulation (1960 – 2003) results validated against observations in the WRB

The blue bars in the figure represent observed forest fire data from 1960 – 2003 in the WRB, for both occurrence (Figure 34a) and extent (Figure 34b). The green bars represent the average result of the 1000 Matlab™ simulations, with 90% quantiles indicated above and below by cross-hairs. The red bars are the same simulations conducted under climate change conditions (2080s A2 scenario), to provide an example of the shifts in fire activity possible under climate change. The model underestimates forest fire occurrence overall, with the upper 90% quantile lying slightly below the observed total occurrence. Average simulated burned area is also underestimated (Figure 34b); however 90% quantiles are within the observed burned area. Despite the underestimation of occurrences, the model is considered reasonable given the total burned area is the final result of the coupled occurrence-extent simulation, and burned area was adequately modelled. The perturbation of temperature and precipitation with climate change has a direct impact on forest fire occurrence, as evidenced on Figure 34. Consistent with literature on increased forest fire activity with climate change (Le Goff, et al., 2009; McCoy & Burn, 2005), this is an example of how substantial this change can be in the model. Figure 35 presents the same results, but broken down by month.

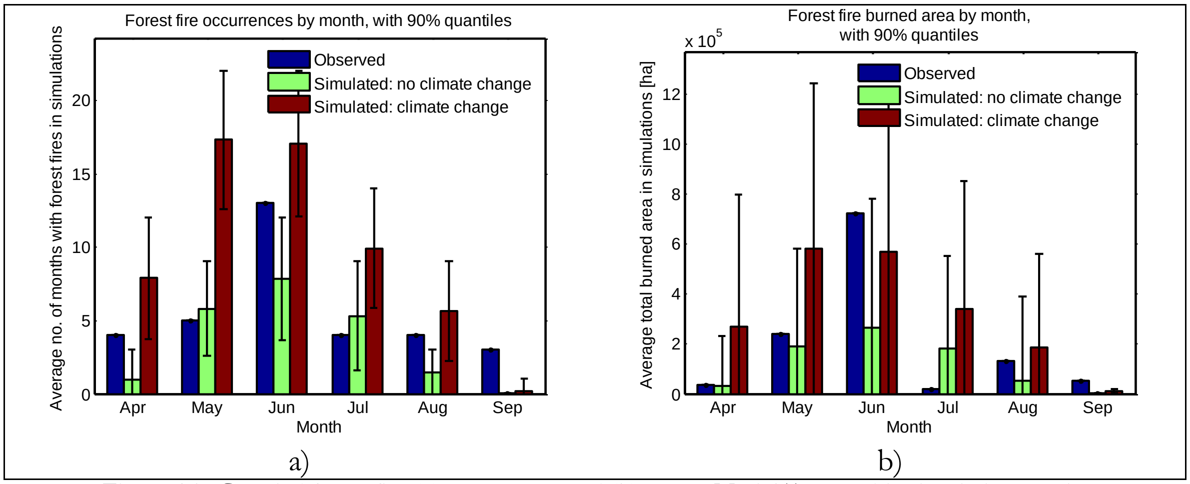

Figure 35 - Coupled forest fire (a) occurrence and (b) extent Matlab™ monthly simulation results

From Figure 35 it can be seen that the greatest amount of forest fire activity occurs in June, in terms of both burned area and occurrence, which is reflected by the coupled model. While significant variability occurs in forest fire extent, every month except September is well within range of observed values. There is very little burned area in the September observed record, but doesn't impact overall results (Figure 34). The model accurately captures and simulates trends in both forest fire occurrence and extent from month to month, and linked with temperature and precipitation perturbations can simulate future forest fires for use in WATFLOOD.

5.2.4 Incorporation of Forest Fire Occurrence and Extent into WATFLOOD

Parameters for the logistic regression and GEV distribution are entered into the landcover simulator parameter file prior to the simulation of landcover. Also customizable using this parameter file are the specific landcovers that are allowed to burn (i.e., some cannot burn, such as water or impervious), months of the forest fire season, and a maximum forest fire size. Including a maximum forest fire extent is optional, and is included to prevent the unlikely (and unrealistic) occurrence of a forest fire that would cover the entire basin. For this thesis, the maximum size was set at 387,743 hectares (~69 grids in the WRB) as the largest fire of record in the WRB (occurring in 1961). The WRB contains 3039 grids, so the maximum forest fire extent would cover ~2.3% of the basin.

In the event that burned area as determined by the GEV distribution is larger than the grid the fire is assigned to, a methodology is required to "spill over" the fire into neighbouring grids. Even fires less than one grid size may require this if water (a non-burnable landcover) is present through most of the grid, reducing the burnable area. Burnable area is determined by summing the total area of each 'burnable' landcover as specified in the parameter file. A simple method is used to burn neighbouring grids when this is necessary that spreads the fire out radially from the grid of origin, as illustrated on Figure 36.

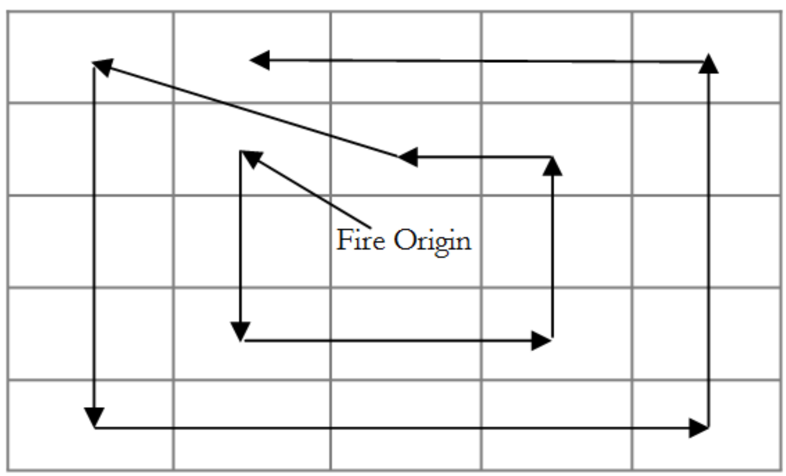

Figure 36 - Graphical depiction of large forest fires being "spilled" to neighboring grid cells

Basically the fire advances from grid-to-grid in a counter-clockwise radial pattern as indicated on the figure, starting at the northwest corner grid until the required amount of hectares is burned according to the GEV distribution. More than one radial ring will be burned if necessary, as is often the case with fires originating in grids on the basin boundary as this algorithm will skip grids not in the basin. This method of transferring fires from grid-to-grid is not physically-based (nor-realistic), nonetheless it's a simplistic method that is easily implemented and computationally efficient. If future studies find that additional complexity would be beneficial, the subroutine governing this process can be modified. For example, if wind direction is added as a standard WATFLOOD forcing, fires could potentially be coded to spread in the direction of current (or prevailing) wind conditions.

After a forest fire occurs in the module, the particular grids that contain the fire enter a recovery phase of predetermined length. No forest fires are permitted to occur by the module in those grids until the recovery period is over (i.e., no re-burn). While this duration is customizable, 20 years was used as approximately the amount of time to recover for areas affected by forest fire based on visual analysis of landcover imagery. This timeline, however, would not necessarily be consistent for other basins. Further details about recovery from forest fires are described in the following section.

5.3 Forest Fire Regeneration Component

Regeneration from forest fire is modelled in the exact same fashion as the natural change component: a first order Markov chain. Transition from burned to other landcover is inherently a natural, gradual process, and is therefore similarly modelled with the same governing assumptions. The main difference lies in the fact that no landcover transitions to burn are permitted in the Markov process, only transitions away from burn to other landcovers. Transition probabilities between two images for this component are determined in a similar fashion to natural change; however the only pixels considered in the calculation are ones that had previously undergone burn in the first image. For Basin 32 (sub-basin with a significant amount of forest fire activity), transition probabilities were calculated between landcover images and tested with the same Matlab™ script described in Section 5.1. Regular and annual probability matrices are shown in Table 20 and Table 21 respectively from 1984 to 1991.

Table 20 - Basin 32 forest fire regeneration transition probabilities [%], 1984 - 1991

	1991							
1984	**conif**	**mixed**	**sparse**	**burn**	**cut**	**bog**	**fen**	**water**
burn	0.6	42.8	20.0	9.3	6.3	5.9	15.0	0.2

Table 21 - Basin 32 forest fire regeneration transition probabilities (annual) [%], 1984 - 1991

	1991							
1984	**conif**	**mixed**	**sparse**	**burn**	**cut**	**bog**	**fen**	**water**
burn	0.1	7.7	3.1	85.0	0.9	0.9	2.3	0.0

Over 1984 – 1991 time period, burned landcover has a 42.8% probability of conversion to mixed forest, 20% to sparse, and only 0.6% to coniferous forest. A slightly different methodology is undertaken for the regeneration component than with the natural change component of Section 5.1.2. The natural change component used transition probabilities from two images (i.e. 1984 and 1991) and simulated from the latter year to a 'future' year (i.e. 1991 – 2003) to see how the probabilities predicted 'future' landcover. In the case of regeneration, a forest fire occurring in the first image (i.e. 1984) experiences regeneration in the preceding years. The probabilities describing this regeneration can be determined using any image after the fire (i.e. 1984 – 1991, and 1984 – 2003). Therefore, a decision must be made on which images to use in the calculation of transition probabilities in the landcover simulator module. In both cases (1984 – 1991 and 1984 – 2003), transition probabilities are calculated and compared to observed in the final year of simulation, to judge the adequacy of the respective time periods. The first case (1984 – 1991) is shown graphically on Figure 37, simulating on a yearly time step using annual probabilities from Table 21.

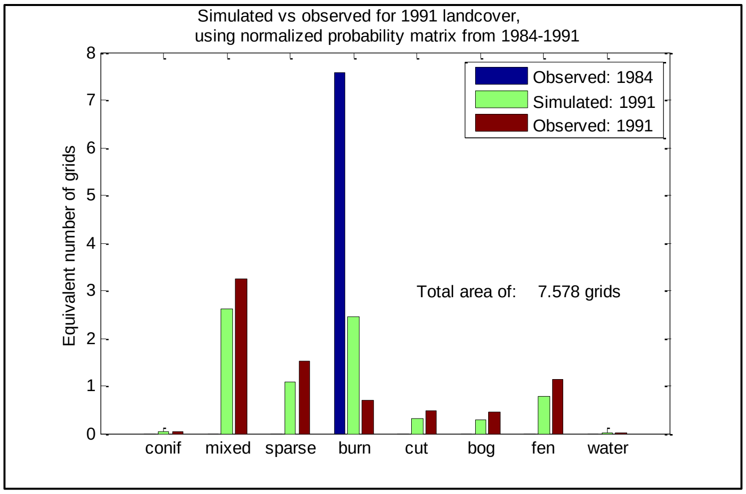

Figure 37 – Basin 32 Matlab™ simulation of forest fire regeneration from 1984 – 1991 (using annual transition probabilities from 1984 – 1991)

As evident from the single blue bar on Figure 37, initially only burned landcover is present in 1984 then is converted to other classes throughout the simulation. Using annual transition probabilities tends to delay the regeneration process as evidenced by the discrepancy between observed and simulated landcover in 1991 (approximately 1.5 equivalent grids). To contrast this, the above simulation was repeated with transition probabilities between 1984 and 2003, effectively skipping the 1994 image. Regular and annual probabilities for this case are presented in Table 22 and Table 23 respectively, with the results of the Matlab™ simulation on Figure 38.

Table 22 - Basin 32 forest fire regeneration transition probabilities [%], 1984 - 2003

	2003							
1984	**conif**	**mixed**	**sparse**	**burn**	**cut**	**bog**	**fen**	**water**
burn	7.2	69.2	9.6	0.4	3.8	1.7	7.5	0.6

Table 23 - Basin 32 forest fire regeneration transition probabilities (annual) [%], 1984 - 2003

	2003							
1984	**conif**	**mixed**	**sparse**	**burn**	**cut**	**bog**	**fen**	**water**
burn	0.4	6.0	0.5	92.3	0.2	0.1	0.4	0.0

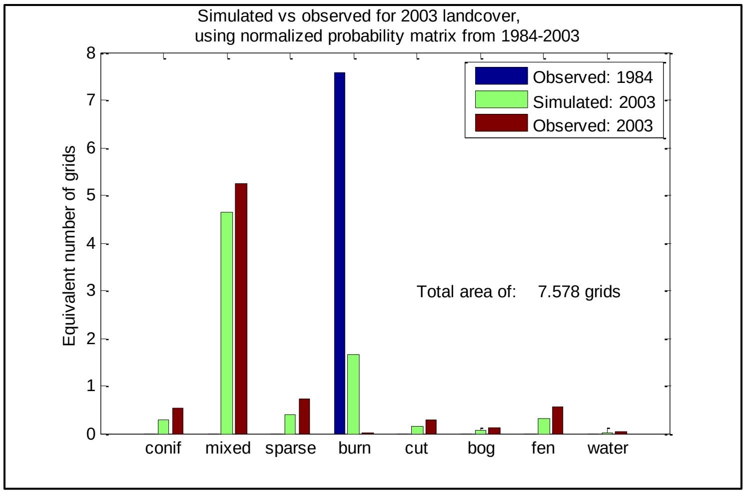

Figure 38 – Basin 32 Matlab™ simulation of forest fire regeneration from 1984 – 2003 (using annual transition probabilities from 1984 – 2003)

For this case, 19 years after the 1984 landcover image all observed burned area is practically removed. During this time period, burned area has a 69.2% probability of conversion to mixed forest, 9.6% to the sparse class, and 7.2% to coniferous forest. This is similar to the previous case (1984 – 1991) with regeneration being dominated by mixed and sparse forest. While the 1984 – 2003 simulation tends to overestimate the amount of burned area at the end of the simulation, with approximately the same ratio of observed starting burned area to simulated burned areas of the previous simulation from 1984 – 1991 (comparing Figure 37 and Figure 38).

Ultimately, one set of transition probabilities from the above two scenarios must be chosen for simulation of regeneration in the WRB. For this thesis, the annual probabilities in Table 21 from 1984 – 1991 are used. While the amount of error in both of simulations is similar, the earlier time period is more appropriate due to a lower overestimation of burned area *over a 20 year period*. With the chosen probabilities, there will be overestimation of burn ~7 years after the fire, however when given 20 years to regenerate, most if not all of the burn will be regenerated. If the 1984 – 2003 probabilities were chosen, a significant amount of burn may still remain after 19 years.

In this chapter, a methodology was constructed to incorporate non-stationary landcover into WATFLOOD through the use of a preprocessing module developed in Fortran 95. The main components are natural change, forest fire occurrence, forest fire extent, and regeneration. The natural change component uses a first order Markov chain based on transition probabilities derived from historical landcover imagery to simulate the future. An analysis was conducted using Matlab™ to determine which images were most appropriate for use in the module. The results of the analysis yielded the 1991 – 2003 probabilities from Basin 32 (burned pixels removed) as the optimal choice, and are used in the module for the rest of this thesis. The forest fire occurrence component utilizes a logistic regression model to simulate forest fires on a monthly time step, with coefficients derived from historical forest fire data. The model itself is a function of monthly average temperature and monthly cumulative precipitation (in the hydrologic year), making it ideally suited to linkage with climate model outputs for climate change simulation. Extent of fire is determined from a generalized extreme value (GEV) distribution, also fit from historical forest fire data. Together, forest fire occurrence and extent were coupled in a series of Matlab™ simulations to determine its effectiveness in simulating forest fires of the WRB. Overall occurrences were found to be underestimated, but actual burned area was well simulated. Regeneration from forest fire is simulated in a similar manner to natural change using a first order Markov chain, as regeneration is inherently a natural process. After some testing, transition probabilities from 1984 – 1991 were selected to be used. The final transition probability matrix combining the regeneration and natural change components is included in Appendix 5. This matrix was input into the landcover simulator module, along with the forest fire parameters for generation of future landcover. In the next chapter, future landcover is generated and used in climate change simulations to determine the effects of climate change on the hydrologic regime of the WRB as well as the uncertainties associated with non-stationary landcover.

Chapter 6 Model Application

In this chapter, landcover is generated with the landcover simulator module for CGCM3.1 data from the A1B, B1, and A2 scenarios, and with no climate change (using historical meteorological input only). Results of the hydrological simulations for the 2050s and 2080s with non-stationary and stationary landcover are discussed. Also discussed are the uncertainties in hydrological prediction that result from using stationary landcover, as is expected in the current hydrological modelling literature (Cuo, et al., 2011; Quilbe, et al., 2008; Samaniego & Bardossy, 2006).

6.1 Historical Streamflow Simulation with Non-Stationary Landcover

Before climate change simulations are conducted, landcover files were generated with the landcover simulator module and used in WATFLOOD from 1971 – 2000 (using 1970 for model spin-up) without climate change (i.e. using historical meteorological forcing). The purpose is to gain an understanding of the degree to which shifts in the hydrologic regime (magnitude and/or timing) are associated with landcover changes as opposed to uncertainty under climate change. Average annual hydrographs on Figure 39 show the green envelope of non-stationary landcover representing the range in 'possible' streamflow simulated from 45 iterations of the landcover simulator module. These results are for the outlet of the WRB at Pine Falls (WSC gauge# 05PF069).

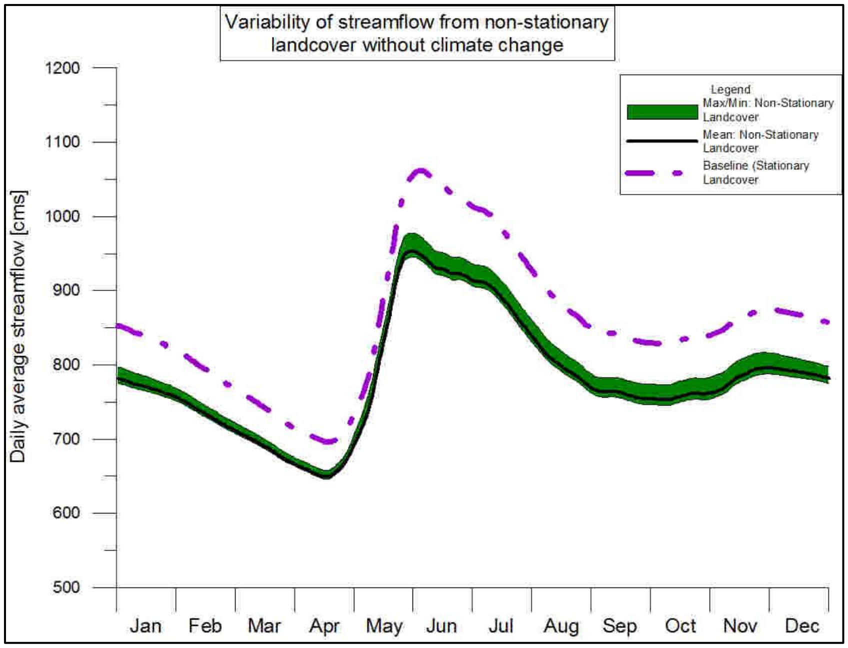

Figure 39 - Annual average hydrographs for WATFLOOD simulations under historical conditions at Pine Falls

The thick black line is the mean of the non-stationary landcover simulations, and the purple dashed line the 'baseline' run with stationary (ortho-image) landcover. Table 24 contains statistics regarding these simulations on a seasonal and annual basis. Included in the table are the mean, max, min, standard deviation of the mean, and percent change from the baseline for the non-stationary landcover simulations. Overall, the non-stationary landcover simulations result in ~8.6% lower flows as compared to stationary landcover. Cumulative distribution functions (CDFs) of these simulations are shown on Figure 40 using all flows in the simulations, not average annual values as on the previous figure. A kernel smoothing function (Gaussian) was used to estimate these CDFs. The 50th percentiles of stationary and non-stationary simulations are 816 cms and 741 cms respectively, and are both lower than the observed flow 50th percentile of 880 cms. The CDF's shape for stationary and non-stationary simulations are the same, indicating that differences between the two simulations are primarily by volume.

Table 24 - Seasonal and annual statistics for WATFLOOD simulations under historical conditions at Pine Falls

	Observed	Baseline	Non-Stationary Landcover	
	Flow [cms]	Flow [cms]	Flow [cms]	% Change from baseline
DJF				
Mean	945.4	833.9	765.4	-8.2
Max	971.5	874.0	816.2	-6.6
Min	914.5	770.2	710.1	-7.8
Std deviation	11.2	31.5	24.2	-23.2
MAM				
Mean	956.8	778.0	724.9	-6.8
Max	1049	1052.0	977.6	-7.1
Min	908.0	695.9	645.5	-7.2
Std deviation	35.7	100.5	89.7	-10.7
JJA				
Mean	886.2	968.1	872.7	-9.8
Max	1007	1062.2	977.5	-8.0
Min	715.1	849.0	762.9	-10.2
Std deviation	96.8	68.4	57.9	-15.3
SON				
Mean	835.7	843.9	766.4	-9.2
Max	948.1	874.1	816.7	-6.6
Min	704.3	827.8	744.9	-10.0
Std deviation	68.4	14.0	13.3	-5.3
Overall				
Mean	906.0	856.1	782.5	-8.6
Max	1049	1062.2	977.6	-8.0
Min	704.3	695.9	645.5	-7.2
Std deviation	78.9	94.1	77.9	-17.2

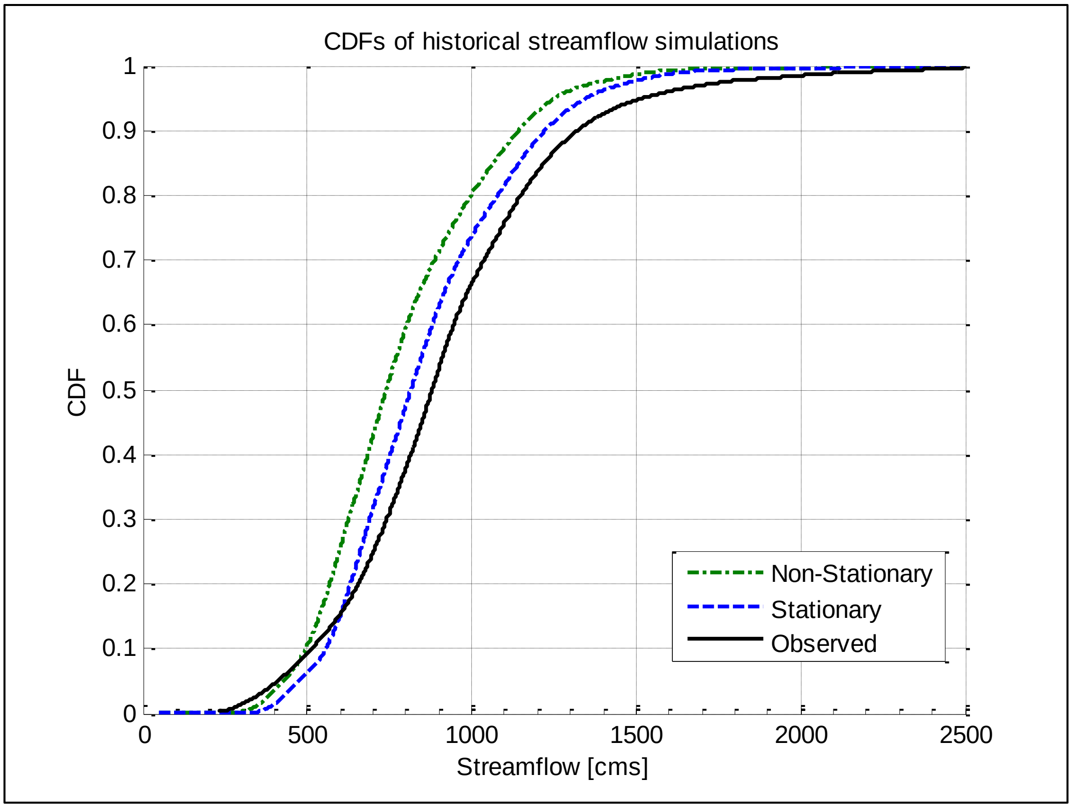

Figure 40 - Historical CDFs of non-stationary and stationary landcover simulations, and observed streamflow at Pine Falls

CDF shape of observed flows is different from that of the two simulations, showing higher flows than the simulated above the 20th and 10th percentiles for stationary and non-stationary landcover, respectively. This difference in CDF shape indicates that differences in volume between simulated (stationary and non-stationary) and observed vary between higher and lower flows.

Lower flows under non-stationary landcover (compared to stationary) are consistent with literature that has examined changes in the flow regime due to increased forest cover, specifically of the deciduous type (Brown, et al., 2013; Eschner & Satterlund, 1966). These studies have attributed decreased flows to increased evapotranspiration (ET) from larger leaf areas found with the transition to deciduous forests.

The landcover changes in this study as described in Chapter 5 involve significant transitions from coniferous to mixed forests over time, and transition of landcover in post-fire grids to predominantly mixed. Deciduous trees present in mixed forest have larger leaf areas and therefore interception capacity relative to other landcover types (reflected in WATFLOOD parameters), which results in increased ET losses in the years (and decades) following a forest fire. This is particularly notable if the dominant landcover pre-fire was coniferous forest. While results from Pomeroy et al. (2012) suggest that while flows can increase immediately after a forest fire, decreased flows are likely to occur in the decades following (i.e., the regeneration period). This phenomenon is illustrated on Figure 41 by the output of one of the non-stationary landcover simulation for a single headwater grid relative to cumulative evapotranspiration (ET) loss. While the simulation begins in 1970, shown on the plot is 1978 – 1981, and the year 2000. Since in this particular simulation a forest fire occurs in 1980 and extends the entire grid, the plots can be inspected preceeding the fire (1978 – 1979), immediately after (1980), and after regeneration (2000).

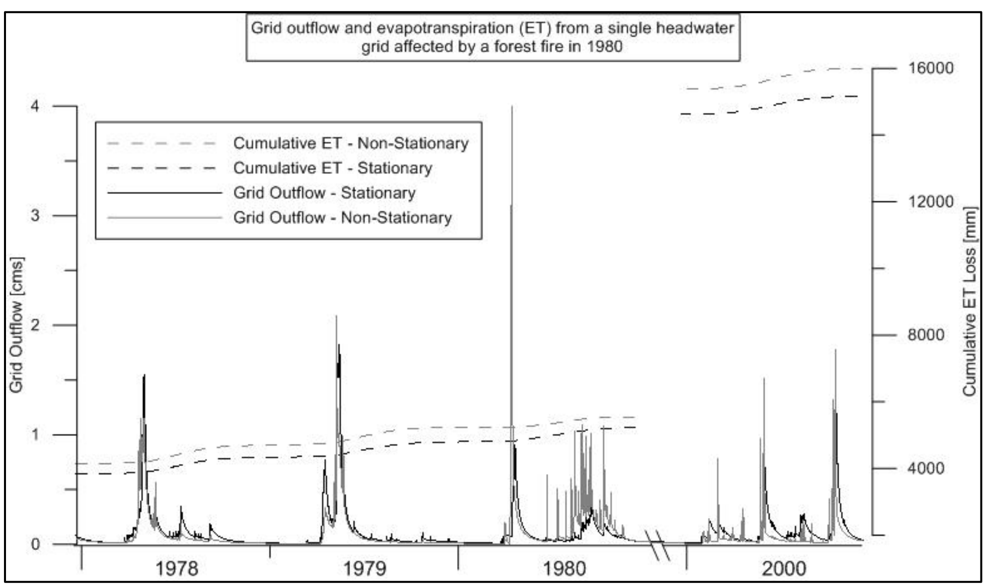

Figure 41 - Streamflow relative to evapotranspiration (ET) for a single headwater grid before and after a forest fire

Measured streamflow is not included as no hydrometric gauge is located in this headwater grid, and given the intent is to show the relative differences in modelled flow that occur between stationary and non-stationary landcover. In the two years preceeding the fire, there is evidence of lower grid outflow (i.e., runoff) ocurring solely from the natural change component of the landcover simulator module due to mixed forest being added to the dominant coniferous forest of that grid. Immediately after the fire, burned area in the grid results in higher flow and a faster runoff response for the non-stationary landcover simulation. About twenty years after the fire, while the runoff responses are still faster during peak flow, there is an overall reduction in flow. From the plot of cumulative ET, increased ET losses (i.e., increased difference between simulations) are a significant factor in this flow reduction. These differences between stationary and non-stationary landcover for both flows and ET are quantified in Table 25, over the entire simulation (1970 – 2000).

Table 25 - Differences in volume of runoff and ET for a headwater grid in the WRB between stationary and non-stationary simulations

Difference in Volume (Stationary – Non-Stationary) [m^3]	Difference in Evapotranspiration (ET) Losses (Stationary – Non-Stationary) [m^3]	Amount of Volume Difference Attributed to ET [%]
-14,450,000	13,830,000	95.70

From this table, 95.7% of the discrepancy in flows between non-stationary and stationary landcover simulations can be explained by ET losses. Specifically, in this case, caused by gradual shifts in landcover from the domimant coniferous class to mixed. The greater amounts of broadleaf trees present in mixed forest consequently yield more ET loss to the atmosphere than their conifer counterparts.

As seen on Figure 41, increased peak flows are represented in the model for non-stationary landcover immediately following a forest fire. These peak flows are averaged-out in the annual hydrographs for the whole watershed and result in overall decreases in flow as shown on Figure 39 and in Table 24. So while the basin-scale average annual hydrograph experiences only decreases in flows (Figure 39), grid-scale hydrologic responses to landcover change (Figure 41) are occurring in both directions, as expected (through forest fires and natural change).

The comparison of percent change in flow from observed for stationary and non-stationary landcover simulations are shown on Figure 42, providing an indication of uncertainty resulting from landcover change. Uncertainty can be defined as the width of the boxes, or the interquartile range (IQR). Whiskers in the figure represent data within IQR*1.5, in which anything outside is considered an outlier.

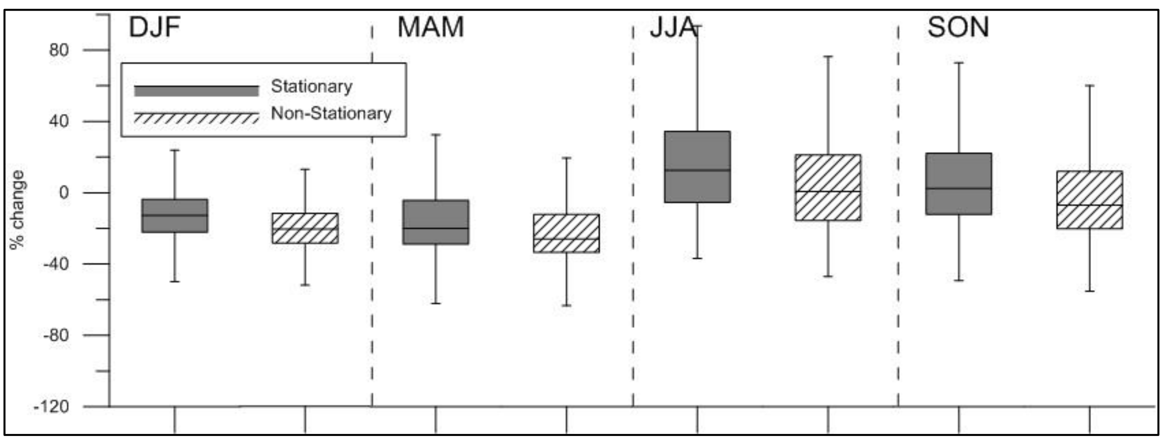

Figure 42 - Seasonal percent change of stationary and non-stationary landcover simulations relative to observed flow under historical climate conditions at Pine Falls

Lower flows with non-stationary compared to stationary landcover are evident from Figure 42, consistent with the average annual hydrographs from Figure 39. Since all simulated flows are plotted in this figure, not calculated average annual values, visualizing the extent of extreme high or low flows is made possible. For both simulations, the median and quartiles range from positive and negative percent changes, the greatest increases in flow occur in summer (JJA). Stationary landcover experiences flows up to 90% greater than observed, with non-stationary landcover up to 70% greater (upper whiskers). In contrast, the lowest flows are more consistent through the seasons ranging from 40% to -60% from observed (lower whiskers). The level of uncertainty (i.e. relative widths of boxes) in streamflow between non-stationary and stationary landcover simulations remains relatively unchanged. The greatest change in IQR occurs in spring (MAM), with stationary landcover being ~3% wider than non-stationary. So while non-stationary landcover simulations experience lower flow than assuming stationarity, the widths of the boxes (i.e., uncertainty) remains relatively constant. Therefore incorporating non-stationary landcover primarily affects runoff volume, as opposed to runoff uncertainty. While this is true for the above simulations using historical meteorological forcing, how climate change projections are affected by non-stationary landcover in the WRB is the focus of the next section.

6.2 Streamflow Simulation under Climate Change with Non-Stationary Landcover

Using the climate deltas from Section 3.4, landcover files are generated and WATFLOOD simulations are conducted under climate change. Results for the scenarios in the 2050s and 2080s are described in this section, with discussion on the differences between stationary and non-stationary landcover simulations. Additionally, the potential effects of climate change on streamflow in general for the Winnipeg River basin are discussed.

6.2.1 2050s: B1, A1B, and A2 Scenarios

The annual average hydrographs produced by WATFLOOD for the B1 CGCM3.1 emissions scenario in the 2050s are shown on Figure 43, with non-stationary and stationary landcover.

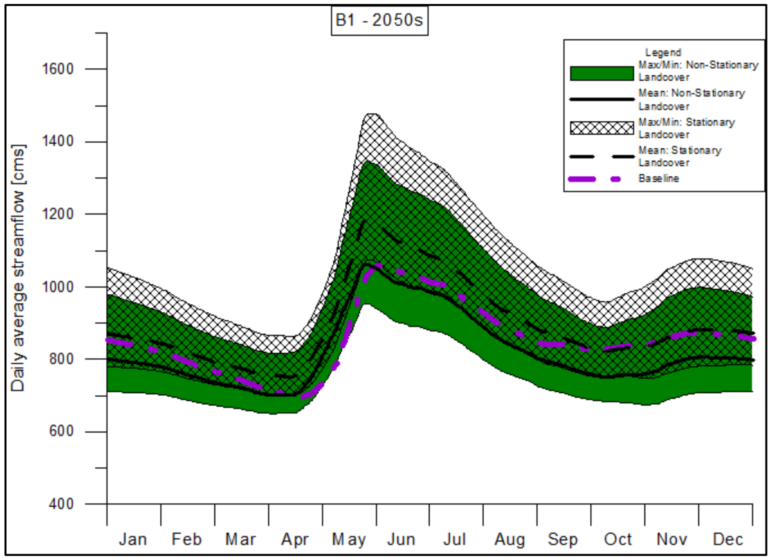

Figure 43 - Annual average WATFLOOD hydrographs for the CGCM3.1 B1 scenario in the 2050s at Pine Falls

The runoff envelopes for this scenario are the result of delta values from five GCM runs, each initialized with different initial conditions. The envelopes on Figure 43 represent the maximum and minimum average annual values from these hydrographs.

Figure 43 is consistent with the results from Section 6.1 in that flows decrease with non-stationary landcover relative to simulations with stationary landcover. The stationary landcover mean (dashed black line) average annual hydrograph is greater than the modelled baseline (dashed purple line) for the entire year, however, indicating an overall increase in future runoff with the stationarity assumption. For non-stationary landcover, the mean hydrograph (solid black line) is reasonably close to the baseline in summer (JJA); exhibiting lower average runoff during fall (SON) and winter (DJF), and higher average runoff during spring freshet (MAM). This implies that increases in future precipitation are offset by increasing water loss via ET resulting from combined increases in both temperature and water availability. In Appendix 6, tables for this scenario (and all others) describing the seasonal variation in mean, maximum, minimum, and standard deviation on the mean are provided. A significant number of non-stationary landcover simulations are, however, greater than the baseline (more area of the green envelope curve lying above the baseline), indicating that higher flows are possible with this scenario. When comparing to historical simulations on Figure 39, the significantly wider envelopes both with stationary and non-stationary landcover under climate change are evident. This increase in variability is largely a result of the differences in delta values from the CGCM3.1 runs, with each run having different initial conditions for the GCM despite being in the same scenario. Also, this range helps represent the uncertainty in natural climate variability, which is non-linear in nature.

Simulation results for the A1B and A2 scenarios in the 2050s are presented on Figure 44 and Figure 45, and represent middle-ground and pessimistic scenarios respectively. These scenarios show similar trends to the B1 scenario: non-stationary landcover (green envelope) predicts lower flows, on average, than stationary landcover (hatched envelope) with climate change.

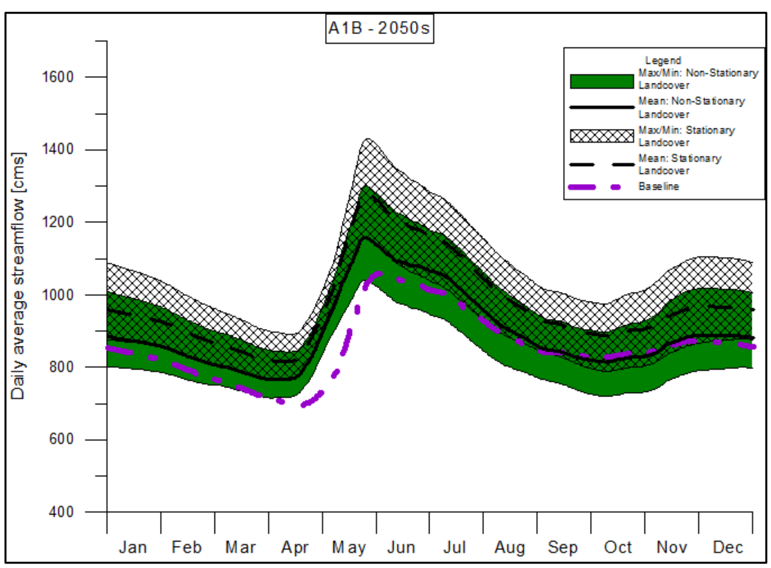

Figure 44 - Annual average WATFLOOD hydrographs for the CGCM3.1 A1B scenario in the 2050s at Pine Falls

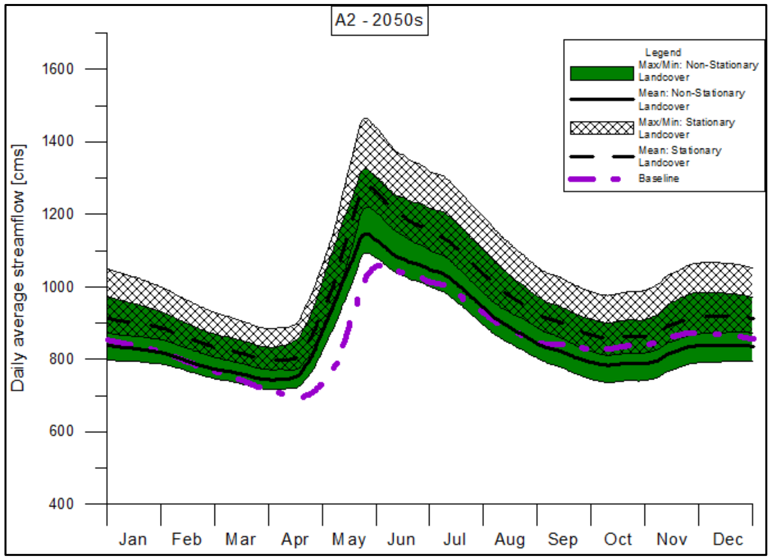

Figure 45 - Annual average WATFLOOD hydrographs for the CGCM3.1 A2 scenario in the 2050s at Pine Falls

Streamflow envelopes for both non-stationary and stationary landcover simulations for the A1B and A2 scenarios are narrower than those predicted under the B1 scenario (Figure 43). While these plots provide a means to compare stationary and non-stationary landcover within each scenario individually, differences over all scenarios are best examined using the box-whisker plots provided on Figure 46, showing the percent change in streamflow from the baseline period (1971 – 2000).

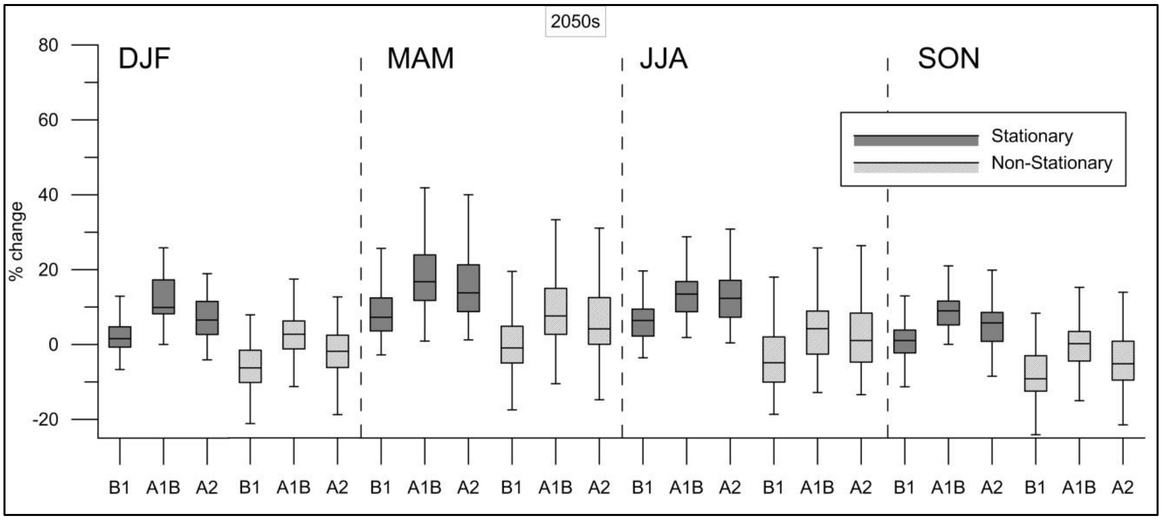

Figure 46 - Seasonal box-whisker plots of the B1, A1B, and A2 CGCM3.1 Scenarios in the 2050s at Pine Falls

Simulations under the A1B and A2 emissions scenarios show greater increases from the baseline during spring freshet (MAM) than the B1 scenario. Increases in freshet flow (MAM) can be explained upon examination of the delta values from Section 3.4. The A1B and A2 scenarios tend to exhibit higher precipitation in winter (DJF) than the B1, as well as increased temperatures for winter and spring (MAM). Such future trends will increase the likelihood of snowpack accumulation throughout the winter, and an earlier spring runoff period than the B1 scenario. Interestingly, fall (SON) delta values show the greatest variability amongst the seasons, while exhibiting little variability in flows (Figure 46). Precipitation increases offset by greater evaporation rates in fall (Slota, 2013), could be a factor in this. Also in late fall, particularly November, snow is common in the WRB, diverting the impact of precipitation changes until spring.

Uncertainty Introduced by Non-Stationary Landcover in the 2050s

Under climate change conditions in the 2050s, differences in projected runoff between stationary and non-stationary landcover is significant with every scenario. From Figure 46 it is clear that there is a general decrease in flows with non-stationary landcover with respect to stationary consistently across all scenarios. Spring (MAM) flows with the A1B scenario have the greatest increase in flow from the baseline in Figure 46, having a median of 16.8% increase under stationary landcover. This reduces to a 7.60% increase after incorporating non-stationary landcover. The greatest decreases in median flows occur in the fall (SON) months for the B1 scenario. Median streamflow under non-stationary conditions in this scenario fall to -9.17% of the baseline, while assuming stationarity projects an increase of 1.07%.

In Section 6.1, it was found that introducing non-stationary landcover into historical simulations did not significantly change the level of uncertainty in streamflow simulations, and that uncertainty was consistent among seasons. Under climate change conditions, however, in the 2050s (Figure 46), the range in possible streamflow (i.e. uncertainty) increases with non-stationary landcover. The interquartile range (IQR) for the B1 scenario in summer (JJA) increases from 7.23% to 12.1% by introducing non-stationary landcover. Other scenarios show similar increases in uncertainty this season, as well as in the fall (SON), with the IQR for the B1 scenario in fall changing from 6.10% to 9.45% when incorporating non-stationary landcover. The summer and fall months experienced the greatest changes in uncertainty with non-stationary landcover, with the winter (DJF) and spring (MAM) experiencing smaller magnitude changes. The spring shows larger amounts of uncertainty in streamflow, not solely attributable to landcover as the uncertainty exists within the stationary runs as well (12.2% and 12.3% for stationary and non-stationary respectively for A1B).

6.2.2 2080s: B1, A1B, and A2 Scenarios

For the 2080s time period Figure 47, Figure 48, and Figure 49 show the average annual hydrographs under climate change for the B1, A1B, and A2 scenarios respectively. Corresponding seasonal and annual statistics can be found in Appendix 6.

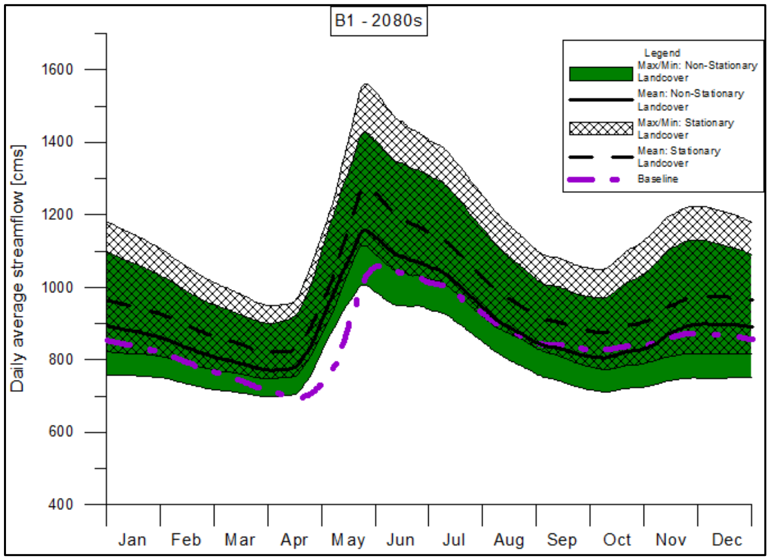

Figure 47 - Annual average hydrographs for the B1 scenario in the 2080s at Pine Falls

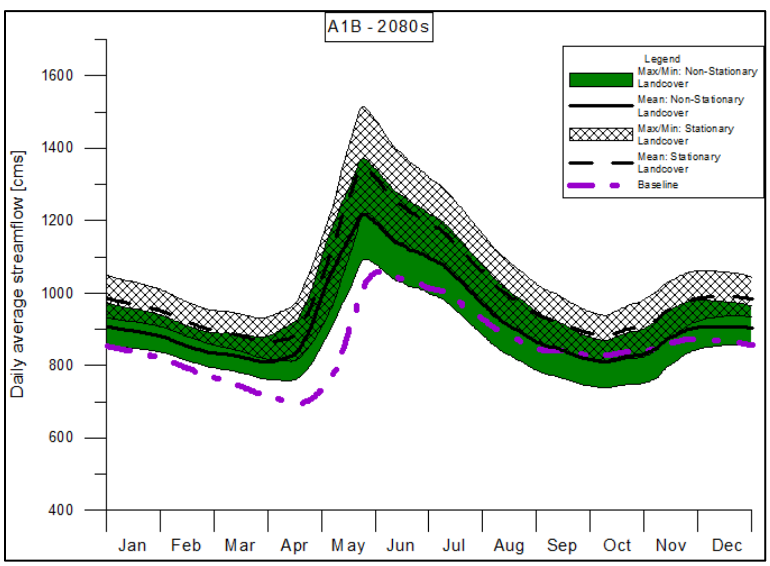

Figure 48 - Annual average hydrographs for the A1B scenario in the 2080s at Pine Falls

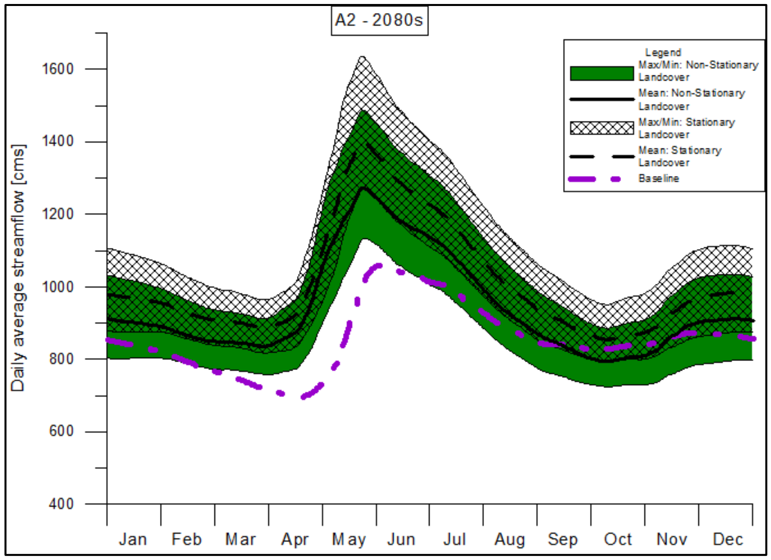

Figure 49 - Annual average hydrographs for the A2 scenario in the 2080s at Pine Falls

What is immediately apparent with the B1 scenario in the 2080s, as compared to the 2050s, is the larger mean and maximum streamflow for non-stationary and stationary landcover simulations, widening the overall envelope. While minimum flows show negligible increases between eras, maximums increase from 1063 cms to 1428 cms for non-stationary landcover, and 1187 cms to 1562 cms for stationary landcover. The means also show an increase of 823.3 cms to 897.2 cms, and 899.3 cms to 970.8 cms for non-stationary and stationary simulations respectively. These trends culminate into the mean overall streamflow for non-stationary landcover being very close to the baseline by July (Figure 47) while increasing by spring freshet. Similarly the A1B scenario has higher spring freshet flow than the baseline, while approaching the baseline by late July. One major difference, however, is that while overall maximum flow for non-stationary landcover tends to increase by a significant amount between eras (~70 cms), the mean flow show much lower increases (~27 cms). This is in contrast to the B1 scenario in that overall mean flow also increases by a large amount between eras (~74 cms for non-stationary landcover). The overall trends for the A2 scenario in the 2080s are consistent with the 2050s; the magnitudes of potential streamflow shifts under this scenario are very large. Being the most pessimistic in terms of GHG emissions, this scenario also commands the greatest increases in temperature and precipitation, of up to 7°C and 70%, respectively (Figure 9). With overall maximum daily average flows (over 30 years) projected to be 40% and 54% higher than the baseline for non-stationary and stationary simulations respectively, future generations will surely experience the consequences of a very different hydrologic regime, at least in spring and early summer.

Percent changes in streamflow relative to baseline flow can be viewed on Figure 50 as box-whisker plots. These plots are divided seasonally, and show the increasing level of uncertainty in streamflow among each scenario. The A2 scenario exhibits the most uncertainty, followed by A1B and B1. As in the 2050s, the spring months (MAM) experience the greatest amount of uncertainty in streamflow (stationary and non-stationary landcover).

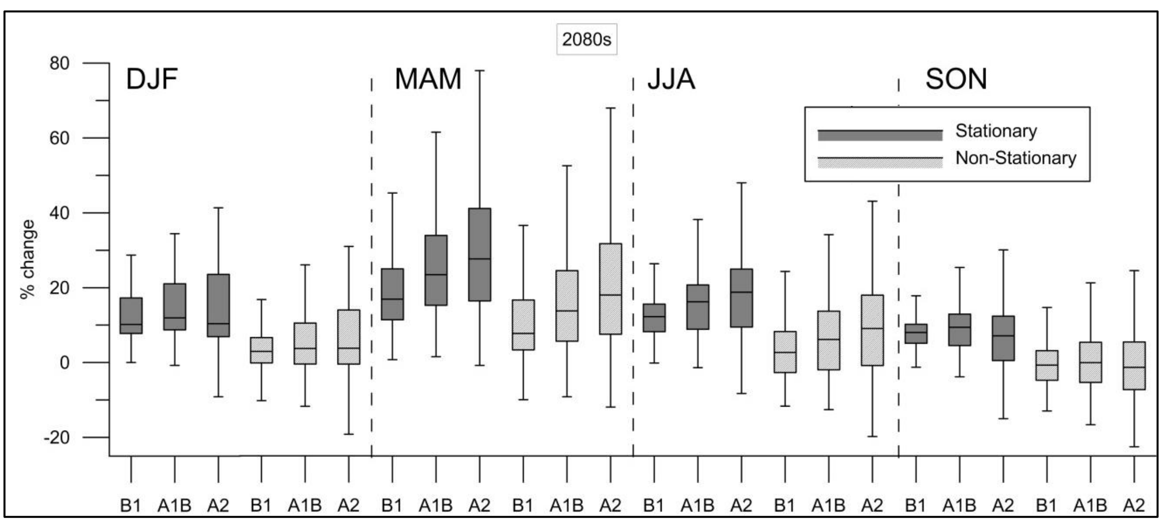

Figure 50 - Seasonal box-whisker plots of the B1, A1B, and A2 CGCM3.1 Scenarios in the 2080s at Pine Falls

Uncertainty Introduced by Non-Stationary Landcover in the 2080s

While spring (MAM) flow exhibits the greatest amount of uncertainty as seen on Figure 50, there is little change between stationary and non-stationary landcover simulations. Summer (JJA) and fall (SON) months however show more uncertainty in flows with non-stationary landcover than assuming stationarity. The greatest increases in uncertainty occur with the A1B scenario in the fall, with the IQR increasing from 11.9% to 15.7%. While these trends in uncertainty for spring, summer, and fall months are consistent with the 2050s, interestingly winter (DJF) is the opposite. The B1 scenario's IQR in winter decreases from 9.47% to 6.77% with the incorporation of non-stationary landcover. The A1B and A2 scenarios also experience a decrease (12.3% to 10.9% and 16.6% to 14.4% respectively). A direct comparison of overall (non-seasonal) uncertainty introduced by non-stationary landcover in the 2050s and 2080s is shown on Figure 51.

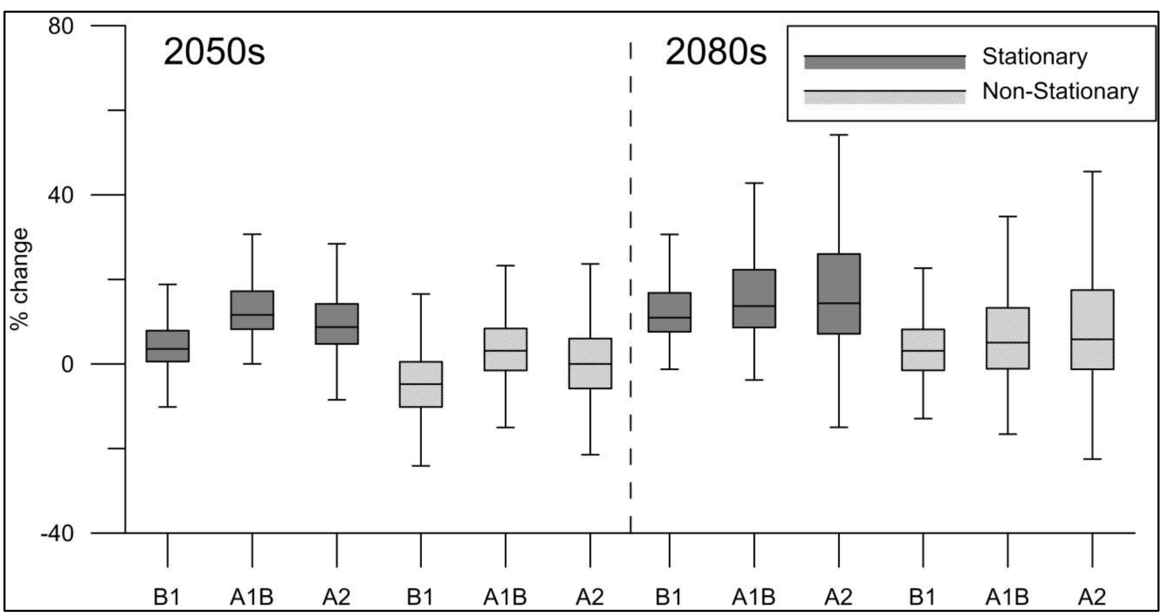

Figure 51 - Box-whisker plots of the B1, A1B, and A2 CGCM3.1 Scenarios in the 2050s and 2080s at Pine Falls

While not taking seasonality into account, there is an increase in uncertainty from introducing non-stationary landcover in most cases. The magnitude is not as high as previously discussed as changes in streamflow over the entire year are considered. In the 2050s the B1 and A2 show the most changes in uncertainty from introducing non-stationarity, from 7.31% to 10.7% and 9.47% to 11.8% respectively. The B1 scenario only experienced a modest increase in uncertainty from 8.9% to 9.9% with non-stationarity. The 2080s simulations show less uncertainty associated with non-stationary landcover. Increases in IQR of 9.22% to 9.67% and 13.7% to 14.4% for the B1 and A1B scenarios reflect this. The A2 actually experiences a slight decrease in uncertainty from 18.9% to 18.7% with non-stationarity. So while a significant amount of uncertainty exists from introducing non-stationarity in the 2050s, it becomes less pronounced in the 2080s.

6.3 Trends in Climate Change Results and Uncertainties in the context of Hydroelectric Generation

All simulations tend towards higher flows under climate change during the spring freshet period (MAM), but diverge with both higher and lower flows (depending on model and scenario) throughout the rest of the year. Since it is unclear which emissions scenario will best represent the future, combining all scenarios into one runoff prediction envelope is useful for gaining an understanding of the possible ranges in streamflow under climate change. Annual average WATFLOOD hydrographs for all scenarios are presented on Figure 52 and Figure 53 for the 2050s and 2080s, respectively. These hydrographs show the percent change in flow as compared to the baseline, and are separated by emissions scenario. They also provide a direct comparison between non-stationary and stationary landcover, in terms of percent increase or decrease in flow. For reference, average annual hydrographs for all scenarios combined are included in Appendix 7.

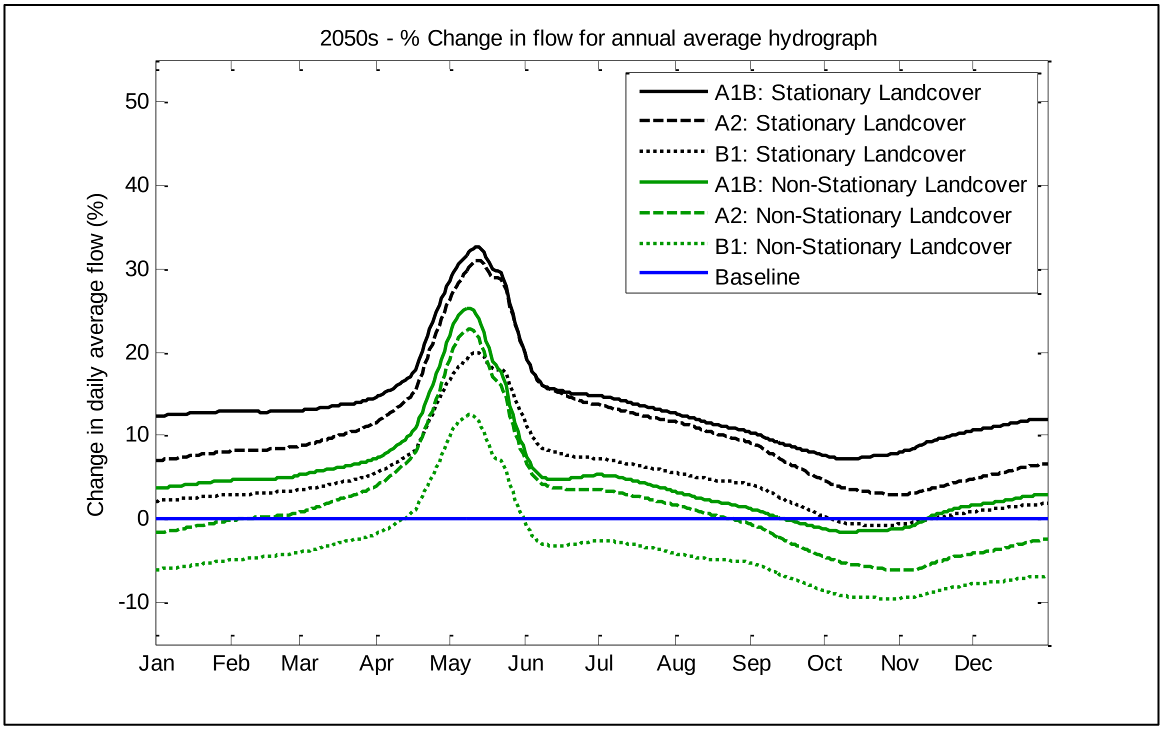

Figure 52 - Percent change in average annual flow for three CGCM3.1 emissions scenarios in the 2050s at Pine Falls

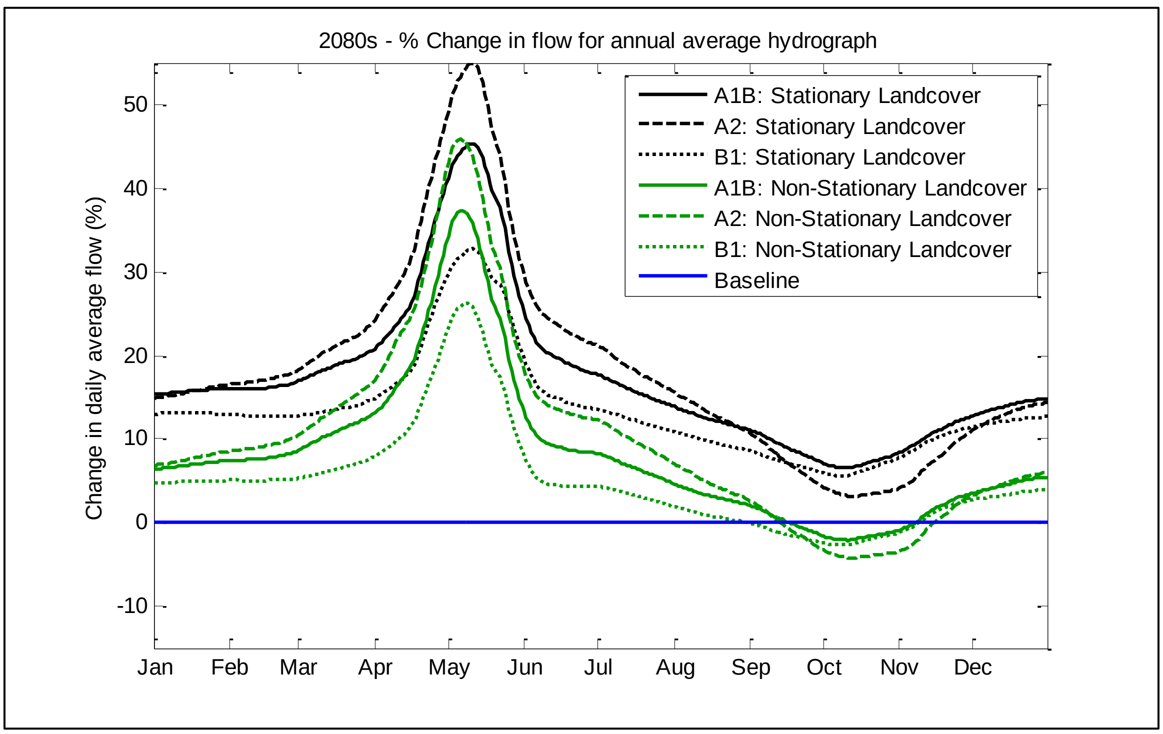

Figure 53 - Percent change in average annual flows for three CGCM3.1 emissions scenarios in the 2080s at Pine Falls

By the 2050s significant shifts in streamflow are anticipated, regardless if stationary or non-stationary landcover is assumed. Simulations generally tend to predict larger increases and decreases over the year, with the range in possible runoff increasing into the 2080s (Figure 63).

One thing that is most obvious by the 2080s is increased significance of the annual snowmelt event. For both simulations (stationary and non-stationary), the greatest changes in annual flow occurs during the spring freshet, and most variability in projections as seen in Section 6.2. Stationary landcover conditions show the greatest increases (up to 55% for A2), with non-stationary simulations remaining closer to the baseline and showing less change in future runoff. This trend is also seen on Figure 50 with upper whiskers of 78% and 68% increase from the baseline for stationary and non-stationary landcover, respectively in the spring (MAM) months.

On Figure 9 it was shown that the 2050s A1B and A2 scenarios have similar delta values and tended to diverge by the 2080s. The consequences of this are apparent on Figure 52 and Figure 53 for the 2050s and 2080s, respectively. For the 2050s the percent changes in flow are quite similar during the spring freshet (with A1B slightly greater than A2), while by the 2080s, no such similarities exist. This holds true for both stationary and non-stationary landcover simulations.

Figure 54 to Figure 56 provide a 'timeline' of percent change in runoff under climate change and are indicators of increased uncertainty under climate change introduced by the non-stationary landcover assumption. For these plots uncertainty is represented as the width of envelope, and its change from present day to 2080 can be viewed.

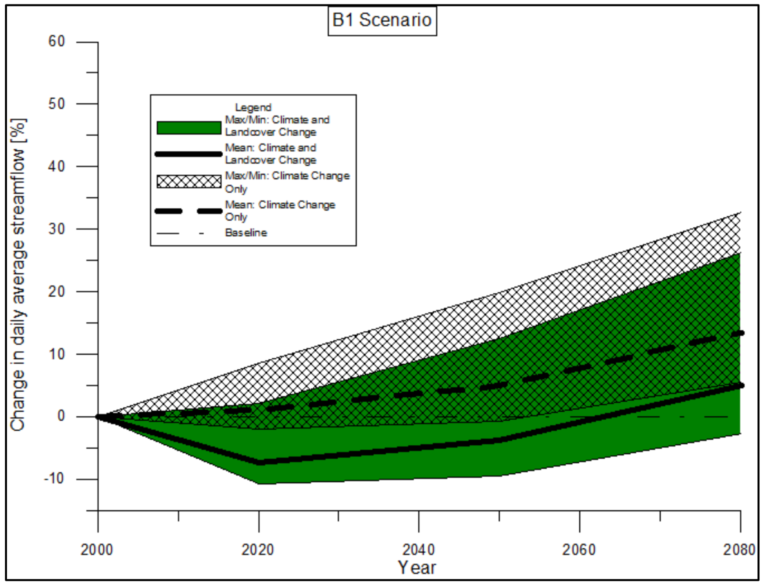

Figure 54 – Trends in daily average streamflow for the CGCM3.1 B1 scenario, as a function of year at Pine Falls

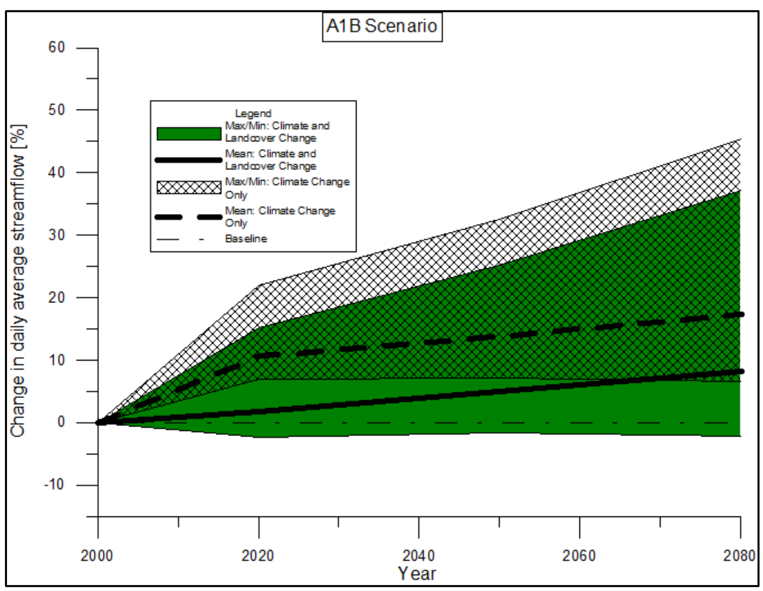

Figure 55 - Trends in daily average streamflow for the CGCM3.1 A1B scenario, as a function of year at Pine Falls

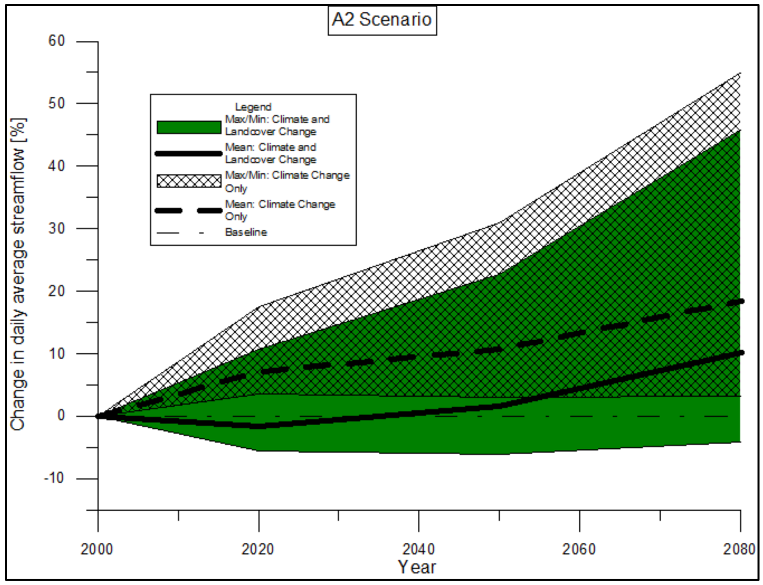

Figure 56 - Trends in daily average streamflow for the CGCM3.1 A2 scenario, as a function of year at Pine Falls

For these plots, the equivalent 2020s runs were conducted to provide a more realistic timeline of future trends from the year 2000 onwards. Therefore four points are included on the plots, 2000, 2020, 2050, and 2080 with linear interpolation between. The most optimistic scenario in terms of GHG emissions (B1, Figure 54), experiences the most significant decrease in runoff, then gradually increases (crossing the baseline to a projected runoff increase by ~2060 for non-stationary landcover). In contrast, the most pessimistic A2 scenario crosses the baseline in ~2030, projecting more significant runoff increases. While a 'pessimistic' scenario in terms of GHG emissions, an increased water supply can be beneficial for hydroelectric operations. All scenarios, with stationary and non-stationary landcover, experience widening of the envelopes into the future with climate change.

There are clear discrepancies between the stationary and non-stationary landcover simulations. The assumption of landcover stationarity would lead to the conclusion that flows will surely increase under climate change regardless of scenario. Whereas the results of this thesis find that alteration of the landscape can significantly affect the hydrologic regime.

In the WRB, the consequence is an offsetting effect where precipitation increases projected by CGCM3.1 under changing landcover do not necessarily result in higher flows relative to stationary simulations. Therefore, it is clear that lower (than baseline) future runoff is also likely to occur and should be taken into account for long term planning, including the design of hydroelectric and control facilities. CDFs of simulated streamflow (using a Gaussian kernel smoothing function) are shown below on Figure 57 and Figure 58 for the 2050s and 2080s respectively. The CDFs indicate the exceedance probability of streamflow under climate change for all scenarios (B1, A1B, A2) combined. The 50th percentiles for stationary and non-stationary flow are 884 cms and 805 cms respectively for the 2050s, and are 938 cms and 861 cms respectively for the 2080s. Also included on the figures is the CDF of all simulated flows in the 2050s, combining both stationary and non-stationary flows (black line). This is included to address the fact that uncertainty inherent in the generation of landcover with the pre-processing module can naturally propagate into the final simulation results (in addition to CGCM and WATFLOOD model uncertainties).

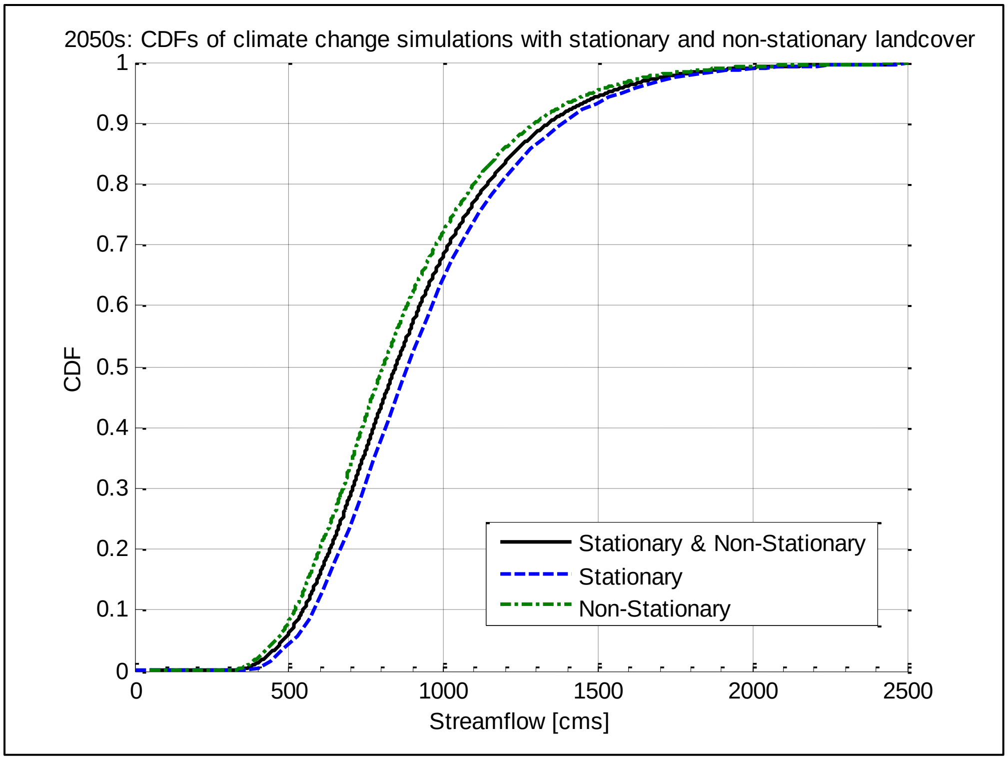

Figure 57 – 2050s climate change CDFs of non-stationary and stationary landcover simulations (B1, A1B, A2 CGCM3.1 scenarios combined) at Pine Falls

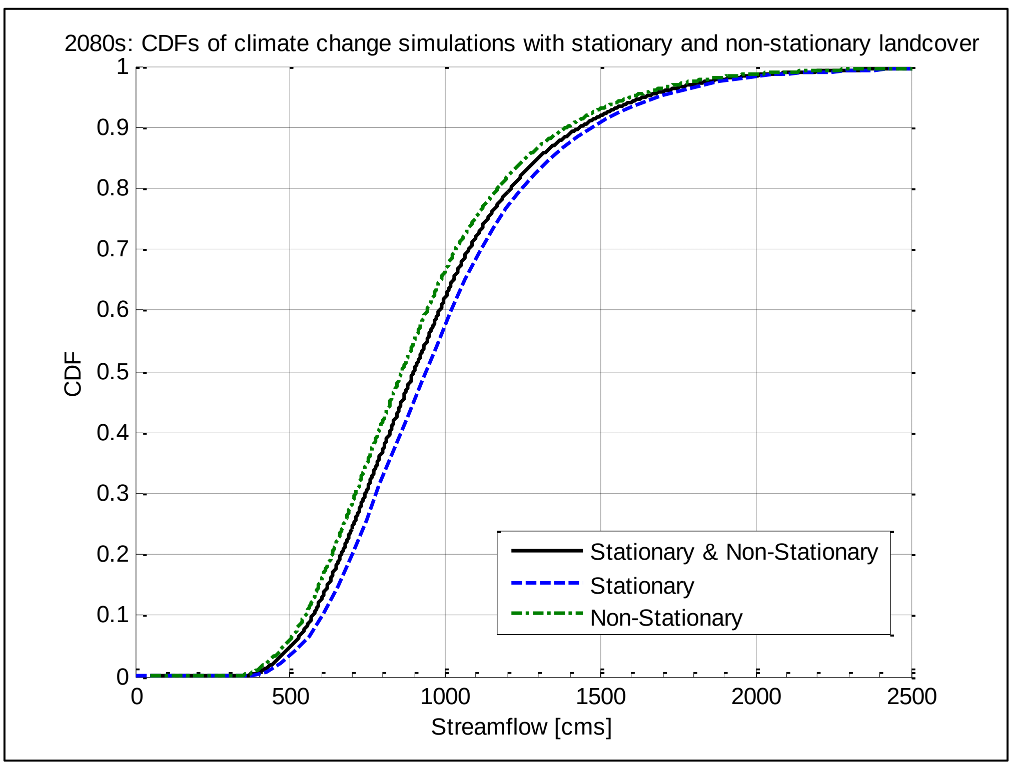

Figure 58 - 2080s climate change CDFs of non-stationary and stationary landcover simulations (B1, A1B, A2 CGCM3.1 scenarios combined) at Pine Falls

It is therefore not unreasonable, for the purposes of policy and future hydroelectric design, to include the stationary landcover simulations in the overall envelope of possible flow regimes. Flows from stationary simulations would be less likely to occur, as changes in the landscape tend to offset the effects of climate change, resulting in lower flows with non-stationarity than with stationarity. The most confidence should be placed in the non-stationary landcover simulation envelope, however, the extreme high flows of the stationary simulations should not be considered outside the realm of possibility. From Figure 54 to Figure 56, a much wider envelope of future streamflow is evident when combining stationary and non-stationary results. With this approach, examining streamflow for stationary, non-stationary, and then combined will assist in establishing the sensitivity of the landcover stationarity assumption for future design.

In this chapter, output from the landcover simulator module was run using WATFLOOD in historical and climate change contexts. In the former, changes in volume and uncertainty in streamflow were investigated and quantified solely as a result of landcover change using historical temperature and precipitation. Volume of flow was most affected by non-stationary landcover, with overall reductions in mean flow of -8.6% as compared to stationary landcover. This decrease was largely accounted for by increased evaporation rates resulting from gradual increases in mixed forest in the WRB as opposed to coniferous forest. The uncertainty in streamflow was relatively unchanged with non-stationary landcover under historical conditions, but did experience increases in uncertainty under climate change. Fall flows in the 2080s A2 CGCM3.1 scenario had the greatest increases in uncertainty with non-stationary landcover, with the IQR of percent changes in flows from the baseline increasing from 11.9% to 15.7%. Under climate change conditions, flows are projected to increase in the WRB overall from increased precipitation, regardless if landcover stationarity or non-stationarity is assumed. The main reason for the difference between these assumptions, based on the results of this thesis, is attributed to changes in volume of flow resulting from increased precipitation. Lower flows with non-stationary landcover (as compared to stationary) are expected, with the 50^{th} percentile decreasing from 884 cms to 805 cms by the 2050s. For the 2080s, 50^{th} percentile flows for stationary and non-stationary landcover are 938 cms and 860 cms respectively, which is higher than the baseline periods 50^{th} percentile of 815.7 cms. If both stationary and non-stationary results are combined, 50^{th} percentile streamflows are 845 cms and 899 cms for the 2050s and 2080s, respectively.

Chapter 7 Conclusions and Recommendations

In this chapter, results of this thesis are summarized, and relevant conclusions outlined. Significance of this research is also discussed in terms of incorporating this new methodology to simulate non-stationary landcover as well as the results pertaining to hydroelectric generation. Recommendations to improve on the methodology, as well as to increase understanding of the effects of non-stationary landcover in the greater Nelson-Churchill River basin are also discussed.

7.1 Summary of Conclusions

From the historical landcover change analysis of Chapter 4, module development and testing of Chapter 5, and application of the module with WATFLOOD climate change simulations in Chapter 6, several conclusions can be made for this thesis and are outlined below:

- Using a semi-automated classification method, it is possible to classify historical satellite imagery into hydrologically-distinct land classes in order to simulate non-stationary landcover for historical hydrologic analysis at the sub-basin scale. This method can improve model results in sub-basins experiencing forest fires, demonstrating the importance of using representative landcover from the modelled time period in WATFLOOD. Additionally, model output uncertainty is very sensitive to choice of landcover for the stationary simulations;

- Non-stationary landcover can be modelled through logistic regression and a generalized extreme value distribution for forest fire occurrence and extent. First order Markov chains can be used for simulation of fire regeneration and natural, gradual change. Applied to the WRB, this methodology results in increased amounts of forest fires under climate change, and a gradual shift in landcover from coniferous to mixed forest. Incorporating climate change to temperature and precipitation inputs also increased the uncertainty in coupled forest fire occurrence and extents produced in the model.
- For historical non-stationary landcover simulations in the entire WRB, 50th percentile flow decreases to 741 cms from the baseline (stationary) case of 816 cms. This is a consequence of increased evapotranspiration from mixed forest being the primary replacement landcover in forest fire regenerated areas, as well as produced in the natural change component. While stationary and non-stationary landcover simulations differ in flow volume, relative uncertainty (i.e. range) in simulated flow remains unchanged.
- With climate change, streamflow increases are expected for all scenarios in the 2080s, with the exception of the fall (SON) season. The largest projected increases occur during the spring freshet period, up to 55% with the A2 stationary landcover scenario, or 45% with non-stationary landcover (Figure 53). The 2050s exhibits more possibilities of decreased flows throughout the year, with the greatest decreases similarly occurring from September to November. Therefore in the future, flows in the WRB can potentially decrease for a period of time through the 2050s, while gradually increasing by the 2080s;

- In contrast to historical simulations, non-stationary landcover is a source of uncertainty in summer and fall climate change projections. The IQR of percent change in flow from the baseline increase from 11.9% to 15.7% when incorporating non-stationary landcover for fall A2 flows in the 2080s. So while changes in volume are still the dominant source of change when incorporating non-stationary landcover, uncertainty can also change. Propagation of data input uncertainty can be a factor in this, considering the wide range of possible burned area under climate change on Figure 34. This figure was a result of 1000 test simulations in Matlab, with fewer simulations actually conducted under climate change simulations in WATFLOOD. However despite this, volume is still the likely dominant source of change when non-stationary landcover is incorporated.

7.2 Significance of Findings

By introducing a novel approach for incorporating non-stationary landcover into a hydrological model, this thesis makes a significant contribution to the field of water resources engineering. It has been shown that by using a relatively small number of well-established methods for simulating landcover, they can be combined, linked to climate model output, and used to dynamically simulate landcover for long periods of time as direct input into a hydrological model. This methodology provides a first step to eliminating the assumption of stationary landcover in long-term hydrological projections under climate change.

Results show that significant changes in the hydrologic flow regime of the Winnipeg River basin are expected under climate change, as soon as the 2050s regardless of scenario. Also shown are that changes in future landcover significantly impact streamflow projections, further emphasising the need to consider non-stationary landcover effects in the Winnipeg River and other basins in the Nelson-Churchill River system. Considering the amounts of hydroelectric energy utilized on the Winnipeg and Nelson Rivers, understanding the effects of climate and landcover change on future flow regimes is of paramount importance for both rehabilitating current stations and the potential development of new ones.

Additionally, application of the landcover simulator module need not be constrained to Boreal regions with large amounts of forest fire activity. The forest fire component in the module can be turned off, with the Markov chain used to simulate other future landcover changes of interest. For example, historical satellite imagery can be used to determine the rate of wetland depletion in other basins, and case studies can be conducted to determine the hydrologic impacts of continued depletion, or restorative measures. In agricultural basins such as the Assiniboine and Red Rivers, the uncertainty in future streamflow can be analyzed from changes in farming practices and dominant crop types. Pasturing, grain crops, and perennial hay crops all have specific hydrologic responses and can change as certain methods of farming become more or less viable with climate change. Urban expansion is also an ongoing phenomenon and can also be investigated.

7.3 Recommendations for Future Work

As this thesis is the first attempt at incorporating non-stationary landcover into WATFLOOD, there are numerous possibilities for extension and improvements of this methodology, which are outlined below:

- Expansion of the historical landcover change analysis of Chapter 4 to other areas of the Winnipeg River basin, potentially including more time periods. The sub-basins were selected for this thesis on the basis of forest fire activity, and available hydrometric records. The images selected for the determination of transition probabilities for the natural, gradual change component was then consequently determined from unburned areas in these sub-basins. This however, does not necessarily need to be the case, if one is solely interested in improving the natural change component. For example, images from several areas of the Winnipeg River basin could be analyzed and transition probabilities calculated, with a methodology developed to incorporate a more spatially representative Markov chain for the entire basin including potential regional differences;

- While the landcover simulator module's inputs are adequate for its current purposes, additional inputs can be investigated and added to increase physical realism as they are included into WATFLOOD. For example, if wind speed and direction are added to WATFLOOD from the results of lake evaporation studies such as those by Slota, (2013), they could be added to the forest fire component as well. While forest fire occurrence is unlikely to see much benefit from such an addition, extent and direction of fire propagation could be made more physically realistic;
- Application of the landcover simulator module on other basins of the Nelson-Churchill River system is necessary to provide the greatest understanding of non-stationary landcover and climate change effects on the totality of Manitoba Hydro's future generating capabilities. As mentioned earlier, the exact methodology as conducted in this thesis may not be required, but can serve as a useful launching point for application on other basins;
- This thesis used one GCM and one hydrological model to examine changes in streamflow and streamflow uncertainty by evolving landcover with climate change. While computationally expensive, determining the sensitivity of this thesis' results to

GCM (or RCM) and hydrological model selection, along with their emissions scenarios, could be valuable.

- The delta-change method was used for downscaling the GCM precipitation and temperature outputs for use in WATFLOOD. Being a mean-based approach, it may not capture the future extreme temperature and precipitation events as quantile-based methods (Ines & Hansen, 2006). Incorporating different downscaling methods in non-stationary landcover simulations is worth consideration.

This thesis serves to provide a methodology and understanding of the effects of climate and landcover changes in the Winnipeg River basin. With this methodology and the results obtained, as well as recommendations for future work, a complete picture of possible hydrologic regimes under climate change throughout Canada and the world can soon be realized.

References

Baldwin, D. J., Desloges, J. R., & Band, L. E. (2000). Physical geography of Ontario. In A. H. Perera, D. L. Euler, & I. D. Thompson (Eds.), *Ecology of a managed terrestial landscape: Patterns and processes of forest landscapes in Ontario* (pp. 12-30). Toronto: UBC Press.

Bingeman, A., Kouwen, N., & Soulis, E. (2006). Validation of hydrological processes in a hydrological model. *Journel of Hydrologic Engineering*, 11: 451-463.

Bohrn, S. K. (2012). Climate change impact assessment and uncertainty analysis of the hydrology of a northern, data-sparse catchment using multiple hydrological models. *MSc thesis, University of Manitoba, Department of Civil Engineering, Winnipeg, MB*, 335.

Brown, A. E., Western, A. W., McMahon, T. A., & Zhang, L. (2013). Impact of forest cover changes on annual streamflow and flow duration curves. *Journal of Hydrology, 483*, 39-50.

Canadian Forest Service. (2010). *Canadian National Fire Database – Agency Fire Data. Natural Resources Canada, Canadian Forest Service, Northern Forestry Centre*. Retrieved Oct 23, 2013, from http://cwfis.cfs.nrcan.gc.ca/en_CA/nfdb

Chen, J., Brissette, F., Poulin, A., & Leconte, R. (2011). Overall uncertainty study of the hydrological impacts of climate change for a Canadian watershed. *Water Resources Research*, 47: 1-16.

Chou, Y. H., & Minnich, R. A. (1993). Mapping probability of fire occurrence in San Jacinto Mountains, California, USA. *Environmental Management, 17*, 129-140.

Cuo, L., Beyene, T., Voisin, N., Su, F., Lettenmaier, D., Alberti, M., & Richey, J. (2011). Effects of mid-twenty-first century climate and land cover change on the hydrology of the Puget Sound basin, Washington. *Hydrological Processes*, 25: 1729-1753.

Diaz-Nieto, J., & Wilby, R. L. (2005). A comparison of statistical downscaling and climate change factor methods: Impacts on low flows in the River Thames, United Kingdom. *Climatic Change, 69*, 245-268.

Duveiller, G., Defourny, P., Desclee, B., & Mayaux, P. (2008). Deforestation in Central Africa: Estimates at regional, national and landscape levels by advanced processing of systematically-distributed Landsat extracts. *Remote Sensing of Environment, 112*, 1969-1981.

Ehman, J., Fan, W., Randolph, J., Southworth, J., & Welch, N. (2002). An integrated GIS and modeling approach for assessing the transient response of forests of the southern Great Lakes region to a doubled CO2 climate. *Forest Ecology and Management, 155*, 237-255.

Environment Canada. (2013). *Calculation of the 1971 to 2000 Climate Normals for Canada*. Retrieved Oct 14, 2013, from http://climate.weather.gc.ca/climate_normals/normals_documentation_e.html

Eschner, A. R., & Satterlund, D. R. (1966). Forest protection and streamflow from an Adirondack watershed. *Water Resources Research, 2*, 765-783.

Evans, A. (in press). Investigation of enhancements to two fundamental components of the statistical interpolation method used by the Canadian Precipitation Analysis (CaPA). *MSc thesis, University of Manitoba, Department of Civil Engineering, Winnipeg, MB*, 307.

Fulton, R. (1995). Surficial materials of Canada, Geological Survey of Canada, Map 1880A, scale 1:5,000,000.

H2O Power Limited Partnership. (2013). *Welcome to H2O Power Limited Partnership*. Retrieved 12 9, 2013, from http://www.h2opower.ca/

Hall, F. G., Botkin, D. B., Strebel, D. E., Woods, K. D., & Goetz, S. J. (1991). Large-scale patterns of forest succession as determined by remote sensing. *Ecology, 72*, 628-640.

Hay, L. E., Wilby, R. L., & Leavesley, G. H. (2000). A comparison of delta change and downscaled GCM scenarios for three mountainous basins in the United States. *Journal of the American Water Resources Association*, 36: 387-397.

Huziy, O., Sushama, L., Khaliq, M., Laprise, R., Lehner, B., & Roy, R. (2013). Analysis of streamflow characteristics over northeastern Canada in a changing climate. *Clim Dyn, 40*, 1879-1901.

Ines, A., & Hansen, J. (2006). Bias correction of daily GCM rainfall for crop simulation studies. *Agricultural and Forest Meteorology, 138*, 44-53.

IPCC. (2000). *Special Report on Emissions Scenarios.* Cambridge, UK: Cambridge University Press.

IPCC. (2007). *Climate Change 2007: Fourth Assessment Report of the Intergovernmental Panel on Climate Change.* Geneva, Switzerland: IPCC.

Jarvis, A., Reuter, H., Nelson, A., & Guevara, E. (2008). Hole-filled SRTM for the globe Version 3, CGIAR-CSI SRTM 90m Database .

Jiang, Y., & Zhuang, Q. (2011). Extreme value analysis of wildfires in Canadian boreal forest ecosystems. *Can. J. For. Res., 41*, 1836-1851.

Kamusoko, C., Aniya, M., Adi, B., & Manjoro, M. (2009). Rural sustainability under threat in Zimbabwe – Simulation of future land use/cover changes in the Bindura district based on the Markov-cellular automata model. *Applied Geography, 29*, 435-447.

Kim, J., Choi, J., Choi, C., & Park, S. (2013). Impacts of changes in climate and land use/cover under IPCC RCP scenarios on streamflow in the Hoeya River basin, Korea. *Science of the Total Environment, 452-453*, 181-195.

Kouwen, N. (2012). WATFLOOD/WATROUTE hydrological model routing and flood forecasting system. Unpublished manuscript [model user's manual].

Kouwen, N., Soulis, E., Pietroniro, A., Donald, J., & Harrington, R. (1993). Grouped Response Units for Distributed Hydrologic Modelling. *Journal of Water Resources Planning and Management*, 119(3): 289-305.

Lake of the Woods Control Board. (2002). Managing the water resources of the Winnipeg River drainage basin. Ottawa, Canada.

Le Goff, H., Flannigan, M. D., & Bergeron, Y. (2009). Potential changes in monthly fire risk in the eastern Canadian boreal forest under future climate change. *Can. J. For. Res., 39*, 2369-2380.

Lillesand, T. M., & Kiefer, R. W. (1994). *Remote sensing and image interpretation* (3rd ed.). New York: John Wiley and Sons, Inc.

Liu, Y., Stanturf, J., & Goodrick, S. (2010). Trends in global wildfire potential in a changing climate. *Forest Ecology and Management*, 259: 685-697.

Manitoba Hydro. (2012). *2011/2012 Annual Report.* Retrieved June 12, 2013, from http://www.hydro.mb.ca/corporate/ar/2011/publish/index.html

Manitoba Hydro. (2013). WATFLOOD Setup of the Winnipeg River basin.

McCoy, V. M., & Burn, C. R. (2005). Potential alteration by climate change of the forest-fire regime in the boreal forest of central Yukon Territory. *Arctic, 58*, 276-285.

Meehl, G., Covey, C., Delworth, T., Latif, M., McAvaney, B., Mitchell, J., . . . Taylor, K. (2007). The WCRP CMIP3 multi-model dataset: A new era in climate change research. *Bulletin of the American Meteorological Society, 88*, 1383-1394.

Minister of Supply and Services. (1989). WreNSs HYDrology . *version 1.1, Rel 11/01/90, Canada*.

Minville, M., Brissette, F., & Leconte, R. (2008). Uncertainty of the impact of climate change on the hydrology of a nordic watershed. *Journal of Hydrology, 358*, 70-83.

MLI. (2013). *Manitoba Land Initiative, Conservation and Water Stewardship*. Retrieved Oct 19, 2013, from http://mli2.gov.mb.ca/

MNR. (2013). *Ontario Ministry of Natural Resources*. Retrieved Oct 19, 2013, from http://www.mnr.gov.on.ca/

Ontario Power Generation . (2011). *OPG Generating Stations*. Retrieved 12 9, 2013, from http://www.opg.com/power/OPGmap0309.pdf

Parisien, M., Peters, V. S., Wang, Y., Little, J. M., Bosch, E. M., & Stocks, B. J. (2006). Spatial patterns of forest fires in Canada, 1980-1999. *International Jounal of Wildland Fire, 15*, 361-374.

Pastor, J., Bonde, J., Johnston, C., & Naiman, R. J. (1993). Markovian analysis of the spatially dependent dynamics of beaver ponds. *Lectures on Mathematics in the Life Sciences, 23*, 5-27.

Pomeroy, J., Fang, X., & Ellis, C. (2012). Sensitivity of snowmelt hydrology in Marmot Creek, Alberta, to forest cover disturbance. *Hydrological Processes, 26*, 1891-1904.

Poulin, A., Brissette, F., Leconte, R., Arsenault, R., & Malo, J. (2011). Uncertainty of hydrological modelling in climate change impact studies in a Canadian, snow-dominated river basin. *Journal of Hydrology, 409*, 626-636.

Prudhomme, C., & Davies, H. (2009a). Assessing uncertainties in climate change impact analyses on the river flow regimes in the UK. Part 1: baseline climate. *Climatic Change, 93*, 177-195.

Prudhomme, C., & Davies, H. (2009b). Assessing uncertainties in climate change impact analyses on the river flow regimes in the UK. Part 2: future climate. *Climatic Change, 93*, 197-222.

Quilbe, R., Rousseau, A. N., Moquet, J. S., Savary, S., Ricard, S., & Garbouj, M. S. (2008). Hydrological responses of a watershed to historical land use evolution and future land use scenarios under climate change conditions. *Hydrology and Earth System Sciences, 12*, 101 - 110.

Raddatz, R. (2007). Evidence for the influence of agriculture on weather and climate through the transformation and management of vegetation: Illustrated by examples from the Canadian Prairies. *Agricultural and Forest Meteorology*, 142: 186-202.

Roberts, J., Pryse-Phillips, A., & Snelgrove, K. (2012). Modeling the Potential Impacts of Climate Change on a Small Watershed in Labrador, Canada. *Canadian Water Resources Journal, 37*(3), 231-251.

Samaniego, L., & Bardossy, A. (2006). Simulation of the impacts of land use/cover and climatic changes on the runoff characteristics at the mesoscale. *Ecological Modelling, 196*, 45-61.

Sanchez, J., & Canton, M. P. (1999). *Space Image Processing.* Boca Raton, Florida: CRC Press LLC.

Scarr, T. A., Ryall, K. L., Piscopo, K. L., & Straight, T. W. (2011, June 6). *Forest Health Conditions in Ontario, 2009.* Retrieved October 6, 2013, from http://www.mnr.gov.on.ca/en/Business/Forests/2ColumnSubPage/STDPROD_087483.html

Schindler, D. (1998). A dim future for Boreal waters and landscapes. *BioScience, 48*(3), 157-164.

Scinocca, J. F., McFarlane, N. A., Lazare, M., Li, J., & Plummer, D. (2008). Technical Note: The CCCma third generation AGCM and its extension to the middle atmosphere. *Atmospheric Chemistry and Physics, 8*, 7055-7074.

Slota, P. M. (2009). Quantifying the impacts of climate change on power generation in the Winnipeg River basin. *BSc thesis, University of Manitoba, Department of Civil Engineering, Winnipeg, MB*, 82.

Slota, P. M. (2013). Evaluation of operational lake evaporation methods in a Canadian Shield landscape. *MSc thesis, University of Manitoba, Department of Civil Engineering, Winnipeg, MB*, 217.

St. George, S. (2007). Streamflow in the Winnipeg River basin, Canada: Trends, extremes and climate linkages. *Journal of Hydrology, 332*, 396-411.

Stadnyk, T., Amour, N., Kouwen, N., Edwards, T., Pietroniro, A., & Gibson, J. (2005). A groundwater separation study in boreal wetland terrain: The WATFLOOD hydrological model compared with stable isotope tracers. *Isotopes in Environmental and Health Studies*, 41: 49-68.

Stadnyk, T., Delavau, C., Kouwen, N., & Edwards, T. (in press). Towards hydrological model calibration and validation: simulation of stable water isotopes using the isoWATFLOOD model. *Hydrological Processes*, doi: 10.1002/hyp.9695.

Stadnyk-Falcone, T. (2008). Mesoscale Hydrological Model Validation and Verification using Stable Water Isotopes: The isoWATFLOOD Model. Ph.D. Thesis, University of Waterloo, Waterloo, ON: 386 pp. http://hdl.handle.net/10012/3970.

Stocks, B. J., Mason, J. A., Todd, J. B., Bosch, E. M., Wotton, B. M., Amiro, B. D., . . . Skinner, W. R. (2003). Large forest fires in Canada, 1959–1997. *Journal of Geophysical Research, 108*, 5-1 - 5-12.

Thompson, I., Flannigan, M., Wotton, B., & Suffling, R. (1998). The effects of climate change on landscape diversity: an example in Ontario forests. *Environmental Monitoring and Assessment, 49*, 213-233.

US Department of the Interior. (2013a). *Federal Wildland Fire Occurrence Data. United States Geological Survey*. Retrieved Oct 23, 2013, from http://wildfire.cr.usgs.gov/firehistory/data.html

US Department of the Interior. (2013b). *Band designations for LandSAT satellites*. Retrieved June 27, 2013, from http://landsat.usgs.gov/band_designations_landsat_satellites.php

US Department of the Interior. (2013c). *Earth Resources Observation and Science Center (EROS). USGS Global Visualization Viewer*. Retrieved Mar 15, 2013, from http://glovis.usgs.gov/

Usher, M. B. (1981). Modelling ecological succession, with particular reference to Markovian models. *Vegetatio, 46*, 11-18.

Van Hulst, R. (1979). On the dynamics of vegetation: Markov chains as models of succession. *Vegetatio, 40*, 3-14.

Veijalainen, N., Dubrovin, T., Marttunen, M., & Vehvilainen, B. (2010). Climate Change Impacts on Water Resources and Lake Regulation in the Vuoksi Watershed in Finland. *Water Resour Manage, 24*, 3437-3459.

Velazquez, J. A., Schmid, J., Ricard, S., Muerth, M. J., St Denis, B. G., Minville, M., . . . Turcotte, R. (2013). An ensemble approach to assess hydrological models' contribution to uncertainties in the analysis of climate change impact on water resources. *Hydrology and Earth System Sciences, 17*, 565 - 578.

Verhegghen, A., Ernst, C., Defourny, P., & Beuchle, R. (2010). Automated land cover mapping and independent change detection in tropical forest using multi-temporal high resolution data set. In Addink, E.A. and F.M.B. Van Coillie (Eds), GEOBIA 2010-Geographic Object-Based Image Analysis. Ghent University, Ghent, Belgium 29 June – 2 July: ISPRS Vol.No. XXXVIII-4/C7, Archives ISSN No 1682-1777: ISPRS Working Groups. Retrieved from http://www.isprs.org/proceedings/XXXVIII/4-C7/pdf/Verhegghen.pdf on June 27, 2013.

Vogelmann, J. E., Howard, S. M., Yang, L., Larson, C. R., Wylie, B. K., & Van Driel, J. N. (2001). Completion of the 1990's National Land Cover Data Set for the conterminous United States. *Photogrammetric Engineering and Remote Sensing, 67*, 650-662.

Vogelmann, J. E., Sohl, T. L., Campbell, P. V., & Shaw, D. M. (1998). Regional land cover characterization using LandSAT thematic mapper data and ancillary data sources. *Environmental Monitoring and Assessment, 51*, 415-428.

Vogt, M. (2012). *Undergraduate student research work term: Landcover classification in the Winnipeg River basin.* Winnipeg, MB: Dept. Civil Engineering, University of Manitoba.

Woolford, D. G., Cao, J., Dean, C. B., & Martell, D. L. (2010). Characterizing temporal changes in forest fire ignitions: Looking for climate change signals in a region of the Canadian boreal forest. *Environmetrics, 21*, 789-800.

WSC. (2013). *Water Survey of Canada*. Retrieved Oct 19, 2013, from http://www.ec.gc.ca/rhc-wsc/

Yip, Q., Burn, D., Seglenieks, F., Pietroniro, A., & Soulis, E. (2012). Climate Impacts on Hydrological Variables in the Mackenzie River Basin. *Canadian Water Resources Journal, 37*(3), 209-230.

Zhao, K. (in press). Validation of the Canadian Precipitation Analysis (CaPA) for hydrological modelling in the Canadian Prairies. *MSc thesis, University of Manitoba, Department of Civil Engineering, Winnipeg, MB*, 173.

Appendix 1: Basin 36 Proportionality Plots

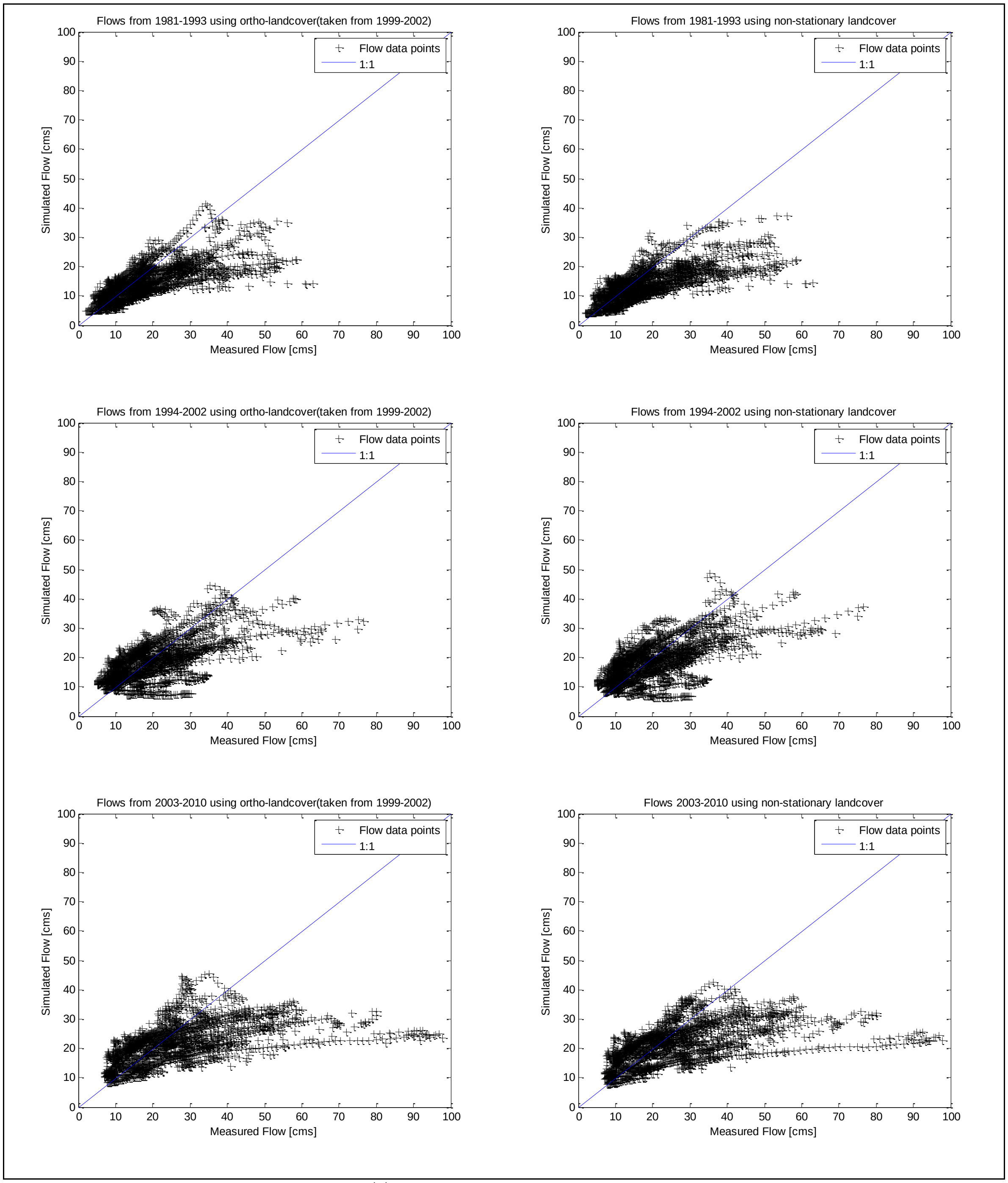

Figure 59 - Proportionality plots for WATFLOOD simulations on Basin 36 (05QC003) for stationary landcover (left column), and non-stationary landcover (right column)

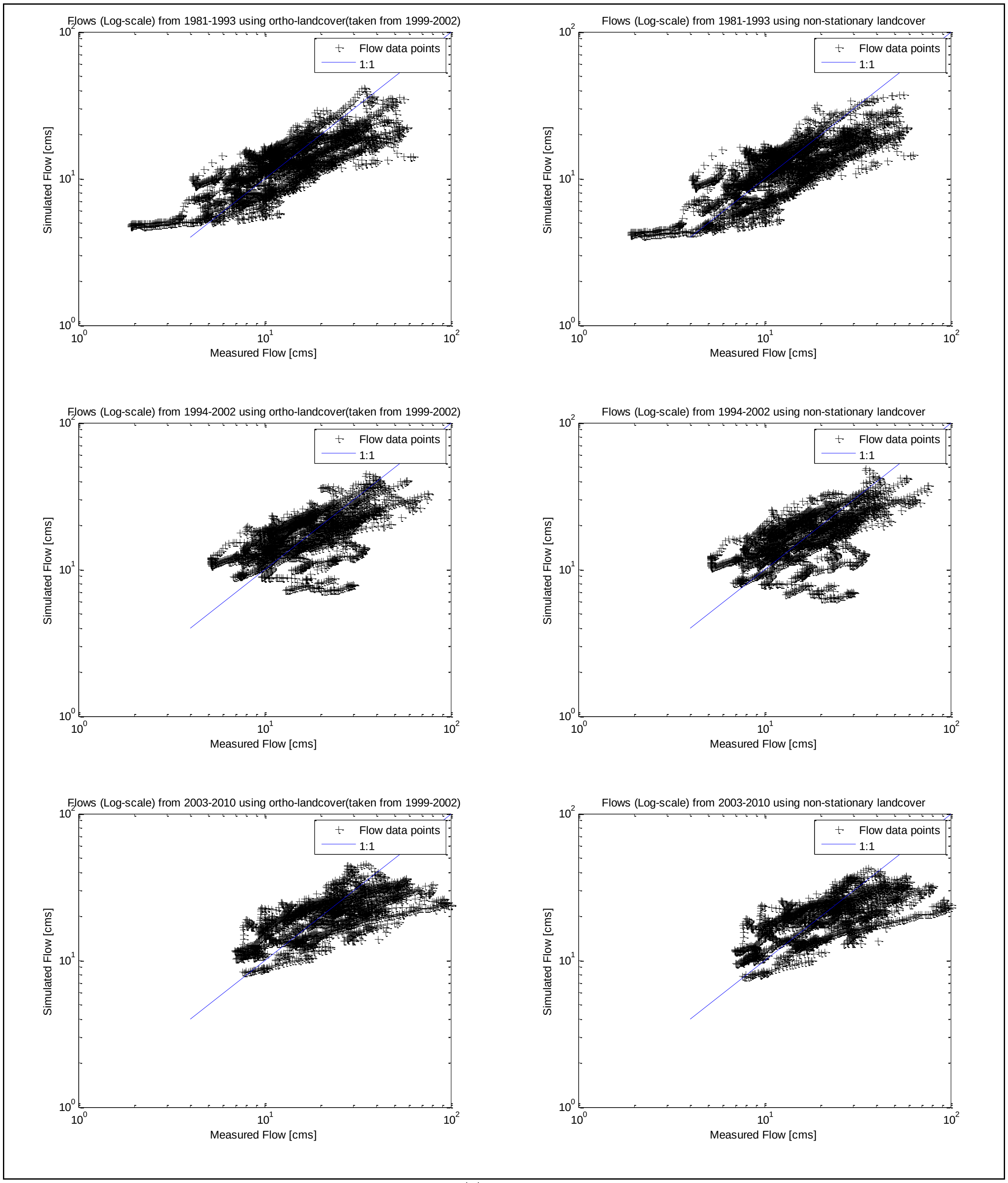

Figure 60 - Proportionality plots (log-scale) for WATFLOOD simulations on Basin 36 (05QC003) for stationary landcover (left column), and non-stationary landcover (right column)

Appendix 2: Parameter File

Below is the parameter file for the landcover simulator module used in this thesis, "#" indicating comments, and ":" parameters:

```
# Landcover Simulator Parameter File
#   Place in directory: bsnm/landcover
#   Run lcsim.exe in bsnm directory
:version        1.0
#
# Input parameters
#Forest fire flag
:ff_flag        y
#Start year
:start      1970
#End year
:finish         2000
#Baseline shd file
:baseshd        basin/wpegr_shd.r2c
#Maximum ff size (max in observation set)
:maxff          387743.
#
# Natural change and regeneration transition probabilities
```

:nClass 21

:BurnClass 13

:BurnableLC 1 1 1 1 1 1 1 1 1 1 1 1 1 1 1 1 1 1 0 0 0

:TransitionProb

(See Appendix 5 for transition probability matrix)

:EndTransitionProb

#

Forest fire simulation

#Logistic regression coefficients

:LogReg_coef -1.107990231 -0.008145903 0.212449707

#GEV coefficients

:GEV_coef 1.58416528799708 3193.34906799923 3830.14211661379

#Simulated months for forest fires

:simmths 0 0 0 1 1 1 1 1 1 0 0 0

#

Simulation List

#Number of climate change simulations to run (45)

:nCCsim 1

:CCsim

2a1b-19

2a1b-20

2a1b-21

2a1b-22

2a1b-23

2a2-15

2a2-16

2a2-17

2a2-18

2a2-19

2b1-17

2b1-18

2b1-19

2b1-20

2b1-21

5a1b-19

5a1b-20

5a1b-21

5a1b-22

5a1b-23

5a2-15

5a2-16

5a2-17

5a2-18

5a2-19

5b1-17

5b1-18

5b1-19

5b1-20

5b1-21

8a1b-19

8a1b-20

8a1b-21

8a1b-22

8a1b-23

8a2-15

8a2-16

8a2-17

8a2-18

8a2-19

8b1-17

8b1-18

8b1-19

8b1-20

8b1-21

:EndCCsim

Appendix 3: Definitions of Parameters

The following are a list of parameters used in the landcover simulator module and their definitions:

:ff_flag – Flag to turn the forest fire component on (“y”) or off (“n”)

:start – Beginning year of the simulation

:finish – Last year of the simulation

:baseshd – Baseline landcover input file, to use as initial conditions

:maxff – Maximum allowable forest fire size in hectares

:nClass – Number of landcover classes (size of transition probability matrix)

:BurnClass – Class # that is the burned landcover

:BurnableLC – Classes that are allowed to burn in the module, “1” if allowed to burn, “0” otherwise

:TransitionProb – Transition probability matrix on following lines

:LogReg_coef – Coefficients of the logistic regression model, for the intercept, cumulative precipitation, and temperature respectively

:GEV_coef – Coefficients of the generalized extreme value distribution, for the shape, scale, and location parameters respectively

:simmths – Months included in the forest fire season, "1" to include, "0" otherwise.

:nCCsim – Number of climate change simulations to run

:CCsim – List of keywords identifying climate change simulations to run in the following lines. Keywords are used as suffixes for the monthly climate delta files, to identify climate change simulations. Keywords are also used as folder names for the output storage folders, to identify them for the user.

Appendix 4: Module Requirements

The folder structures used by the landcover simulator module and file requirements are shown with Figure 61 on the next page. The module is executed in the same directory as all other WATFLOOD executables, namely *bsnm*/, or directory specific to the watershed. More information on how WATFLOOD is set up in general can be found in (Kouwen, 2012). Any new files used by the module, in addition to the output, are under a new folder *bsnm*/landcover/. The term *CCSIM*, refers to the keywords listed in the parameter file under **:CCsim** to identify climate change scenarios (as explained in Appendix 3), and are specified by the user to organize module inputs and outputs. After the module has been executed, the use of batch files is recommended to facilitate the transfer of landcover files to *bsnm*/basin/ for climate change simulation.

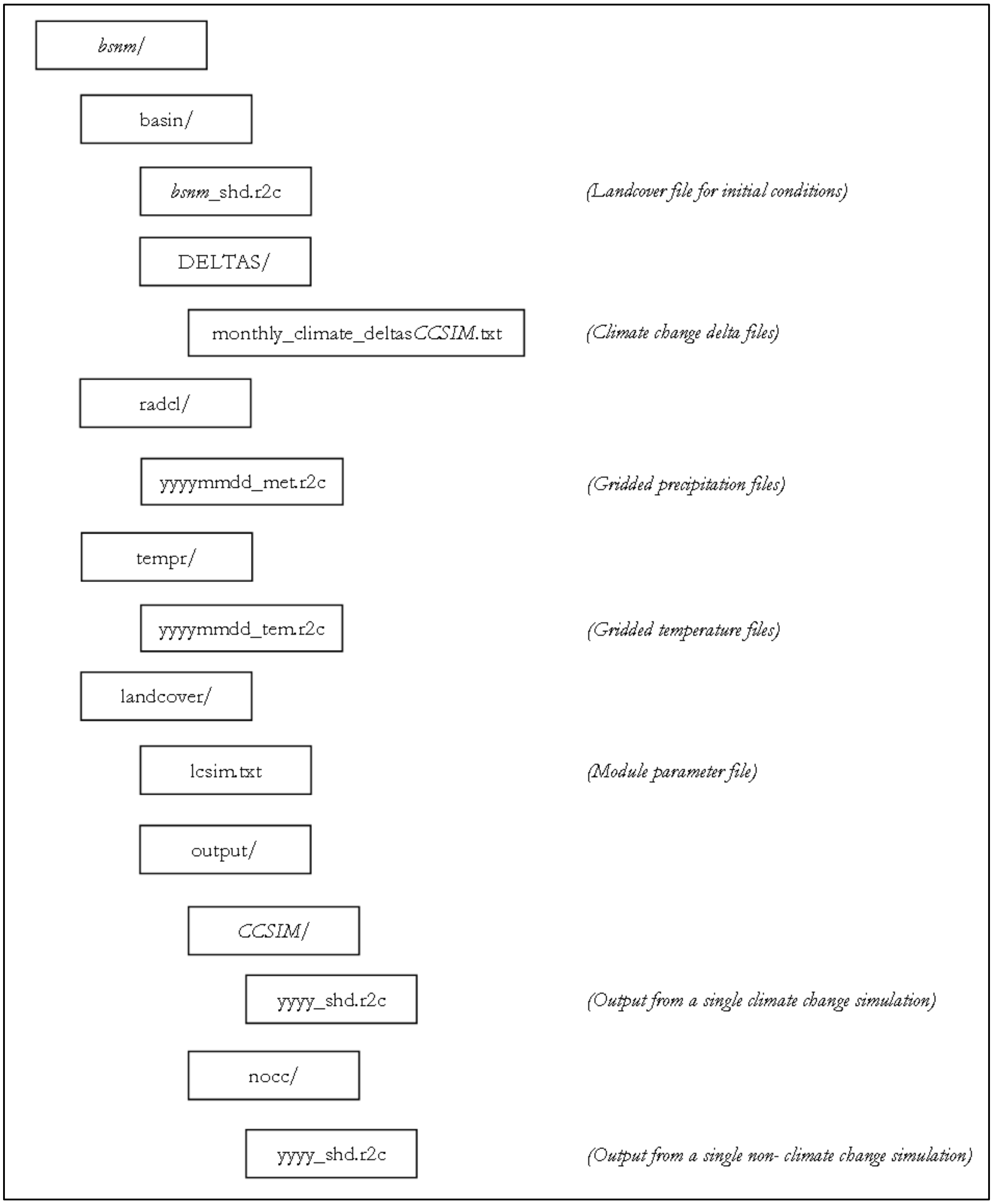

Figure 61 - Folder structure and file requirements for the landcover simulator module

Appendix 5: Natural Change and Regeneration Transition Probability Matrix

The final transition probability matrix, as input to the landcover simulator module, is included on the next page in Table 26. A smaller number of land classes were used in the historical landcover change analysis of Chapter 4 than is included in the transition probability matrix, due to the WATFLOOD model setup of the WRB. This is primarily due to the basin residing in three jurisdictional areas, which has differing landcover classification methodologies. While essentially similar, some irregularities in the classification can occur when crossing borders, and have consequently been included as separate classes in the model setup. For example, three classes in this setup can be described as coniferous forest, each residing in a different province or state. Since transition probabilities derived in Chapter 4 are from basins in Ontario only, an assumption is made that they are equivalent in other jurisdictions. Therefore, descriptions of each land class from every jurisdiction was inspected, and grouped into an equivalent class in Ontario, with grouped classes colour coded in Table 26.

Table 26 - Final transition probability matrix for the natural change and regeneration components

	crops_1	grass_2	decid_3	decid_4	decid_5	conif_6	everg_7	conif_8	mixed_9	mixed_10	mixed_11	tr_rck_12	burns_13	fr_cut_14	bogs_15	bogs_16	openbog17	wetland	wetland	water	imper_21
crops_1	1	0	0	0	0	0	0	0	0	0	0	0	0	0	0	0	0	0	0	0	0
grass_2	0	1	0	0	0	0	0	0	0	0	0	0	0	0	0	0	0	0	0	0	0
decid_3	0	0	1	0	0	0	0	0	0	0	0	0	0	0	0	0	0	0	0	0	0
decid_4	0	0	0	1	0	0	0	0	0	0	0	0	0	0	0	0	0	0	0	0	0
decid_5	0	0	0	0	1	0	0	0	0	0	0	0	0	0	0	0	0	0	0	0	0
conif_6	0	0	0	0	0	0.9731	0	0	0.0058	0	0.0102	0	0	0.0105	0	0.0001	0	0.0003	0	0	0
everg_7	0	0	0	0	0	0	0.9731	0	0.0058	0	0.0102	0	0	0.0105	0	0.0001	0	0.0003	0	0	0
conif_8	0	0	0	0	0	0	0	0.9731	0.0058	0	0.0102	0	0	0.0105	0	0.0001	0	0.0003	0	0	0
mixed_9	0	0	0	0	0	0.0074	0	0	0.9135	0	0.0551	0	0	0.0108	0	0.0039	0	0.0093	0	0	0
mixed_10	0	0	0	0	0	0.0218	0	0	0.0131	0.9499	0	0	0	0.0078	0	0.0017	0	0.0058	0	0	0
mixed_11	0	0	0	0	0	0.0218	0	0	0.0131	0	0.9499	0	0	0.0078	0	0.0017	0	0.0058	0	0	0
tr_rck_12	0	0	0	0	0	0.0074	0	0	0	0	0.0551	0.9135	0	0.0108	0	0.0039	0	0.0093	0	0	0
burns_13	0	0	0	0	0	0.000899	0	0	0.031353	0	0.076615	0	0.850397	0.00923	0	0.008601	0	0.022905	0	0	0
fr_cut_14	0	0	0	0	0	0.0009	0	0	0.0082	0	0.0532	0	0	0.9248	0	0.0046	0	0.0083	0	0	0
bogs_15	0	0	0	0	0	0.0059	0	0	0.0123	0	0.0904	0	0	0.0051	0.8863	0	0	0	0	0	0
bogs_16	0	0	0	0	0	0.0059	0	0	0.0123	0	0.0904	0	0	0.0051	0	0.8863	0	0	0	0	0
openbog17	0	0	0	0	0	0.0059	0	0	0.0123	0	0.0904	0	0	0.0051	0	0	0.8863	0	0	0	0
wetland	0	0	0	0	0	0.0045	0	0	0.0120	0	0.0864	0	0	0.0055	0	0	0	0.8916	0	0	0
wetland	0	0	0	0	0	0	0	0	0	0	0	0	0	0	0	0	0	0	1	0	0
water	0	0	0	0	0	0	0	0	0	0	0	0	0	0	0	0	0	0	0	1	0
imper_21	0	0	0	0	0	0	0	0	0	0	0	0	0	0	0	0	0	0	0	0	1

Legend

- No change
- Coniferous
- Mixed
- Mixed/Sparse
- Burn
- Cuts
- Bogs
- Fens

Appendix 6: Non-Stationary Landcover Climate Change Simulation Tables

Table 27 - Seasonal and annual statistics for WATFLOOD simulations with the CGCM3.1 B1 scenario in the 2050s

2050s - B1	Baseline	Stationary Landcover		Non-Stationary Landcover	
	Flow [cms]	Flow [cms]	% Change	Flow [cms]	% Change
DJF					
Mean	833.9	853.1	2.3	784.9	-5.9
Max	874.0	1078	23.3	998	14.2
Min	770.2	732.2	-4.9	674.1	-12.5
Std deviation	31.5	26.5	-16.0	20.4	-35.3
MAM					
Mean	778.0	861.7	10.8	798.5	2.6
Max	1052	1479	40.5	1347	28.1
Min	695.9	703.5	1.1	650.0	-6.6
Std deviation	100.5	143.6	42.9	122.9	22.3
JJA					
Mean	968.1	1032	6.6	934.3	-3.5
Max	1062	1476.0	39.0	1337	25.8
Min	849.0	799.3	-5.9	727.4	-14.3
Std deviation	68.4	87.4	27.9	74.8	9.4
SON					
Mean	843.9	849.2	0.6	774.0	-8.3
Max	874.1	1078	23.3	998.1	14.2
Min	827.8	747.2	-9.7	674.7	-18.5
Std deviation	14.0	19.1	36.4	17.5	24.8
Overall					
Mean	856.1	899.3	5.1	823.3	-3.8
Max	1062	1479	39.2	1347	26.8
Min	695.9	703.5	1.1	650.0	-6.6
Std deviation	94.1	115.2	22.5	97.9	4.1

Table 28 - Seasonal and annual statistics for WATFLOOD simulations with the CGCM3.1 A1B scenario in the 2050s

2050s - A1B	Baseline	Stationary Landcover		Non-Stationary Landcover	
	Flow [cms]	Flow [cms]	% Change	Flow [cms]	% Change
DJF					
Mean	833.9	936.1	12.3	864.7	3.7
Max	874.0	1105.2	26.5	1018.2	16.5
Min	770.2	812.5	5.5	752.6	-2.3
Std deviation	31.5	30.6	-2.9	24.7	-21.6
MAM					
Mean	778.0	941.5	21.0	877.5	12.8
Max	1052	1431	36.1	1300	23.5
Min	695.9	767.4	10.3	715.3	2.8
Std deviation	100.5	157.7	56.9	136.3	35.6
JJA					
Mean	968.1	1102	13.8	1008	4.1
Max	1062	1417.0	33.4	1282	20.7
Min	849.0	848.7	0.0	772.0	-9.1
Std deviation	68.4	96.1	40.7	84.3	23.4
SON					
Mean	843.9	916.4	8.6	840.9	-0.3
Max	874.1	1103	26.2	1017	16.3
Min	827.8	788.6	-4.7	718.9	-13.1
Std deviation	14.0	23.2	65.9	21.7	54.8
Overall					
Mean	856.1	974.4	13.8	898.0	4.9
Max	1062	1432	34.8	1300	22.4
Min	695.9	767.4	10.3	715.3	2.8
Std deviation	94.1	120.3	27.9	104.5	11.1

Table 29 - Seasonal and annual statistics for WATFLOOD simulations with the CGCM3.1 A2 scenario in the 2050s

2050s - A2	Baseline	Stationary Landcover		Non-Stationary Landcover	
	Flow [cms]	Flow [cms]	% Change	Flow [cms]	% Change
DJF					
Mean	833.9	893.6	7.2	821.9	-1.4
Max	874.0	1068	22.2	985.1	12.7
Min	770.2	808.7	5.0	748.8	-2.8
Std deviation	31.5	25.4	-19.5	19.7	-37.6
MAM					
Mean	778.0	923.1	18.7	854.9	9.9
Max	1052	1464	39.2	1325	25.9
Min	695.9	770.4	10.7	715.7	2.9
Std deviation	100.5	164.4	63.6	140.6	39.9
JJA					
Mean	968.1	1093	13.0	992.7	2.5
Max	1062	1441	35.7	1305	22.9
Min	849.0	887.3	4.5	803.1	-5.4
Std deviation	68.4	98.3	43.8	85.1	24.5
SON					
Mean	843.9	883.5	4.7	806.3	-4.5
Max	874.1	1066	21.9	984.3	12.6
Min	827.8	811.1	-2.0	736.2	-11.1
Std deviation	14.0	20.6	46.9	18.9	35.0
Overall					
Mean	856.1	948.9	10.8	869.4	1.5
Max	1062	1464	37.8	1325	24.7
Min	695.9	770.4	10.7	715.7	2.9
Std deviation	94.1	129.3	37.4	111.3	18.3

Table 30 - Seasonal and annual statistics for WATFLOOD simulations with the CGCM3.1 B1 scenario in the 2080s

2080s - B1	Baseline	Stationary Landcover		Non-Stationary Landcover	
	Flow [cms]	Flow [cms]	% Change	Flow [cms]	% Change
DJF					
Mean	833.9	939.5	12.7	870.8	4.4
Max	874.0	1224	40.1	1130.6	29.4
Min	770.2	773.9	0.5	719.3	-6.6
Std deviation	31.5	33.7	7.1	27.7	-12.1
MAM					
Mean	778.0	943.1	21.2	881.6	13.3
Max	1052	1562	48.5	1428	35.7
Min	695.9	748.3	7.5	698.6	0.4
Std deviation	100.5	154.8	54.0	134.7	34.1
JJA					
Mean	968.1	1089	12.5	998.0	3.1
Max	1062	1541	45.1	1407	32.4
Min	849.0	832.7	-1.9	761.2	-10.3
Std deviation	68.4	100.0	46.3	87.4	27.9
SON					
Mean	843.9	909.8	7.8	837.2	-0.8
Max	874.1	1224	40.1	1131	29.4
Min	827.8	773.1	-6.6	711.5	-14.0
Std deviation	14.0	29.9	113.3	27.7	97.5
Overall					
Mean	856.1	970.8	13.4	897.2	4.8
Max	1062	1562	47.0	1428	34.4
Min	695.9	748.3	7.5	698.6	0.4
Std deviation	94.1	117.9	25.3	102.6	9.0

Table 31 - Seasonal and annual statistics for WATFLOOD simulations with the CGCM3.1 A1B scenario in the 2080s

2080s - A1B	Baseline	Stationary Landcover		Non-Stationary Landcover	
	Flow [cms]	Flow [cms]	% Change	Flow [cms]	% Change
DJF					
Mean	833.9	961.0	15.2	886.6	6.3
Max	874.0	1062.2	21.5	980.3	12.2
Min	770.2	858.8	11.5	795.3	3.3
Std deviation	31.5	29.2	-7.4	23.3	-26.0
MAM					
Mean	778.0	1005	29.1	934.5	20.1
Max	1052	1514	43.9	1371	30.3
Min	695.9	811.8	16.7	758.2	9.0
Std deviation	100.5	171.8	70.9	147.8	47.1
JJA					
Mean	968.1	1125	16.2	1032	6.6
Max	1062	1480	39.4	1345	26.6
Min	849.0	864.0	1.8	787.5	-7.3
Std deviation	68.4	111.1	62.5	98.7	44.4
SON					
Mean	843.9	919.8	9.0	844.0	0.0
Max	874.1	1061	21.3	979.8	12.1
Min	827.8	807.1	-2.5	737.9	-10.9
Std deviation	14.0	30.2	116.0	27.6	97.4
Overall					
Mean	856.1	1003	17.2	924.7	8.0
Max	1062	1514	42.5	1371	29.1
Min	695.9	807.1	16.0	737.9	6.0
Std deviation	94.1	129.8	37.9	114.6	21.7

Table 32 - Seasonal and annual statistics for WATFLOOD simulations with the CGCM3.1 A2 scenario in the 2080s

2080s - A2	Baseline	Stationary Landcover		Non-Stationary Landcover	
	Flow [cms]	Flow [cms]	% Change	Flow [cms]	% Change
DJF					
Mean	833.9	960.2	15.1	893.1	7.1
Max	874.0	1114	27.5	1034	18.4
Min	770.2	840.3	9.1	774.1	0.5
Std deviation	31.5	22.9	-27.2	19.5	-38.1
MAM					
Mean	778.0	1045	34.3	975.5	25.4
Max	1052.0	1635	55.4	1487	41.3
Min	695.9	817.6	17.5	758.5	9.0
Std deviation	100.5	188.5	87.5	161.9	61.1
JJA					
Mean	968.1	1150	18.7	1062	9.7
Max	1062	1590	49.6	1454	36.9
Min	849.0	854.0	0.6	776.3	-8.6
Std deviation	68.4	126.1	84.5	113.0	65.2
SON					
Mean	843.9	895.9	6.2	831.8	-1.4
Max	874.1	1101	26.0	1024	17.2
Min	827.8	794.2	-4.0	724.3	-12.5
Std deviation	14.0	33.7	140.8	31.8	127.3
Overall					
Mean	856.1	1013	18.3	941.2	9.9
Max	1062	1635	53.9	1487	40.0
Min	695.9	794.2	14.1	724.3	4.1
Std deviation	94.1	149.5	58.9	132.8	41.1

Appendix 7: Climate Change Simulation Plots, All Scenarios

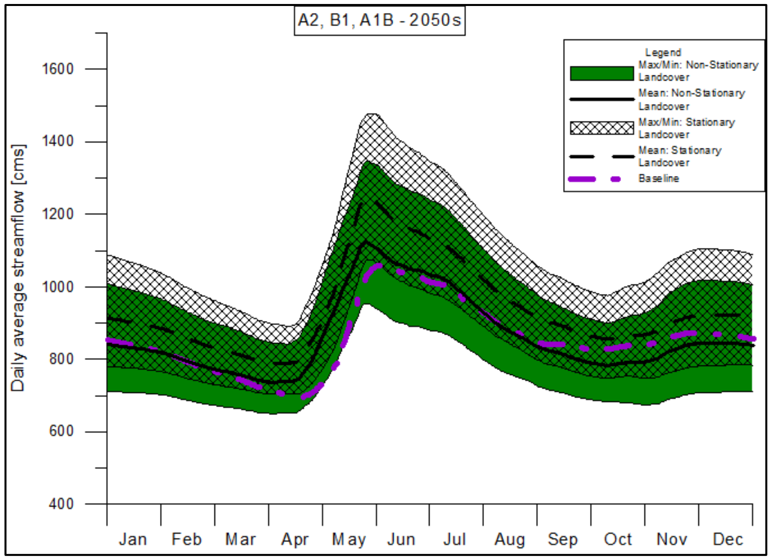

Figure 62 – Annual average WATFLOOD hydrographs for three CGCM3.1 emissions scenarios in the 2050s

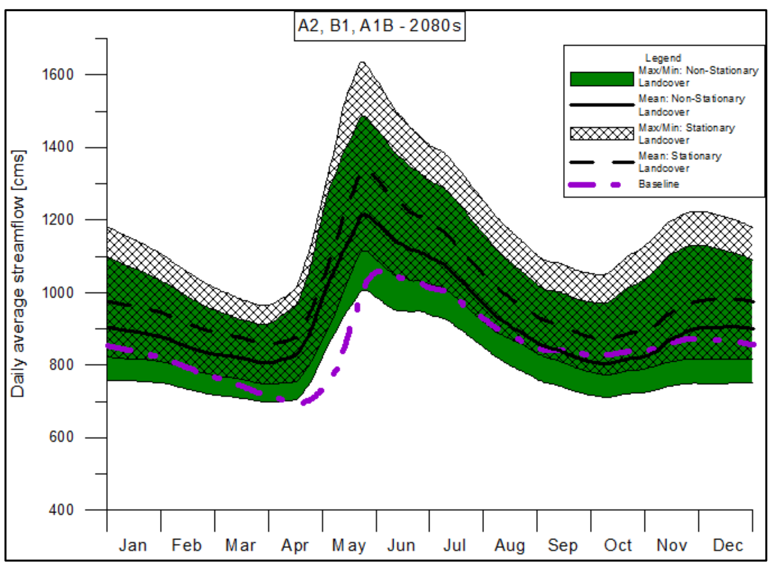

Figure 63 - Annual average WATFLOOD hydrographs for three CGCM3.1 emissions scenarios in the 2080s